Seventh Quarterly Report
Phase II
July 1, 2011

Prepared by
Prof. Nariman Farvardin
Principal Investigator and EERC Project Director

Prof. Balakumar Balachandran, Chair
EERC Project Deputy Director

Dr. Azar Nazeri
EERC Research Manager

THE UNIVERSITY OF MARYLAND AND THE PETROLEUM INSTITUTE OF ABU DHABI, UAE

EERC Key Contributors

University of Maryland – College Park, MD, USA

Shapour Azarm
Balakumar Balachandran
Avram Bar-Cohen
David Bigio
Hugh A. Bruck
Nikil Chopra
Serguei Dessiatoun
Ashwani K. Gupta
Satyandra K. Gupta
Yunho Hwang
P.K. Kannan
Mohammad Modarres
Michael Ohadi
Reinhard Radermacher
Amir Shooshtari

Petroleum Institute – Abu Dhabi, UAE

Youssef Abdel-Majid
Ahmed Al Shoaibi
Saleh Al Hashimi
Ebrahim Al-Hajri
Ali Almansoori
Mohamed Alshehhi
Ali Elkamel
Sai Cheong Fok
Afshin Goharzadeh
Hamad Karki
Isoroku Kubo
Peter Rodgers
Abdennour Seibi

Table of Contents

Executive Summary

The following is a summary of the major project activities that have taken place over the completed quarter. For more detail, see the individual reports in the last section of this report.

Thrust 1: Energy Recovery and Conversion

Sulfur Recovery from Gas Stream using Flameless and Flame Combustion Reactor

A.K. Gupta, A. Al Shoaibi

- Continued progress on experimental part of the project. Examined the formation of CS_2 and the elementary chemical reactions that may form it.
- Modified experimental setup to overcome previous challenges such as prolonged gas sampling time, clogged sampling lines, and burner issues.
- Examined the effect of presence of CO_2 in acid gas.
- Wrote technical paper draft for presentation and publication at the International Energy Conversion Engineering Conference (IECEC) in July/August 2011.

Separate Sensible and Latent Cooling with Solar Energy

R. Radermacher, Y. Hwang, I. Kubo

- Modeled Organic Rankine Cycle
- Validated Organic Rankine Cycle model
- Investigated turbine inlet cooling
- Optimized two configurations of gas turbine combined cycle with double-pressure steam cycle
- Optimized two configurations of split design gas turbine triple-combined cycle with double-pressure steam cycle and absorption chillers.

Waste Heat Utilization in the Petroleum Industry

R. Radermacher, Y. Hwang, S. Al Hashimi, P. Rodgers

- Finished the refrigerant loop
- Ran a shakedown test of the complete cycle
- Installed tachometers for the sensible and desiccant wheel

Thrust 2: Energy-Efficient Transport Process Projects

Multidisciplinary Design and Characterization of Polymer Composite Seawater Heat Exchanger Module

P. Rodgers, A. Bar-Cohen, S.K. Gupta, D. Bigio, H.A. Bruck

- Submitted full draft for a technical paper entitled "Polymer Heat Exchangers – An Enabling Technology for Water and Energy Savings" to IMECE Conference to be held on November 11-17 2011 in Denver, Colorado.
- Manufactured several heat exchanger prototypes made of different polymers using fused deposition modeling, which will be used at the HX test rig at the University of Maryland.
- Developed and utilized thermomechanical finite element model to assess thermal and structural performance of polymer composite heat exchangers and assess feasibility of replacing metallic heat exchangers at the Das Island liquefied natural gas facility with polymer composite heat exchangers.
- Developed processing methodology for comparing experimentally measured fiber orientation to Moldflow® predictions.
- Experimentally validated developed model simplification technique.
- Developed a technique for characterizing mixing of polymer composites in a Twin Screw Extruder (TSE).
- Submitted a full draft for a technical paper entitled "Modeling and Validation of Prototype Thermally Enhanced Polymer Heat Exchanger" to the 2011 International Mechanical Engineering Congress & Exposition in Denver, Colorado.
- A paper entitled "An Integrated Approach to Design of Enhanced Polymer Heat Exchangers" was accepted for publication at the Journal of Mechanical Design.
- Submitted abstract and draft paper entitled "An Integrated Approach to Design of Enhanced Polymer Heat Exchangers" to DETC Conference to be held on August 29-31 2011 in Washington, DC.
- Submitted abstract entitled "Polymer Heat Exchangers – An Enabling Technology for Water and Energy Savings" to IMECE Conference to be held on November 11-17 2011 in Denver, Colorado.

Study on Microchannel-Based Absorber/Stripper and Electrostatic Precipitators for CO_2 Separation from Flue Gas

S. Dessiatoun, A. Shooshtari, M. Ohadi, A. Goharzadeh, E. Al-Hajri

- Improved experimental setup.
- Continued experimental study of absorption of CO_2 in a single microchannel reactor for various diameters.
- Designed/fabricated a second-generation laboratory-scale microchannel CO_2 separator.

Microreactors for Oil and Gas Processes Using Microchannel Technologies

S. Dessiatoun, A. Shooshtari, A. Goharzadeh, E. Al-Hairi

- Evaluated different applications for microreactors and their impact on UAE industry economics.
- Determined that the application of microreactors in the polymerization of ethylene and propylene is feasible and may provide significant economic benefits.

Thrust 3: Energy System Management

Integration of Engineering and Business Decisions for Robust Optimization of Petrochemical Systems

S. Azarm, P.K. Kannan, A. Almansoori, S. Al Hashimi

- Continued the development of the dashboard for oil refinery performance management, with user-interface and improved functions.
- Implemented and integrated a non-regret learning algorithm for simulating the decision-making process by the decision-maker.
- Developed and tested two case study scenarios for a demonstration of dashboard. The case study showed the applicability of the proposed dashboard for oil refinery performance management. It also indicated that the decision-maker was able to make more informed decisions and improve profit.
- Submitted an abstract titled "An Agent-Based Approach to an Integrated Corporate Dashboard for Oil Refinery" to the Canadian Society of Chemical Engineering Conference 2011.
- Finished and submitted an abstract of a book chapter titled "Robust Multi-Objective Genetic Algorithm with Interval Uncertainty."
- Continued progress on other recent joint publications.

Dynamics and Control of Drill Strings

B. Balachandran, H. Karki, Y. Abdelmagid, S.C. Fok

- Expanded on the model previously presented by specifically explaining what motions the model is able to capture. Most notably, the model is able to predict backward whirling while in contact with the outer shell.
- Performed experiments on a vertical drill string in the absence of an outer shell. This allows us to explore the dynamic effect that is due to geometry, and this effect is expected to play a dominant role in horizontal drilling.
- Made modifications to enhance the experimental apparatus.

Studies on Mobile Sensor Platforms

B. Balachandran, N. Chopra, H. Karki, S.C. Fok

- Performed experiments to demonstrate SLAM.
- Performed simulation work on the feature extraction and data association algorithms.

Development of a Probabilistic Model for Degradation Effects of Corrosion-Fatigue Cracking in Oil and Gas Pipelines

M. Modarres, A. Seibi

- Continued theoretical effort in support of model development.
- Conducted experiments in support of corrosion and creep model development:
  - Experiments on Al-7075-T6 materials
  - Experiments on X-70 carbon steels

Individual Project Reports

Thrust 1
Energy Recovery and Conversion

Sulfur Recovery from Gas Stream using Flameless and Flame Combustion Reactor

UMD Investigators: Ashwani K. Gupta
GRA: Hatem Selim
PI Investigators: Ahmed Al Shoaibi
Start Date: October 2006

1. Objectives/Abstract

The main objective is to obtain fundamental information on thermal process of sulfur recovery from sour gas by conventional flame combustion as well as flameless combustion, using numerical and experimental studies. Our ultimate goal is to determine optimal operating conditions for enhanced sulfur conversion. Therefore, an experimental study of the flameless combustion processes of the Claus furnace is proposed so that the results can be used in the normal flame process for determining improved performance. In this study we will explore different operating conditions and perform in flame and exhaust gas analyses of both flame and flameless modes of reactor operation in order to seek our quest for better understanding of the process with the goal to attain enhanced sulfur capture efficiency.

Specific objectives are to provide:

- A comprehensive literature review of the existing flame combustion process for sulfur removal with special reference to sulfur chemistry
- Near isothermal reactor conditions and how such conditions assist in the enhanced sulfur recovery process
- CFD simulation of the flame and flameless combustion in the furnace.
- Determination of the chemical kinetics and the major reaction pathways to seek for high performance
- Design of a reactor for experimental verification of the numerical results
- Measurements and characterization of the combustion furnace under various conditions, including the conditions that utilize high temperature air combustion principles for flameless combustion
- Experiments with different sulfur content gas streams using the flame and flameless combustion furnace modes of operation.
- Installation of the appropriate diagnostics for quantification of stable and intermediate sulfur compounds in the process and exit stream
- Flow, thermal and chemical speciation characteristics of the reactor
- Product gas stream characteristics and evaluation of sulfur recovery and performance in the process

2. Deliverables

- Further examination of hydrogen sulfide combustion in methane/air flame in a plug flow reactor (interpretation of the formation of carbon disulfide from the chemical kinetics point of view).
- Experimental setup has been modified to suit the experiment of CO_2 effect on Claus reactions. Previous geometry did not allow stable flame.
- Start the investigation of CO_2 presence in the acid gas stream on Claus process reactions.
- Finish writing a draft technical paper about the results presented in the previous quarterly report. The paper will be submitted and published at the forthcoming International Energy Conversion Engineering Conference (IECEC), in July/August 2011.

3. Executive Summary

During the reported quarter, progress continued with major focus on the experimental part of the project. In continuation of the study presented in the March 2011 quarterly report, an interpretation on the formation of CS_2 is examined further in the present report. A group of elementary reactions provide the possible channel of CS_2 formation during the chemical reaction.

Some modifications to the experimental setup were carried out in order to perform the experiments. The previous burner could not provide a stable flame for our examination. The burner tubes were replaced with smaller diameter tubes in order to increase the speed of reactants. Several challenges were faced during the experiments, such as a prolonged gas sampling time, the sampling line clogging with condensed sulfur on the walls, and the gas sampling tip becoming too close to the burner. All challenges were addressed and overcome during this quarter.

The effect of presence of carbon dioxide in acid gas was examined. Carbon dioxide was mixed with hydrogen sulfide to produce a mixture of different acid gases. Oxygen was used as an oxidizer (in place of air) in order to rule out the effect of nitrogen on the chemical reaction. Gas sampling was conducted along the centerline of the reactor using a sonic-throat sampling probe, which offers the advantages of rapid cooling of the gases due to sudden expansion of the gases downstream of the sonic throat.

A draft technical paper was also written on the results presented in the previous quarterly report. The paper has been accepted for presentation and publication at the forthcoming International Energy Conversion Engineering Conference (IECEC), July/August 2011, to be held in San Diego.

4. Progress

4.1 Interpretation of the formation of carbon disulfide

The results presented in the previous quarterly report were further examined in order to seek an interpretation on the formation of CS_2, given below.

Figures 1 and 2 show the distribution of carbon disulfide mole fraction at Φ=3.0 and Φ =1.0. Note that CS_2 was not observed under lean conditions (Φ=0.5). The formation of carbon disulfide is attributed primarily to the chemical reaction of methane and sulfur compounds. Reactions 1, 2, and 3 describe the possible channels for CS_2 formation [1]:

$$CH_4 + 2\ S_2 \Leftrightarrow CS_2 + 2\ H_2S \quad (1)$$

$$CH_4 + 2\ S \Leftrightarrow CS_2 + 2\ H_2 \quad (2)$$

$$CH + 2\,H_2S \Leftrightarrow CS_2 + 4H_2 \quad (3)$$

Under Claus conditions and stoichiometric conditions it is more common for these reactions to take place. However, under lean conditions, it is more common for oxidation of H_2S and CH_4 to form SO_2 and CO_2, respectively. Under Claus conditions, the CS_2 mole fraction is almost one order of magnitude higher than the CS_2 value under stoichiometric conditions. This is mainly due to the rarity of CH and S radicals where the availability of more oxygen will transform these radicals to SO and OH. The latter radicals will dictate the reaction to form other end-products, such as, SO_2, H_2O, and CO_2.

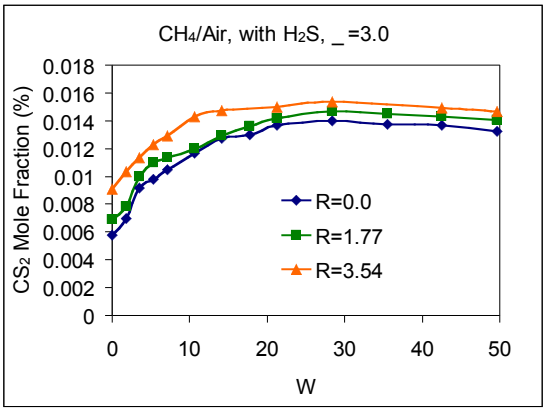

Figure 1. Carbon disulfide mole fraction. Flame conditions: methane/air with H_2S, Φ =3.0.

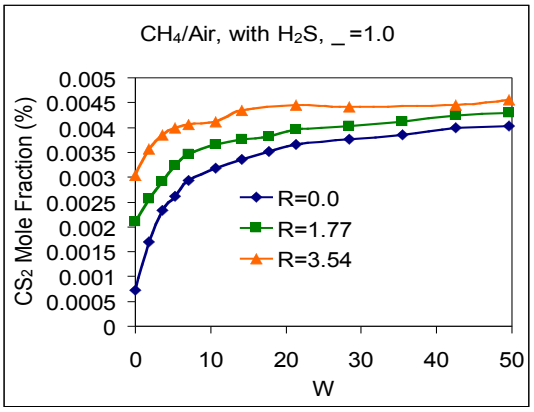

Figure 2. Carbon disulfide mole fraction. Flame conditions: methane/air with H_2S, Φ =1.0.

4.2 Effect of CO_2 in acid gas stream on Claus reactions

We faced several issues during this quarter in order to perform the experiments on the effect of CO_2 in acid gas stream. Several modifications were made on the experimental setup to resolve these issues and to facilitate demonstration of the experiments.

4.2.1 Issues

Oxygen was used as an oxidizer in order to decouple its effect from the effect of CO_2 in the acid gas. The use of oxygen as an oxidizer posed several problems:

- Very low flow speed produced a highly unstable flame
- Gas sampling was very problematic near flame zone because of the high tendency of flame extinction
- Gas sampling time was excessively increased due to the low reactant flow rates
- Formation of relatively high sulfur amounts caused the sampling probe to clog. Figure 3 shows the sampling line clogging with sulfur deposits

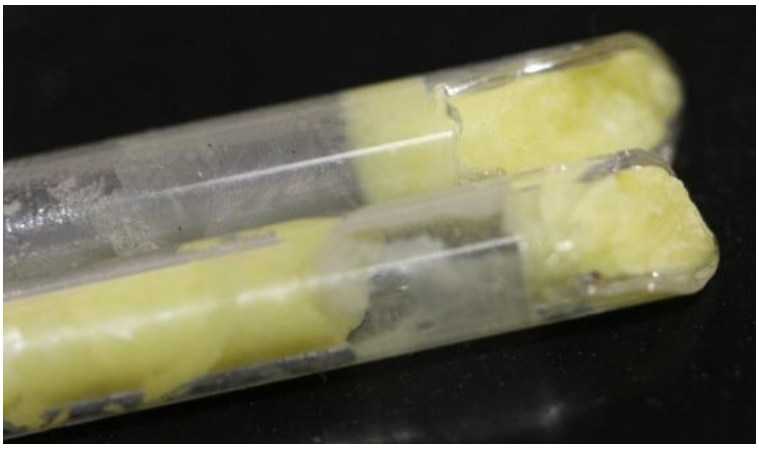

Figure 3. Sampling probe clogged with sulfur.

In order to resolve these issues several modifications were made to the experiment setup. These include:

- Fabrication of a new burner with smaller dimensions in order to increase the speed of reactants flow to enhance flame stability, which subsequently facilitated gas sampling near the burner zone. Figure 4 shows a schematic of the new burner with dimensions.

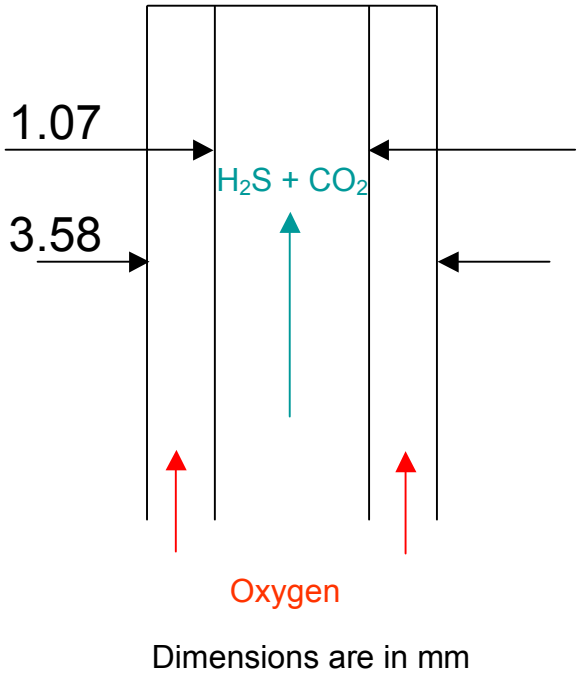

Figure 4. Schematic of the new burner.

- A make-up gas stream was mixed with the sampled gas to increase the sampling flow velocity and reduce the time required for each sample analysis. Argon or air was used as the make-up gas. Figure 5 shows a schematic of the sampling line.

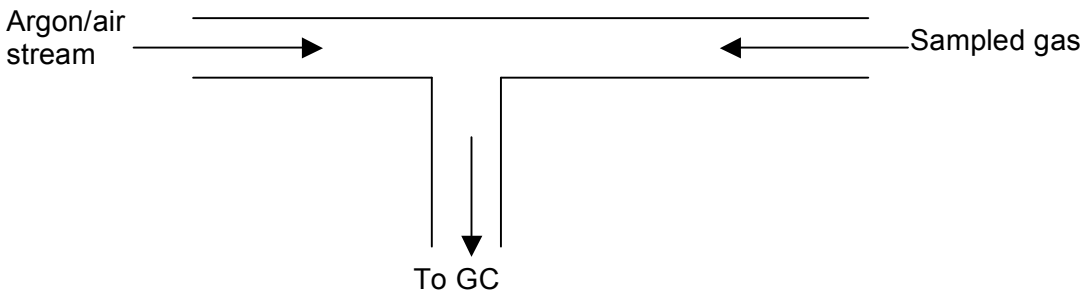

Figure 5. Schematic of the sampling line

- A sulfur collector was fabricated and used to collect sulfur deposits in order to avoid clogging of the sampling line with sulfur. Figure 6 shows a schematic of the sulfur collector.

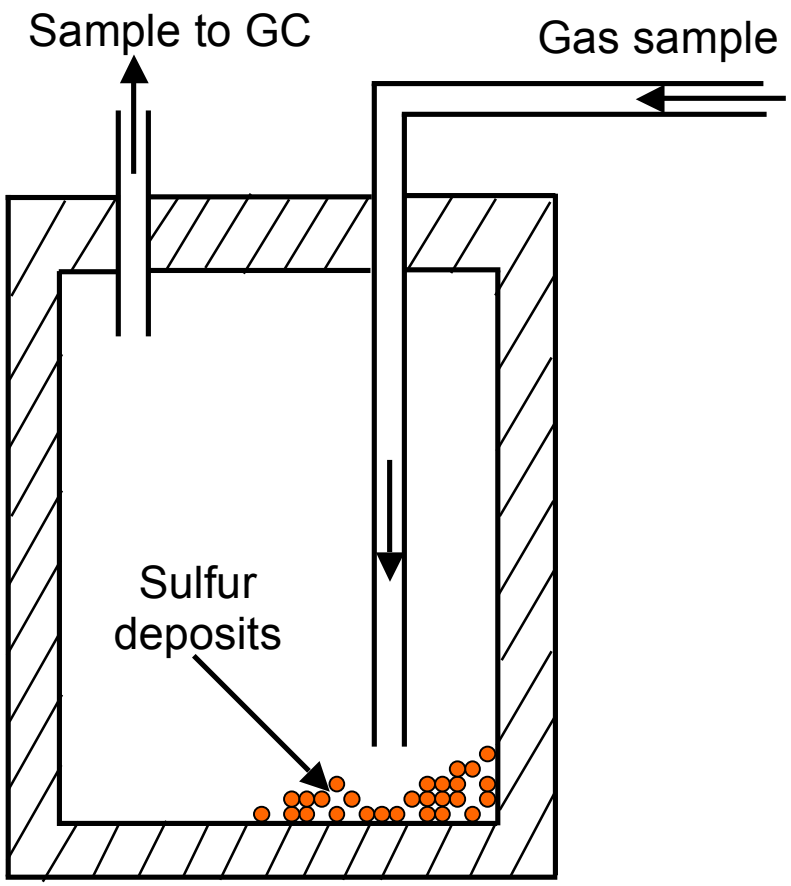

Figure 6. Schematic of the sulfur collector

4.2.2 CO_2-laden acid gas experiments

The carbon dioxide flow rate was changed in order to produce different acid gas compositions while hydrogen sulfide and oxygen flow rates were kept constant. Table 1 shows the experimental conditions used in the experiments.

Table 1. Experimental conditions

	H_2S (cm^3/min)	CO_2 (cm^3/min)	O_2 (cm^3/min)
Acid Gas composition (100% H_2S, 0% CO_2)	**80**	**0**	**40**
Acid Gas composition (90% H_2S, 10% CO_2)	**80**	**9**	**40**
Acid Gas composition 80% H_2S, 20% CO_2)	**80**	**20**	**40**

Temperature measurement

Figure 7 shows the temperature distribution along the reactor centerline. The figure represents both cases of (100% H_2S) acid gas and (80% H_2S, 20% CO_2%) acid gas. Injection of carbon dioxide reduces the temperature of the flame immediately upon injection. Temperature tends to be equivalent downstream. This is attributed to the higher amounts of H_2S combusted due to the liberated oxygen from CO_2. Temperature measurement at the burner tip could not be measured due to problems of flame extinction.

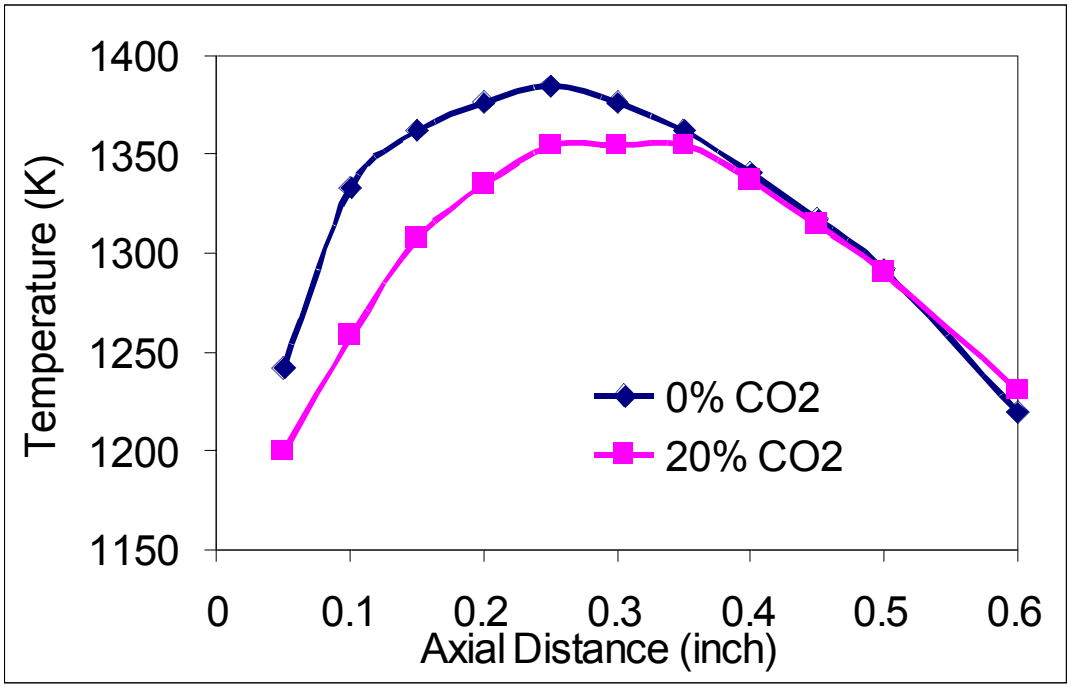

Figure 7. Temperature distribution along the reactor centerline.

Figure 8 shows mole fractions of hydrogen sulfide and sulfur dioxide for 100% H_2S acid gas case. The reaction starts between H_2S and O_2 to form SO_2 while reaction between H_2S and SO_2 takes place downstream (~ 1 inch away from the burner).

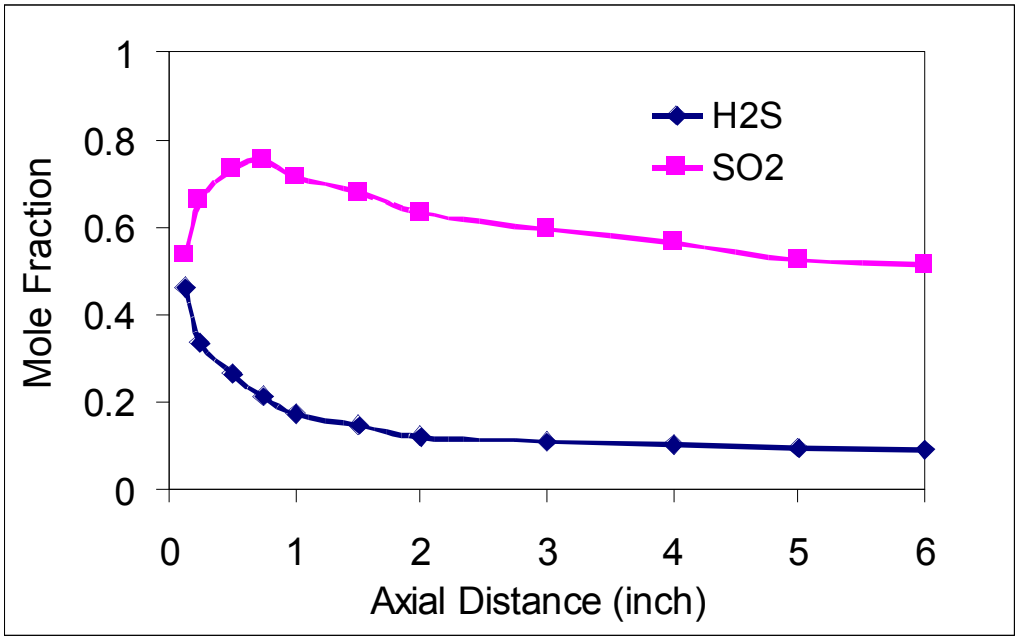

Figure 8. Hydrogen sulfide and sulfur dioxide mole fractions (100% H_2S acid gas).

Figure 9 shows the mole fractions of hydrogen sulfide and sulfur dioxide for the 90% H_2S, 10% CO_2 acid gas case. The reaction between H_2S and SO_2 takes place on a smaller scale due to the presence of CO_2. Carbon dioxide dissociation acts as an oxygen provider into the chemical reaction pool.

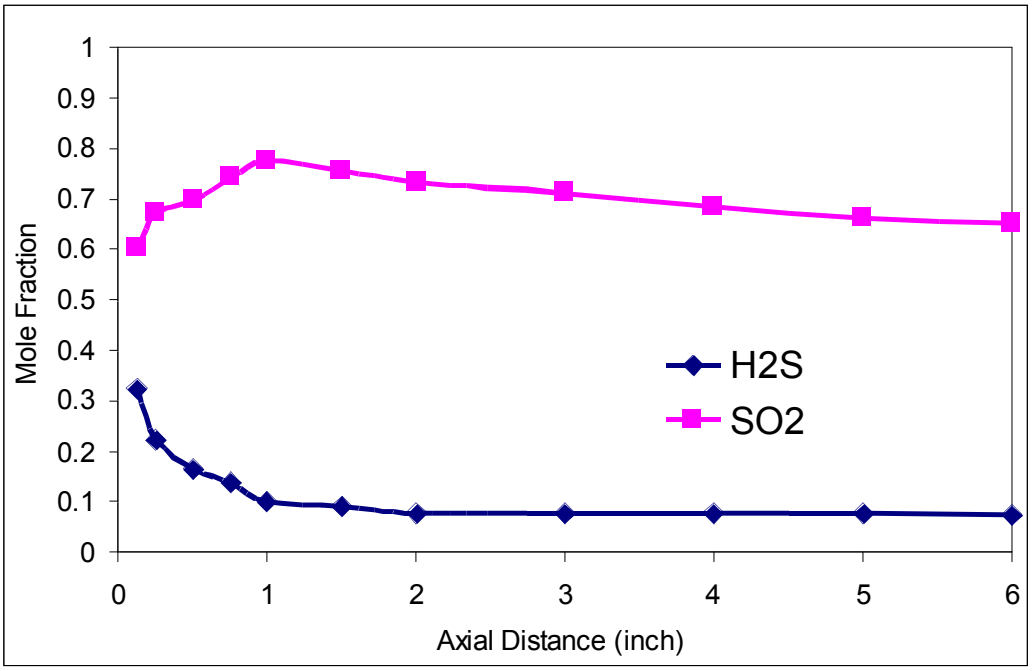

Figure 9. Hydrogen sulfide and sulfur dioxide mole fractions (90% H_2S, 10% CO_2 acid gas).

Figures 10 and 11 depict the mole fractions of carbon dioxide (CO_2) and carbon monoxide (CO), respectively, for the 90% H_2S and 10% CO_2 case. Figure 10 shows the decrease of carbon dioxide where it dissociates to carbon monoxide and atomic oxygen. Atomic oxygen contributes to the reaction as an oxidizer for the H_2S to SO_2 reaction route. Figure 11 shows the carbon monoxide mole fraction that is emanated from the dissociation of CO_2.

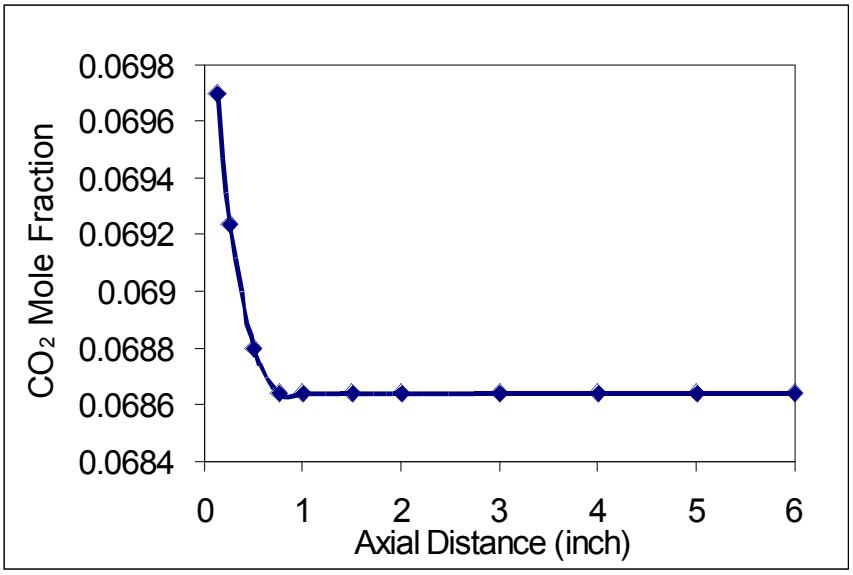

Figure 10. Carbon dioxide mole fraction (90% H_2S, 10% CO_2 acid gas).

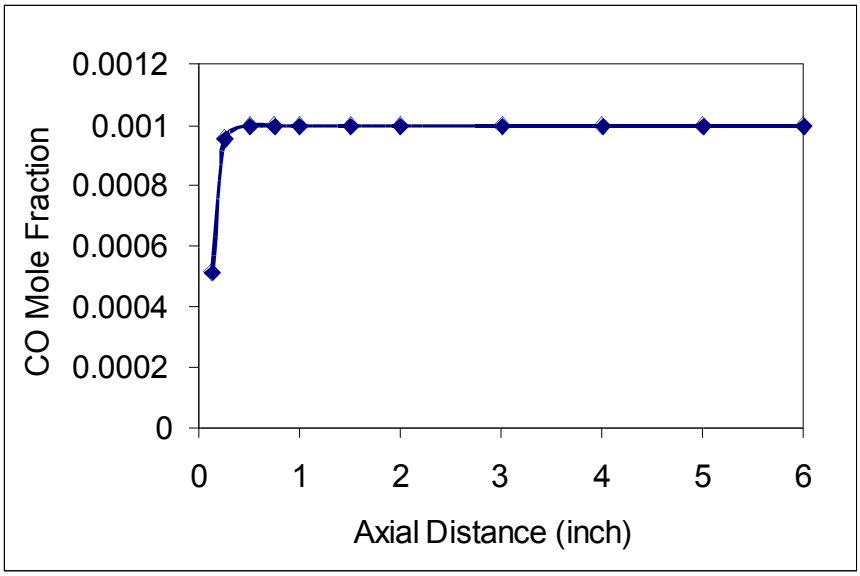

Figure 11. Carbon monoxide mole fraction (90% H_2S, 10% CO_2 acid gas).

Figure 12 shows the mole fractions of hydrogen sulfide and sulfur dioxide for the 80% H_2S and 20% CO_2 acid gas case. Sulfur dioxide reaches almost an asymptotic value at ~ 2 inches, which indicates that reaction between H_2S and SO_2 does not take place. This is attributed to the greater addition of carbon dioxide, which leads to more CO_2 dissociation rates. Subsequently, it is conjectured that higher amounts of liberated oxygen exist in the reaction pool.

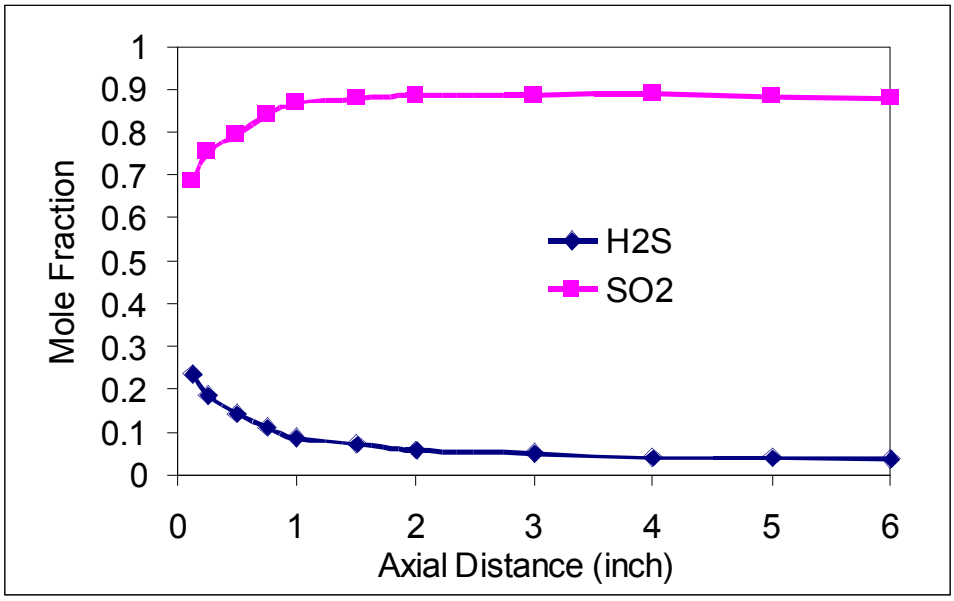

Figure 12. Hydrogen sulfide and sulfur dioxide mole fractions (80% H_2S, 20% CO_2 acid gas).

Figures 13 and 14 show mole fraction of carbon dioxide (CO_2) and carbon monoxide (CO), respectively, for the 80% H_2S and 20% CO_2 mixture case. Similarly to the previous case with 10% CO_2 (see Figures 10 and 11), a decrease of CO_2 and increase of CO is observed, but on a bigger scale.

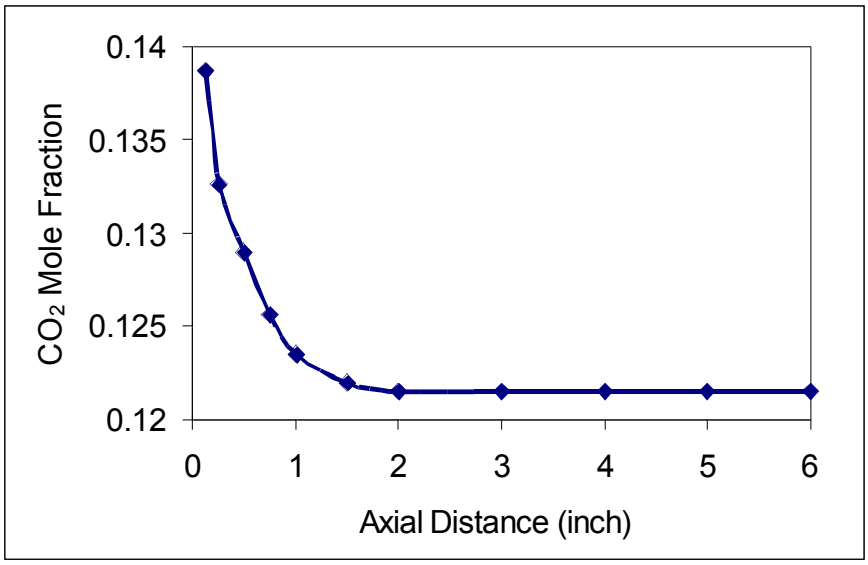

Figure 13. Carbon dioxide mole fraction (80% H_2S, 20% CO_2 acid gas).

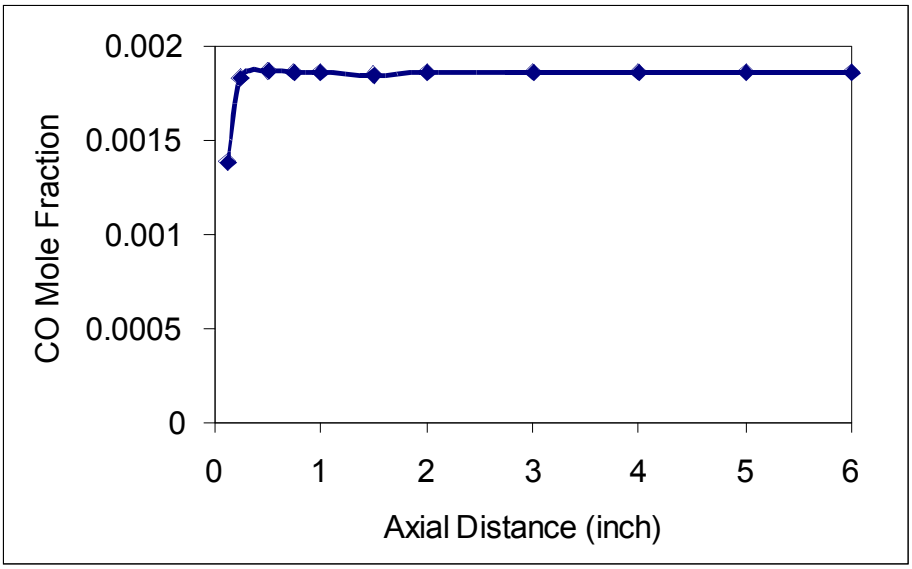

Figure 14. Carbon monoxide mole fraction (80% H_2S, 20% CO_2 acid gas).

4.3 Technical papers

During the past quarter we wrote a technical paper and submitted to the forthcoming International Energy Conversion Engineering Conference (IECEC), in July/August 2011. The paper title is "Spatial Speciation of H_2S Combustion in Methane/Air Flame." This paper was also closely coordinated with faculty from PI, who also provided much input to the paper.

5. Summary

The study begun in the past quarter has been conducted in this quarter. An explanation of the formation of carbon disulfide from the chemical kinetics point of view is given. It was found that carbon disulfide is formed due to the presence of methane, which reacts with sulfur compounds to form CS_2. On the other hand, other intermediate species, such as CH, react with H_2S to form CS_2 as well. Moreover, investigation of the effect of CO_2 presence in the acid gas stream was performed. The experimental setup was modified in order to conduct such a type of experiments with good reliability and robustness of data. A new burner was designed and fabricated, as the previous burner did not provide stable flame. A sulfur collector was fabricated to avoid sampling line clogging. The experiments showed a negative effect of CO_2 on the Claus reaction. Addition of CO_2 into the acid gas stream dwindled the SO_2/H_2S reaction to produce sulfur. This was attributed to CO_2 dissociation to form carbon monoxide and oxygen. The latter oxidizes hydrogen sulfide to form higher amounts of SO_2. Finally, a conference paper was written and submitted to the forthcoming International Energy Conversion Engineering Conference (IECEC), in July/August 2011. The paper title "Spatial Speciation of H_2S Combustion in Methane/Air Flame." This paper was reviewed by 2 different reviewers and has been accepted for presentation at the conference and publication.

6. Difficulties Encountered/Overcome

None

7. Deliverables for the Next Quarter

- Further investigation of the effect of CO_2 in the acid gas stream at higher reactants flow rates.
- Examine the effect of nitrogen presence in acid gas stream on Claus reactions.
- Examine the combined effect of CO_2 and N_2 in the acid gas stream
- Write technical paper for journal and conference publication.

8. References

[1] Thacker, C. M., Miller, E., "Carbon Disulfide Production," Industrial Engineering Chemistry, Vol. 36, Issue 2, 1944, pp. 182-184.

9. Publications

Conference Publications

1. Gupta, A. K. and Sassi, M. "Sulfur Recovery from Acid Gas Using the Claus Process and High Temperature Air Combustion Technology," American J. of Environmental Sciences, Vol. 4, No. 5, 2008, pp. 502-511.
2. Selim, H., Gupta, A. K. and Sassi, M. "Variation of Optimum Claus Reactor temperature with Acid Gas Composition," IECEC Conference, Cleveland, OH, July 28-30, 2008, Paper No. AIAA-2008-5797.
3. Selim, H., Gupta, A. K. and Sassi, M. "Reduced Mechanism for Hydrogen Sulfide Oxidation," 47th AIAA Aerospace Sciences Conference, Orlando, FL, January 5-8, 2009, Paper No. AIAA-2009-1392.
4. Selim, H. and Gupta, A. K. "Nonreactive Study for the Reactants Mixing in Claus Reactions," 7th Intl. Energy Conversion Engineering Conference (7th IECEC), Denver, CO, August 2-5, 2009, Paper No. AIAA-2009-4506.
5. Selim, H, Gupta, A. K. and Sassi, M. "Reduction and Validation of Detailed Kinetic Reactions in Thermal Stage of Claus Process," 48th AIAA Aerospace Sciences Conference, Orlando, FL, (accepted for presentation and Publication), January 3-7, 2010, Paper AIAA-2010-1355.
6. Al Amoodi, N., Selim, H., Gupta, A. K., Sassi, M. and Al Shoaibi, A. "Numerical Simulations of the Thermal Stage in Claus Process: Equilibrium and Kinetic Investigation," 48th AIAA Aerospace Sciences Conference, Orlando, FL, January 3-7, 2010, AIAA-2010-1356.
7. Selim, H. Vijayan, V., Al Shoaibi, A., and Gupta, A. K., "Numerical and Experimental Studies on Mixing and Product Species Distribution in a Claus Reactor," 8th Intl. Energy Conversion Engineering Conference (8th IECEC), Nashville, TN, August 2-5, 2010, Paper No. AIAA-2010-7183.
8. Selim, H, Al Shoaibi, A., and Gupta, A. K., "Examination of Emission Spectra from Hydrogen Sulfide Flames," 49th AIAA Aerospace Sciences Conference, Orlando, FL, January 4-7, 2011, AIAA-2011-440.
9. Selim, H, Al Shoaibi, A., and Gupta, A. K., "Spatial Speciation of H_2S Combustion in Methane/Air Flame," To be submitted to 9th International Energy Conversion Engineering Conference (9th IECEC), San Diego, CA, July 31-August 3, 2011.

Journal Publications

1. Selim H et al. Novel error propagation approach for reducing H_2S/O_2 reaction mechanism. Appl Energy (2011), doi:10.1016/j.apenergy. 2011.01.047.
2. Selim, H., Al Shoaibi, A., Gupta, A. K., "Effect of H_2S in methane/air flames on sulfur chemistry and products speciation," The Journal of Applied Energy, Vol. 88, Issue 8, August 2001, pp. 2593-2600.
3. Selim, H., Al Shoaibi, A., Gupta, A. K., "Experimental examination of flame chemistry in hydrogen sulfide-based flames," The Journal of Applied Energy, Vol. 88, Issue 8, August 2001, pp. 2601-2611.

Appendix

Justification and Background

Hydrogen sulfide is present in numerous gaseous waste streams from natural gas plants, oil refineries, and wastewater treatment plants, among other processes. These streams usually also contain carbon dioxide, water vapor, trace quantities of hydrocarbons, sulfur, and ammonia. Waste gases with ammonia are called sour gases, while those without ammonia are called acid gases. Sulfur must be recovered from these waste streams before flaring them. Sulfur recovery from sour or acid gas typically involves application of the well-known Claus process, using the reaction between hydrogen sulfide and sulfur dioxide (produced at the Claus process furnace from the combustion of H_2S with air and/or oxygen), yielding elemental sulfur and water vapor: $2H_2S(g) + SO_2(g) = (3/n)\ S_n(g) + 2H_2O(g)$ with ΔH_r= -108 kJ/mol. Therefore, higher conversions for this exothermic, equilibrium-limited reaction call for low temperatures, which lead to low reaction rates that dictate the use of a catalyst. The catalytic conversion is usually carried out in a multistage, fixed-bed, adsorptive reactor process, which counteracts the severe equilibrium limitations at high conversions. This technology process can convert about 96% to 97% of the influent sulfur in H_2S to S. However, higher removal requires critical examination of the process and use of a near isothermal reactor, since the conversion is critically dependent upon the exothermic and endothermic conditions of the reactions.

Flameless combustion has been shown to provide uniform thermal field in the reactor so that the reactor temperature is near uniform. Reactor size can also be reduced and combustion-generated pollutants emissions can be reduced by up to 50%. Energy efficiency can be increased by up to 30%. The application of this technology appears to offer great advantages for the processes under consideration. The UAE, which pumps about 2.4 million bpd of crude oil, is also home to the world's fifth biggest gas reserves at about 200 trillion cubic feet. Abu Dhabi Gas Industries (GASCO), an operating company of the Abu Dhabi National Oil Company (ADNOC), is leading a drive to boost gas production in the UAE from five to seven billion cubic feet per day. This calls for sulfur recovery capacity of over 3,000 metric tons per day with the associated SOx and NOx emissions. Therefore, the adoption and further development of flameless combustion technology for sulfur recovery among other commercial and industrial heating processes is expected to be crucial and beneficial, both economically and environmentally.

The conventional sulfur recovery process is based upon the withdrawal of sulfur by in situ condensation within the reactor. The selective removal of water should, however, be a far more effective technique, as its effect on the equilibrium composition in the mass action equation is much greater. The in situ combination of the heterogeneously catalyzed Claus reaction and an adsorptive water separation seems especially promising, as both reaction and adsorption exhibit similar kinetics, and pressure can be adapted to the needs of the adsorptive separation. Such an adsorptive reactor will lead to almost complete conversion as long as the adsorption capacity is not exhausted. There are numerous possibilities for implementing these two functions, ranging from fixed-beds with homogeneous catalyst/adsorbent mixtures to spatially structured distributions or even fluidized beds. Most of the previous studies have concentrated on the Claus catalytic conversion reactors and the TGTU. However, some previous studies have identified the Claus furnace as one of the most important yet least understood parts of the modified Claus process. The furnace is where the combustion reaction and the initial sulfur conversion (through an endothermic gaseous reaction) take place. It is also where the SO_2 required by the downstream catalytic stages is produced and the contaminants (such as ammonia and BTX (benzene, toluene, xylene) are supposedly destroyed. The main two reactions in the Claus furnace are: $H_2S + 3/2\ O_2 = SO_2 + H_2O$, with ΔH_r= -518 kJ/mol, and $2H_2S + SO_2 = 3/2\ S_2 + 2H_2O$, with ΔH_r= +47 kJ/mol. This last endothermic reaction is responsible for up to 67% conversion of the sulfur at about 1200 °C. Moreover, many side reactions take place in the furnace; these side reactions reduce sulfur recovery and/or produce unwanted components that end up as ambient

pollutant emissions. Therefore, it would be useful to combine the endothermic and exothermic process using an isothermal reactor offered by flameless oxidation combustion.

Approach

Critical review

We propose to conduct a critical review of the various approaches used for sulfur removal from the sour gas. The emphasis here will be on sulfur chemistry with due consideration to the fate of ammonia. Following the review, an experimental and a CFD numerical study of the flameless oxidation of the fuel will be conducted as follows:

CFD simulation

A numerical simulation study of the flame under normal and flameless oxidation of fuels in the furnace will be conducted using the available codes. Global features of the flow and thermal behavior will be obtained using the Fluent CFD and Chemkin computer codes. These codes provide detailed simulation of the flow, thermal and chemical behaviors (i.e., detailed chemistry) in the reactor flow using gas-phase reactants. The sulfur in the fuel is in gas phase, so we will be able to simulate and monitor the fate of sulfur during various stages of endothermic and exothermic reactions and over a range of temperature regimes, including those covered in the Claus furnace process. The simulation results will also guide the final design of the flameless furnace. The simulations will also help assist in the experimental program for data validation with the eventual goal of implementing the process for sulfur removal.

Experimental study

An experimental study of the flameless vs. normal flame combustion process for the conditions examined in the theoretical study, including that of Claus furnace, will be conducted. We will explore the operating conditions and the exhaust gas analysis under conditions of both flame and flameless modes to determine the extent of sulfur conversion under the two conditions over the temperatures that can simulate endothermic and exothermic conditions in the Claus furnace. The goal is to seek conditions that yield the highest sulfur recovery from a process. To some extent, these conditions will be based on the composition of the acid/sour gas, from sulfur-rich (> 50% H_2S) to lean (< 20% H_2S). It is expected that our fundamental information will contribute to the eventual design guidelines of an advanced sulfur recovery process furnace operating under flameless combustion mode.

Separate Sensible and Latent Cooling with Solar Energy

UMD Investigators: Reinhard Radermacher, Yunho Hwang
GRA: Ali Al-Alili
PI Investigator: Isoroku Kubo
Start Date: August 2007

1. Objective/Abstract

The main objective of this project is to design, fabricate and test a solar cooling system with the highest possible cooling COP measured to date. The approach involves combining a very efficient concentrating PV-T collector with a separate sensible and latent cooling approach developed at CEEE. This solar cooling system is expected to operate under the UAE's harsh climate conditions.

2. Deliverables for the Completed Quarter

These are the accomplished tasks:

- Finished the refrigerant loop
- Ran a shakedown test of the complete cycle
- Installed tachometers for the sensible and desiccant wheel

3. Summary of Project Activities for the Completed Quarter

The focus of this quarter was to carry out a shakedown test of the complete experiment. Once the refrigerant loop was constructed and tested, all the sensors were connected to the DAQ, and LABVIEW was expanded. The shakedown test showed that all the temperatures and relative humidity sensors are working as expected. The test revealed some minor air leakages, which are under repair.

3.1 The refrigerant loop

The refrigerant copper lines for the sensible vapor compression cycle were cut and shaped to fit the available space. All the connections were brazed, as shown in Figure 1. A high pressure was applied to the loop using nitrogen in order to check for leaks. The leakage locations were identified using soap. Once the leaking problem was solved, the system's pressure was monitored to ensure stable pressure readings, shown in Figure 2.

Figure 1. The sensible vapor compression cycle.

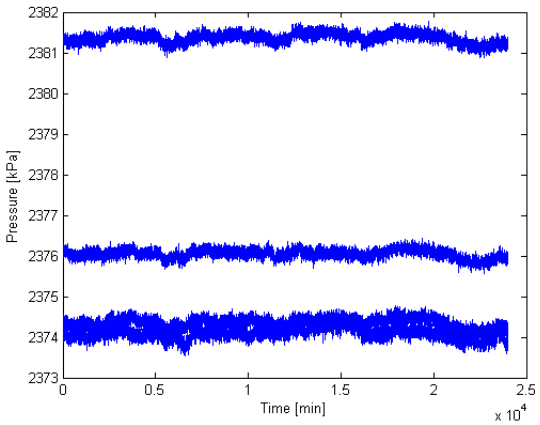

Figure 2. Pressure at different locations of the refrigerant loop.

3.2 Shakedown testing

A shakedown test was necessary to ensure that all the equipments and sensors were operating as expected. While we were carrying the shakedown test, the chamber unit started to lose pressure due to a leak in one of the valves. The process of fixing the leak started with recovering the refrigerant, replacing the valve, charging the system with nitrogen, carrying out a leakage test, applying a vacuum test, then charging the system with the appropriate refrigerant.

The chamber was maintained at constant temperature to check the temperature sensors' consistency. Figure 3 shows the temperatures at nine state points in the air-side recorded using thermocouples and RTDs. The figure shows that there are no defects in the installed sensors.

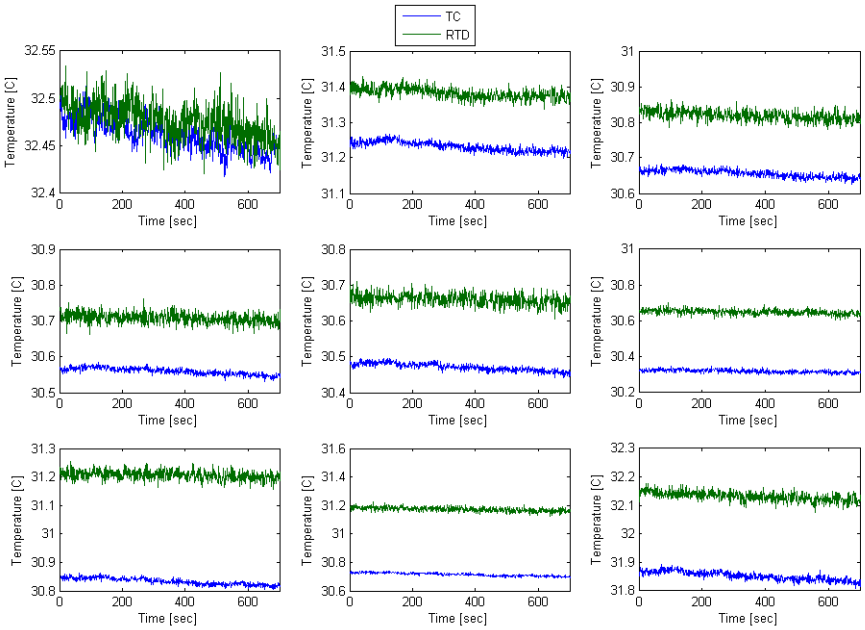

Figure 3. Thermocouples vs. RTDs at different state points.

Preliminary test results are shown in Figure 4. The figure shows the dehumidification at the desiccant wheel and the sensible cooling at the sensible wheel. It also shows the mixing before the vapor compression cycle and the sensible cooling of the vapor compression cycle.

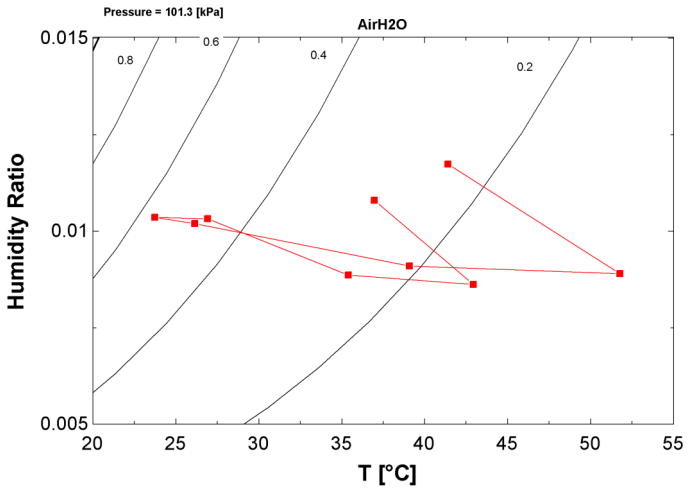

Figure 4. State points in the air-side.

3.3 Tachometers

Two tachometers were needed to record the rotational speed of the sensible and desiccant wheels. The main problem faced was that the rotational speeds were very low, lower than the lower limit of the tachometers. The problem was solved by using the rotational speed of their motors, then calculating the rotational speed of the wheels. The tachometers were installed and connected to the DAQ.

4. Difficulties Encountered/Overcome

- Fixing the chamber condensing unit
- Finding the leaks in the refrigerant loop

5. Planned Project Activities for the Next Quarter

The following activities are to be conducted in the next quarter:

- Finish the shakedown test
- Start the actual test

6. References

[1] Stine, W.B., Geyer, W.B., 2001, Power from the sun, www.powerfromthesun.net.
[2] Threlkeld,.J, Kuehn, T., Ramsy, J.,1998, Thermal Environmental Engineering, Prentice-Hall, Inc, USA
[3] http://www.nrel.gov/rredc/solar_data.html
[4] http://rredc.nrel.gov/solar/old_data/nsrdb/tmy2/State.html
[5] Notton , G. , Poggi, P. , Cristofari, C., 2006, Predicting hourly solar irradiations on inclined surfaces based on the horizontal measurements: Performances of the association of well-known mathematical models, Energy Conversion and Management, 47 1816–1829
[6] http://rredc.nrel.gov/solar/old_data/nsrdb/1991-2005/siteonthefly.cgi?id=724060
[7] ASHRAE, 1999, Applications Handbook, CH.32
[8] Kreith, F. and Kreider, J.F., 1978, Principles of solar engineering, Hemisphere publishing corporation Washington USA
[9] Kalogirou, S., 2004, Solar thermal collectors and applications, Progress in Energy and Combustion Science 30 pp. 231–295
[10] Goswami, Y., Kreith, F. and Kreider, J.F., 2000, Principles of solar engineering, Taylor and Francis, PA, USA,
[11] Duffie, J.A., Beckman, W.A., 1991, Solar engineering of thermal processes, Second edition, John Wiley & Sons, Inc., New York, ISBN: 0-471-51056-4.
[12] Pasupathy, A., Velraj, R., Seeniraj, R.V., 2008, Phase change material-based building architecture for thermal management in residential and commercial establishments, Renewable and Sustainable Energy Reviews, pp.39–64
[13] Dieng, A., Wang, R. , 2001 Literature Review on Solar Adsorption Technologies of Ice-making and Air Conditioning Purposes and Recent Developments in Solar Technology, Renewable and Sustainable Energy Reviews 5 pp.313–342
[14] Sumathy, K., Yeug, K, Yong, L., 2003, Technology Development in the Solar Adsorption Refrigeration Systems, Progress in Energy and Combustion Science 29 pp 301–327
[15] Roger, A. Messenger, J. V., 2005, Photovoltaic Systems Engineering, 2nd ed. Taylor & Francis
[16] http://www.nfpa.org/
[17] http://ieeexplore.ieee.org/iel5/7946/21930/01019771.pdf?arnumber=1019771
[18] TRANE, "Product Data: 4DCZ6036A through 4DCZ6060A" (2008), 22-1815-03
[19] METEONORM, "Global Meteorological Database for Engineers, Planners and Education,"(2007)

Waste Heat Utilization in the Petroleum Industry

UMD Investigators: Reinhard Radermacher, Yunho Hwang
GRAs: Amir Mortazavi, Abdullah Alabdulkarem
PI Investigators: Saleh Al Hashimi, Peter Rodgers
Start Date: October 2006

1. Objective/Abstract

The main objective of this project is to minimize overall energy consumption of gas or oil processing plants and reduce their CO_2 emission by utilizing waste heat and/or improving cycle design with CO_2 capture and sequestration. Consideration will include the use of absorption chillers and steam cycles, among other options.

2. Deliverables for the Completed Quarter

The following were modeled using HYSYS:

- Modeled organic Rankine cycle
- Validated organic Rankine cycle model
- Investigated turbine inlet cooling
- Optimized two configurations of gas turbine combined cycle with double-pressure steam cycle
- Optimized of two configurations of split design gas turbine triple-combined cycle with double-pressure steam cycle and absorption chillers.

3. Summary of Project Activities for the Completed Quarter

HYSYS was used to model an Organic Rankine Cycle (ORC). ORC generates power using waste heat. The ORC model was validated against experimental data with good agreement. Further, the increase in power due to turbine inlet cooling was investigated.

Two configurations each of the gas turbine combined cycle with double-pressure steam cycle and the gas turbine triple-combined cycle with double pressure steam cycle and absorption chillers were optimized as an APCI LNG plant driver cycle. The best option according to our models consumes 38.2% less fuel than the baseline cycle.

3.1 Organic Rankine Cycle Model

An ORC model was developed using HYSYS software as shown in Figure 1. The working fluid is evaporated to high temperature, e.g., 130°C, in a boiler and then expanded in a turbine. The expanded fluid then condenses in a condenser and is pumped in a pump to the pressure of the boiler. The working fluid used is R123. The developed model was validated against experimental data from Quoilin *et al.* (2007). The equation of state used in this model is the Peng-Robinson equation of state. The experimental setup is shown in Figure 2. The validation results are tabulated in Table 1.

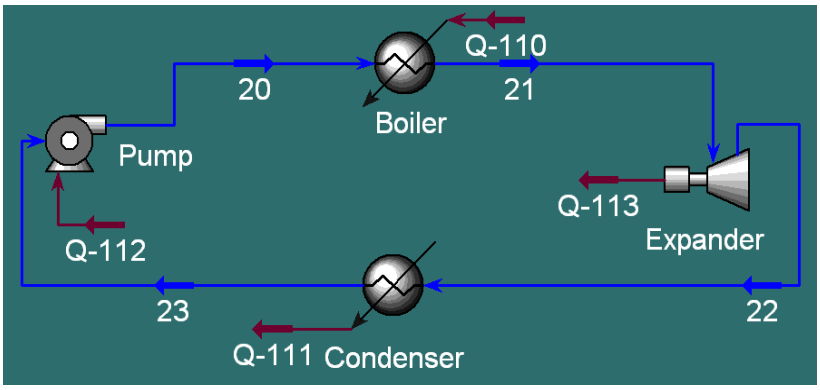

Figure 1. HYSYS organic Rankine cycle model.

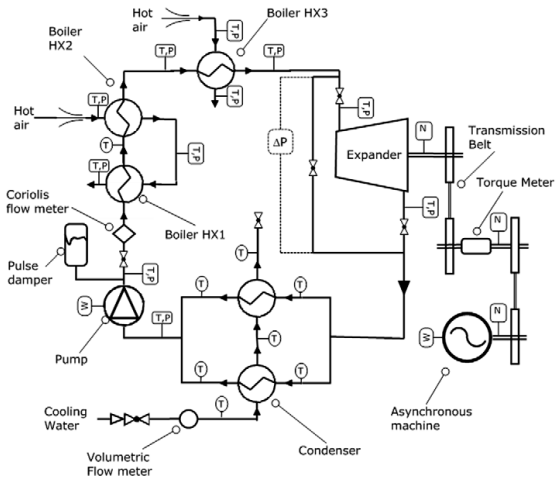

Figure 2. Organic Rankine cycle model experimental setup Quoilin *et al.* (2007).

Table 1. ORC HYSYS model validation results

	Experimental Data	HYSYS Model	Discrepancy
Temp. Inlet to Expander (°C)	131.8	131.8	-
Pressure Inlet to Expander (bar)	8.18	8.18	-
Expander Pressure Ratio	3.76	3.76	-
Pump Isentropic Eff.	0.15	0.15	-
Expander Isentropic Eff.	61.6	61.6	-
Refrigerant Flow Rate (kg/s)	0.067	0.067	-
Subcooling (K)	16.72	16.72	-
Superheating (K)	31.26	29.72	1.54 K
Expander Power (W)	1,067	1,047.7	-1.84%
Cycle Efficiency (%)	5.4	5.403	0.05%

A simple modification on the ORC can be made by introducing a recuperator heat exchanger to preheat the refrigerant before it goes to the boiler using the expanded fluid, as shown in Figure 3. Different refrigerants were explored, and the results are tabulated in Table 2.

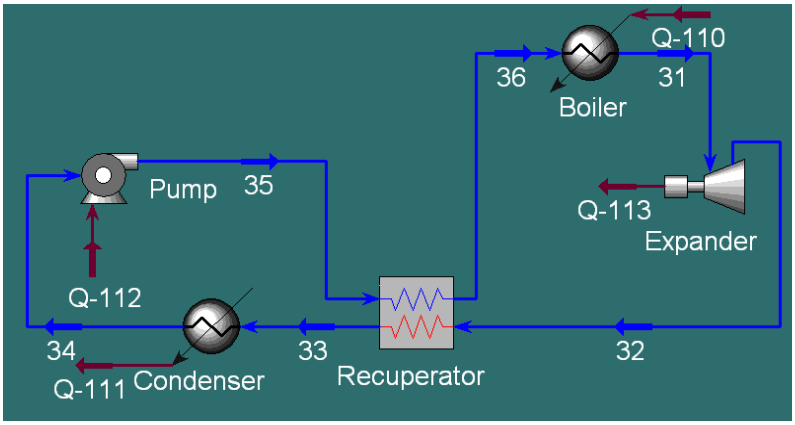

Figure 3. HYSYS Organic Rankine cycle model with a recuperator heat exchanger.

Table 2. ORC performance with different refrigerants

	Refrigerant	W_Exp (MW)	W_pump (MW)	Eff. (%)
Base case	R123	14.03	0.527	14.620
Modified case	R123	14.74	0.573	15.344
Base case	R141b	14.20	0.412	14.929
Modified case	R141b	14.65	0.447	15.381
Base case	Methanol	14.82	0.092	15.952
Modified case	Methanol	14.15	0.095	15.223
Base case	R11	14.84	0.531	15.500
Modified case	R11	14.88	0.549	15.522
Base case	R113	13.77	0.312	14.576
Modified case	R113	14.94	0.364	15.787

3.2 Turbine inlet cooling

Gas turbine power output drops when the ambient temperature increases due to lower air mass flow rate. This power drop can be prevented by employing absorption chillers that run by waste heat to cool the inlet air.

An HYSYS model for a gas turbine with inlet air cooler was used that is based on Mortazavi's *et al.* (2010) gas turbine model. The results of air inlet cooling are tabulated in Table 3 and plotted in Figure 4. As shown in Figure 4, the total combined cycle power increases from 138.189 MW at 50°C ambient temperature to 158.485 MW at 10°C, or a 14.68% increase in produced power.

Table 3. Turbine inlet cooling results

T_{air} (°C)	$Q_{cooling}$ (MW)	W_{GT} (MW)	W_{ST} (MW)	W_{Tot} (MW)	Eff
50	0	78.87	59.319	138.189	41.35%
45	1.903	80.92	59.521	140.441	41.37%
40	3.866	83.03	59.742	142.772	41.40%
35	5.89	85.21	59.963	145.173	41.42%
30	7.979	87.47	60.184	147.654	41.44%
25	10.14	89.8	60.425	150.225	41.47%
20	12.37	92.21	60.675	152.885	41.49%
15	14.67	94.7	60.935	155.635	41.51%
10	17.05	97.29	61.195	158.485	41.54%

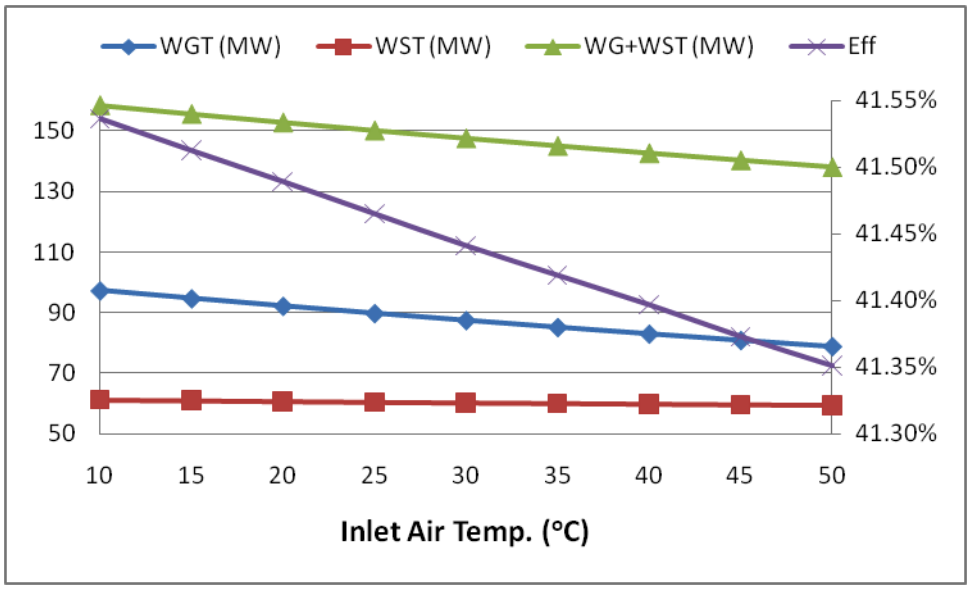

Figure 4. Turbine inlet cooling results.

3.3 Optimization of different gas turbine triple combined cycle configurations:

In order to investigate the potential of gas turbine, steam and absorption chiller combined cycles as an APCI LNG plant driver, the performance of the driver system should be optimized. Moreover, to fully appreciate the benefits of this system it should be compared to the optimized conventional technologies. Matlab software was used as an optimization tool. It was connected to HYSYS, which was used to model the driver cycles. The comparison of different driver technologies is shown in Table 3. As shown in Table 3, the most efficient driver configuration is the gas turbine double-pressure steam and single-effect water/LiBr absorption chiller triple combined cycle. This configuration has the least fuel consumption. Moreover, it maintains its advantages by varying the steam turbine efficiency and minimum exhaust temperature. Its efficiency is 38.2% higher than conventional gas turbines and 2% higher than the gas turbine and double pressure steam combined cycle with reheat drivers. Moreover, as shown in Table 3, the cycles with auxiliary burner are not more efficient than the normal cycles. However, they are not considered in double pressure cycles since optimization results showed zero fuel mass flow rate to the burner.

Table 3. Comparison of different driver cycle technologies

Steam Turbine Efficiency (%)	86	90	90	86	90	90	86	90	90
Exhaust Temperature (°C)	180	180	110	180	180	110	180	180	110
Cycle	**Fuel Consumption (kg/s)**			**Efficiency (%)**			**Efficiency Enhancement (%)**		
Base Cycle With Gas Turbine as a Driver	6.575	6.575	6.575	33.52	33.52	33.52	---	---	---
Combined Gas Turbine and Double-Effect Absorption Chiller	5.174	5.174	5.174	42.59	42.59	42.59	21.31	21.31	21.31
Combined Gas Turbine and Single-Pressure Steam Cycle	4.571	4.541	4.407	48.21	48.53	50.00	30.48	30.93	32.98
Triple Cycle with Double-Effect Absorption Chiller	4.704	4.641	4.641	46.85	47.48	47.48	28.46	29.41	29.41
Triple Cycle with Single-Effect Absorption Chiller	4.251	4.235	4.219	51.84	52.03	52.23	35.35	35.59	35.84
Split Design Triple Cycle with Double-Effect Absorption Chiller	4.581	4.556	4.556	48.10	48.37	48.37	30.33	30.71	30.71
Split Design Triple Cycle with Single-Effect Absorption Chiller	4.594	4.585	4.556	47.97	48.06	48.37	30.13	30.27	30.71
Triple Cycle with Double-Effect Absorption Chiller with Auxiliary Burner	4.704	4.641	4.641	46.85	47.48	47.48	28.46	29.41	29.41
Triple Cycle with Single-Effect Absorption Chiller Auxiliary Burner	4.251	4.235	4.219	51.84	52.03	52.23	35.35	35.59	35.84
Combined Gas Turbine and Double-Pressure Steam Cycle with Reheat	4.438	4.367	4.140	49.65	50.46	53.22	32.5	33.58	37.03
Triple Cycle with Double-Pressure Steam Double-Effect Absorption Chiller with Reheat	4.791	4.707	4.707	46	46.82	46.82	27.13	28.41	28.41
Triple Cycle with Double-Pressure Steam Single-Effect Absorption Chiller with Reheat	4.241	4.195	4.066	51.96	52.53	54.20	35.50	36.20	38.16
Split Design Triple Cycle with Double-Pressure Steam Double-Effect Absorption Chiller with Reheat	4.395	4.347	4.325	50.14	50.59	50.95	33.16	33.89	34.22
Split Design Triple Cycle with Double-Pressure Steam Single-Effect Absorption Chiller with Reheat	4.269	4.236	4.152	51.62	52.02	53.07	35.07	35.57	36.85
Combined Gas Turbine and Double-Pressure Steam Cycle without Reheat	4.571	4.541	4.407	48.21	48.53	50.00	30.48	30.93	32.98

4. Difficulties Encountered/Overcome

5. Planned Project Activities for the Next Quarter

The following activities are to be conducted in the next quarter:

- Optimization of steam cycles with steam extraction for CO_2 regeneration
- Optimization of the gas turbine, dual-pressure steam and absorption chiller triple combined-cycle split designs
- Optimization of mobile LNG plants using robust optimization

6. References

[1] Dopazo J. A., and Fernández-Seara J., 2010, "Experimental evaluation of a cascade refrigeration system prototype with CO_2 and NH_3 for freezing process applications," International Journal of Refrigeration, pp. 1-11.

[2] Venkatarathnam G., 2008, Cryogenic Mixed Refrigerant Processes, Springer-Verlag New York, LLC,.

[3] Paradowski H., Bamba M. O., and Bladanet C., 2004, "Propane Precooling Cycles for Increased LNG Train Capacity," 14th International Conference and Exhibition on Liquefied Natural Gas, pp. 1-18.

[4] Alefeld, G., Radermacher, R., 1994, "Heat conversion systems", CRC Press, Boca Raton.

[5] Al-Hamdan, Q.Z., Ebaid, M.S.Y., 2006, "Modeling and simulation of a gas turbine engine for power generation", ASME Journal of Engineering for Gas Turbines and Power, Vol. 128, pp. 302-311.

[6] LNG technology selection, http://www.fwc.com/publications/tech_papers/files/TariqLNG.pdf, Last access, June, 2008

[7] Haring, H., 2008, " Industrial Gas Processing", Wiley-VCH, Weinheim

[8] ASHRAE, 2002, "ASHRAE Refrigeration Handbook", American Society of Heating, Refrigeration and Air-Conditioning Engineers, Atlanta, GA, USA.

[9] ASHRAE, 2005, "ASHRAE Fundamentals Handbook", American Society of Heating, Refrigeration and Air-Conditioning Engineers, Atlanta, GA, USA.

[10] Brant, B., Brueske, S., Erickson, D.C., Papar, R., 1998, "New waste-heat refrigeration unit cuts flaring, reduces pollution", Oil & Gas Journal, May 18, pp.61-64.

[11] Brooks, F.J., 2000 "GE gas turbine performance characteristics", GE Power Systems Schenectady, NY, GER-3567H.

[12] Cohen, H., Rogers, G.F.C., Saravanamuttoo, H.I.H., 1996, "Gas turbine theory", 4th edition, Longman Scientific & Technical, Singapore.

[13] Erickson, D.C., 2000 "LPG recovery from reformer treat gas", US Patent 6,158,241.

[14] Erickson, D.C., Anand, G., Papar, R.A., Tang, J., 1998, "Refinery waste heat powered absorption refrigeration – cycle specification and design", Proceeding of the ASME Advanced Energy System Division, AES-Vol. 38, pp.391-402.

[15] Erickson, D.C., Kelly, F., 1998, "LPG recovery from refinery by waste heat powered absorption refrigeration", IECEC-98-079, 33rd Intersociety Engineering Conference on Energy Conversion, Colorado Springs, CO.

[16] Giampaolo, T., 2003, "The gas turbine handbook: principles and practices", 2nd edition, The Fairmont Press, Lilburn, GA.

[17] Herold, K.E.; Radermacher, R., Klein, S, 1996, "Absorption chillers and heat pumps", CRC Press, Boca Raton.

[18] Kim, T.S., Hwang, S.H., 2006, "Part load performance analysis of recuperated gas turbine considering engine configuration and operation strategy", Energy, Vol. 31, pp., 260-277.

[19] Klein, S.A., 2005, "Engineering Equation Solver" F-Chart Software.

[20] Kurz, R., 2005, "Gas turbine performance", 44th Turbomachinery Symposium, pp.131-146.

[21] Kurzke, J., 2003, “Model based gas turbine parameter corrections”, GT2003-38234, Proceedings of 2003 ASME TURBO EXPO: Power for Land, Sea, & Air, Atlanta, GA, USA.
[22] Li, Y.G., Pilidis, P., Newby, M.A., 2006, “An adaptation approach for gas turbine design-point performance simulation”, Journal of Engineering for Gas Turbines and Power, Vol. 128, pp. 789-795.
[23] Orlando, J. A., 1996, “Cogeneration design guide”, American Society of Heating, Refrigeration and Air-Conditioning Engineers, Atlanta, GA.
[24] Pande, M., 1996, “Tools for fractionator design in ammonia-water absorption machines”, Master Thesis, University of Maryland, College Park.
[25] Walsh, P.P., Fletcher, P., 1998, “Gas turbine performance”, Blackwell Science, Oxford.

Appendix

Justification and Background

Waste heat utilization opportunities are abundant in the oil and gas industry. Proper use of waste heat could result in improved cycle efficiency, reduced energy usage, reduction in CO_2 emissions, and increased production capacity.

CEEE at the University of Maryland has extensive experience in the design and implementation of integrated combined cooling, heating, and power (CCHP) projects. The faculty at PI has experience in the design and operation of petroleum processing plants. Jointly the team is well equipped to address the challenge posed by this project.

Thrust 2
Energy-Efficient Transport Processes

Multidisciplinary Design and Characterization of Polymer Composite Seawater Heat Exchanger Module

PI Investigator: Peter Rodgers
UMD Investigators: Avram Bar-Cohen, Satyandra K. Gupta, David Bigio, H.A. Bruck
GRAs: Juan Cevallos, F. Robinson, T. Hall, W. Pappas
Start Date: Oct 2006

1. Introduction

Heat exchangers are extensively used in all oil and gas processing operations with seawater as the preferred coolant in near-shore operations. The performance and cost effectiveness of conventional metallic heat exchangers in such environments are severely constrained by corrosion and scale deposits. Polymer heat exchangers, currently under investigation by the EERC team, offer a promising alternative to metallic heat exchangers for the fossil fuel industry. Recent advances in carbon-fiber polymer composites, yielding polymer materials with thermal conductivities equal to or higher than titanium, can be applied to the development of low-cost and low-weight compact heat exchangers for corrosive fluids. These attributes, combined with the low energy investment in the formation and fabrication of these polymer heat exchangers and their ease of manufacturing, appear to make near-term applications of seawater polymer heat exchangers viable. Numerical simulations and laboratory experiments, performed by the UMD/PI EERC team in the first phase of this research, strongly support these conclusions.

2. Milestones/Deliverables for the Completed Quarter

3.1 Submitted full draft for a technical paper entitled “Polymer Heat Exchangers – An Enabling Technology for Water and Energy Savings” IMECE Conference to be held on November 11-17 2011 in Denver, Colorado. (Task A2)

3.2 Manufactured several heat exchanger prototypes made of different polymers were manufactured using fused deposition modeling, which will be used at the HX test rig at the University of Maryland. (Task A1)

3.3 Developed and utilized thermomechanical finite element model to assess thermal and structural performance of polymer composite heat exchangers and assess feasibility of replacing metallic heat exchangers at the Das Island liquefied natural gas facility with polymer composite heat exchangers. (Task A2)

3.4 Developed processing methodology for comparing experimentally-measured fiber orientation to Moldflow® predictions. (Task B2)

3.5 Experimentally validated developed model simplification technique. (Task B1)

3.6 Developed a technique for characterizing mixing of polymer composites in a Twin Screw Extruder (TSE). (Task C1)

3.7 Submitted full draft for a technical paper entitled “Modeling and Validation of Prototype Thermally Enhanced Polymer Heat Exchanger” to the 2011 International Mechanical Engineering Congress & Exposition in Denver, Colorado. (Task A2)

3.8 A paper entitled “An Integrated Approach to Design of Enhanced Polymer Heat Exchangers” was accepted for publication at the Journal of Mechanical Design. (Task B1)

3.9 Submitted abstract and draft paper entitled “An Integrated Approach to Design of Enhanced Polymer Heat Exchangers” to DETC Conference to be held on August 29-31 2011 in Washington, DC. (Task A2)

3.10 Submitted abstract entitled “Polymer Heat Exchangers – An Enabling Technology for Water and Energy Savings” to IMECE Conference to be held on November 11-17 2011 in Denver, Colorado. (Task A2)

3. Summary of Project Activities for the Completed Quarter

3.1 Submitted full draft for a technical paper entitled “Polymer Heat Exchangers – An Enabling Technology for Water and Energy Savings” to IMECE Conference to be held on November 11-17 2011 in Denver, Colorado. (Task A2)

In this paper we explored the intertwined relationship between energy and water and identified the need for a novel cooling technology that reduces energy use and water demand. It was noted that implementation of PHXs could offer increased electricity output while alleviating demand for freshwater.

Three different case studies were used to present the potential energy and water savings achievable by the use of polymer heat exchangers for seawater cooling—specifically, heat exchangers made with thermally enhanced polymers. In general, an energy efficient heat exchanger requires a lightweight material with relatively good thermal conductivity and low embodied energy. Table 1 compares relevant properties of candidate materials for seawater heat exchangers.

Table 1. Thermal conductivity and embodied energy of corrosion resistant materials

Material	Density (g/cm^3)	Thermal conductivity (W/m·K)	Embodied Energy (MJ/kg)	Embodied Energy (GJ/m^3)
Unfilled polymer	1.20	0.25	24	29
Low-k composite	1.49	5	145	216
Medium-k composite	1.65	10	187	309
High-k composite	1.79	20	219	392
Titanium	4.50	20	1000	4500
Copper-nickel	8.90	45	72	641
Aluminum Alloy 5052	2.68	138	306	820

Case Study 1: Liquefaction of natural gas using seawater. The overall energy expenditures related to a 1MW methane cooler were compared for all materials by taking into account the embodied energy and the energy required to pump both fluids, as shown in Figure 1, for a heat exchanger life of 10 years. The values in the plot reveal that the high-k composite requires the least amount of energy, followed by copper-nickel, aluminum, and the other enhanced polymers. Titanium and the unfilled polymer require the most energy of the six materials.

Even with a ten-year life, most of the energy used by a titanium heat exchanger (70%) is related to the material’s embodied energy. A 1MW-heat exchanger using an enhanced polymer composite with a thermal conductivity of 20 W/mK uses around 6.5 TJ less than a titanium heat exchanger; even a composite with one fourth of the conductivity of titanium uses 6.2 TJ less. A copper-nickel alloy uses 240 GJ more than a high-k composite, and 170 GJ more than a medium-

k polymer composite. An aluminum alloy uses 420 GJ more than a high-k composite, and 340 GJ more than a medium-k polymer composite.

Finally, a methane cooler requires 124 billion kilograms (roughly 125 billion liters) of water a year. If seawater is used instead of freshwater, the reduction in freshwater withdrawals can be significant given that a heat exchanger of only 1 MW requires such large amounts of water.

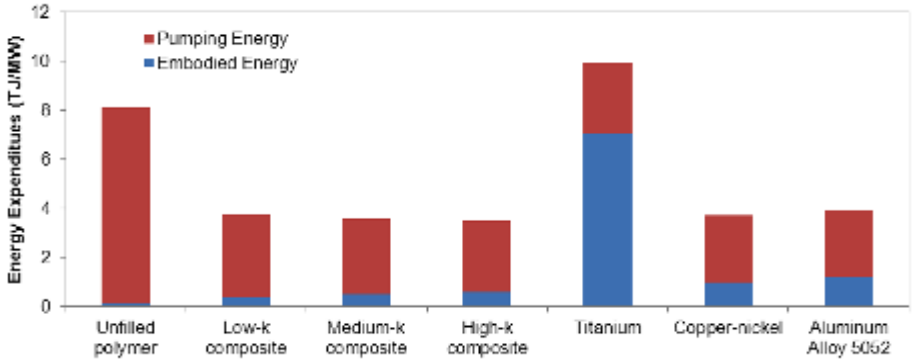

Figure 1. Energy expenditures of a 1MW methane cooler for a 10-year life (L=W=1m, t_b=t=2mm, H=10mm, 20 water-side fins, 80 air-side fins, $m_{methane}$=0.1kg/s, $m_{seawater}$=15kg/s, $T_{methane,inlet}$=60C, $T_{water,inlet}$=35C).

Case Study 2: Water-to-seawater heat exchanger. The overall energy expenditure of a 1MW-heat exchanger was compared for all materials, as shown in Figure 2. The enhanced composites were again the most energy efficient, followed by copper-nickel. In this case, the low-k polymer is the better of the composites instead of the high-k polymer in Case Study 1. The marginal improvements in heat transfer rate provided by the medium-k and high-k composites are offset by the increase in embodied energy due to the higher carbon-fiber fraction.

Over a life of 10 years, a 1MW-heat exchanger using an enhanced polymer composite with a thermal conductivity of 5 W/mK uses 7.5 TJ less than a titanium heat exchanger, while a composite with a conductivity of 20 W/mK uses 7.3 TJ less than titanium. A copper-nickel alloy uses 600 GJ more than a low-k composite, and 415 GJ more than a high-k polymer composite. An aluminum alloy uses 900 GJ more than a low-k composite, and 720 GJ more than a high-k polymer composite.

Finally, a 1MW water-to-seawater exchanger requires 142 billion kilograms (roughly 143 billion liters) of seawater in a year. If freshwater were used as a coolant instead of seawater, the increase in freshwater withdrawals would be significant.

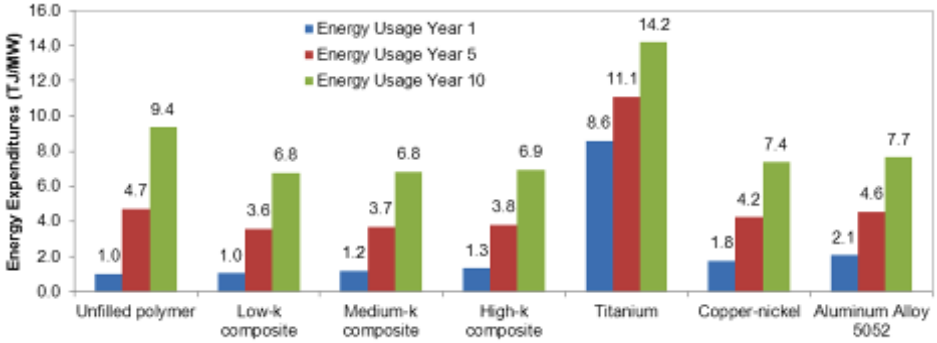

Figure 2. Overall energy expenditures of a 1MW water-to-seawater heat exchanger (L=W=1m, t_b=t=2mm, H=10mm, 20 water-side fins, 20 seawater-side fins, m_{water}=15kg/s, $m_{seawater}$=15kg/s, $T_{seawater,inlet}$=90C, $T_{water,inlet}$=35C).

Case Study 3: Ocean Thermal Energy Conversion (OTEC). Figure 3 shows the energy expenditures of a 2MW ammonia evaporator for materials compatible with OTEC. The aluminum alloy uses significantly less energy than every other material. The high-k composite follows as the second most energy-efficient material. The increase of embodied energy with respect to the other composites is offset by the significantly improved thermal performance. The overall energy expenditures reveal just how critical the thermal conductivity is for an OTEC application. When the composite conductivity is only 5 W/mK, the extra pumping power needed to provide 2MW of heat duty is such that over ten years, the heat exchanger requires 300 GJ more than a titanium heat exchanger, even when the embodied energy of titanium is almost seven times higher. On the other hand, an HX made with a high-k composite requires 4.4 TJ less than if titanium were used.

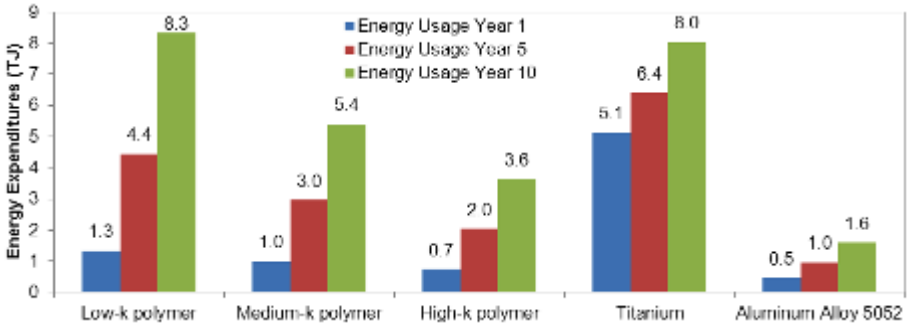

Figure 3. Overall energy expenditures of a 2MW ammonia evaporator (Seawater: 0.2 m^3/s, T_{inlet}=26 C, ammonia: 0.0016 m^3/s, T_{inlet}=17 C).

3.2 Manufactured several heat exchanger prototypes made of different polymers were manufactured using fused deposition modeling, which will be used at the HX test rig at the University of Maryland. (Task A1).

Three heat exchangers (HX) were built using fused deposition modeling. The candidate materials chosen were polycarbonate, polyetherimide (ULTEM), and a filled polycarbonate resin with enhanced thermal conductivity.

The geometry chosen for these HX was the webbed-tube heat exchanger that was discussed in previous progress reports. Figure 4 shows a 3D sketch of the heat exchanger, while Figure 5 shows dimensions of the same WTHX.

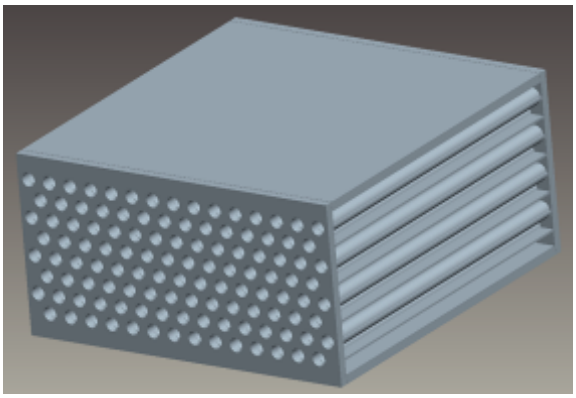

Figure 4. 3D Sketch of WTHX.

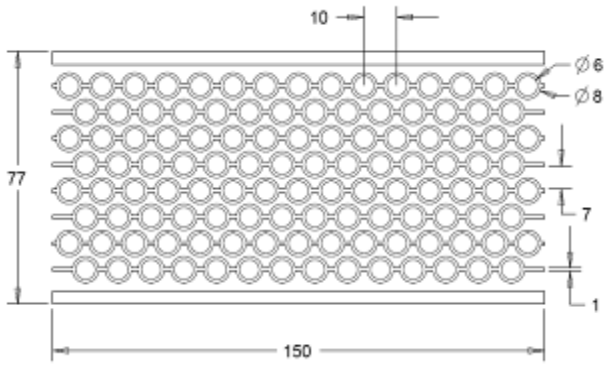

Figure 5 WTHX dimensions in mm.

The layer-by-layer deposition process has some restrictions with respect to the orientation in which the part is built. Specifically, the support material cannot be trapped inside a cavity. With this in mind, the direction of layer addition was aligned with the water tubes axes, i.e., the direction perpendicular to plane shown in Figure 5.

In addition to the build orientation, some features were added to the geometry to avoid using any support material. The features included 45° cones around the tube walls (shown in Figure 6), and 45° inside-chamfers at the intersection of the vertical walls and the ceiling. The purpose of these features was to create a structure that could be built without support material and would support the tube sheet on top of the exchanger (see the front face of the HX in Figure 4). The resulting structure is shown in Figure 7 below.

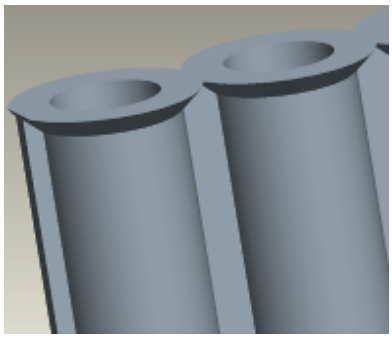

Figure 6. 45° cones around tube wall.

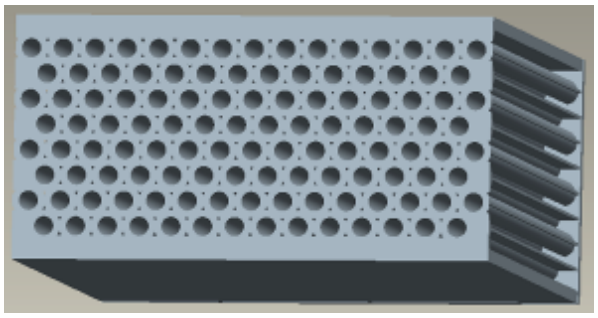

Figure 7. Supporting surface for tube.

3.3 Developed and utilized thermomechanical finite element model to assess thermal and structural performance of polymer composite heat exchanger and assess feasibility of replacing metallic heat exchangers at the Das Island liquefied natural gas facility with polymer composite heat exchangers (PCHXs)

Structural analysis was performed under combined pressure and convection loading to assess the effects of anisotropic thermomechanical properties on the stress distributions in the heat exchanger. Analysis was completed using a water flowrate of 60 cm^3/s, inlet temperature of 15°C and pressure of 500 kPa. The air flowrate was 3000 cm^3/s, the pressure was 500 kPa or 5000 kPa and the inlet temperature was 50°C or 150°C. The maximum stresses resulting from thermomechanical loading of the PCHX are shown in Figure 8.

The results show that stress development from thermal loading is more sensitive to material discontinuities, such as those that occur at the juncture between fins and plates as shown in

Figure 9. This result is evident in the large stress magnitudes for the combined loading scenarios when the inlet air temperature was 150°C. The stresses developing from application of pressure loads only and from the combined application of pressure loads and convection from air with a modest inlet temperature of 50°C were much smaller in magnitude than those that developed from the combined application of pressure loads and convection from air with an inlet temperature of 150°C. For example, in the y-direction, when the air pressure was 500 kPa, the increase in stress magnitude relative to structural only loading for combined loading with an inlet temperature of 50°C was 1.9%; the increase was 302% for an inlet temperature of 150°C.

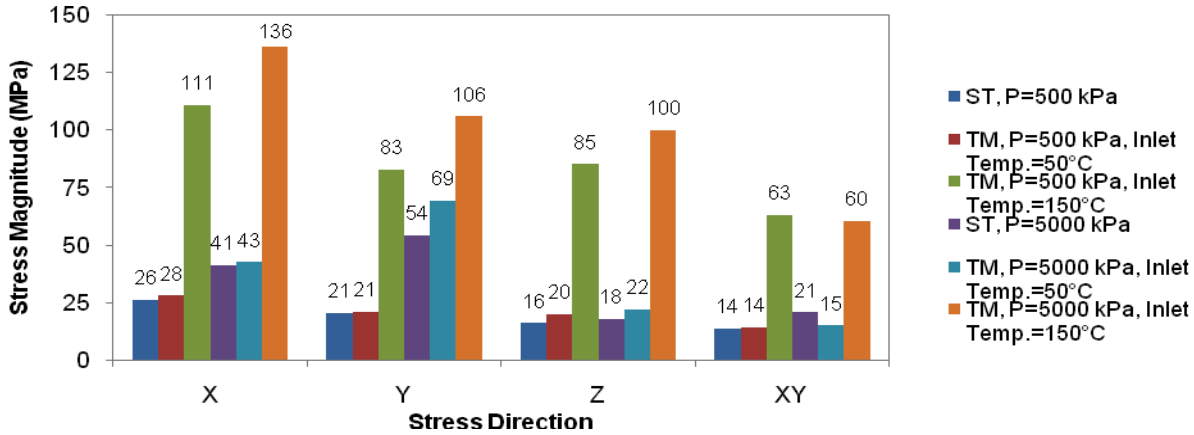

Figure 8. Maximum stress development from thermomechanical loading of PCHX (ST: structural only loading. TM: thermomechanical loading).

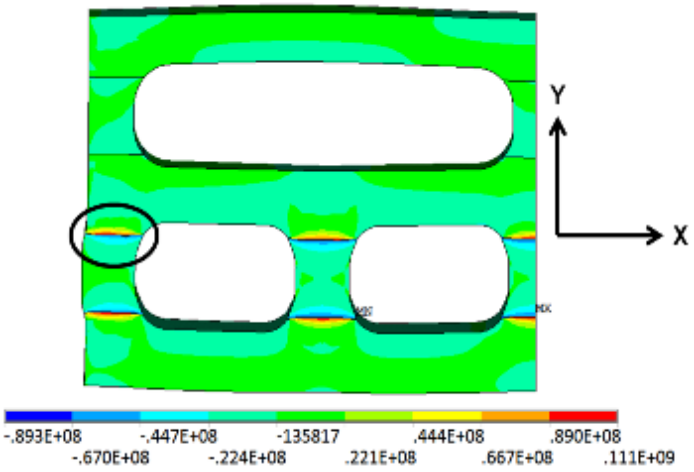

Figure 9. Y-direction stresses under combined loading for (units: Pa).

Relative to the stresses seen in the high temperature scenarios (150°C airside inlet temperature), the increase in airside pressure from 500 kPa to 5000 kPa had modest effects on stress development. The biggest discrepancy in stress magnitude occurred in the x- and y-directions, where the stresses increased by 57% and 164%, respectively. Nonetheless, the structural only y-direction stress magnitude for an airside pressure of 5000 kPa was only 51% of the y-direction stress magnitude for combined loading with an airside pressure of 5000 kPa and inlet temperature of 150°C.

Please note that the current model provides the most extreme anisotropy for the current geometry. Injection molding of PCHXs will generate gradual transitions in material properties as the flow front advances through the mold cavity, which means that the stress development at the juncture between fins and plants will be less significant. Regardless, the discontinuous

thermomechanical properties must be carefully considered to ensure that stress development between adjacent regions with significantly different fiber orientations does not cause failure of PCHXs.

3.4 Developed processing methodology for comparing experimentally-measured fiber orientation to Moldflow® predictions.

Motivation: With the image processing technique for extracting fiber information from experimental images complete, a processing methodology for comparing these values to Moldflow® predictions is required.

Action Plan: Fiber orientation tensor values are calculated based on measured fiber geometry within a varying region size and compared directly to predicted tensor values from Moldflow®.

Findings: For each found fiber, the geometric parameters used for calculating tensor values, including the length of the minor and major axes, m and M, respectively, are determined using Equation (1) based on the fiber cross-section shown in Figure 10.

$$m = \sqrt{(x_3 - x_4)^2 + (y_3 - y_4)^2}$$

$$X = x_2 - x_1, Y = y_2 - y_1 \quad (1)$$

$$M = \sqrt{(x_2 - x_1)^2 + (y_2 - y_1)^2}$$

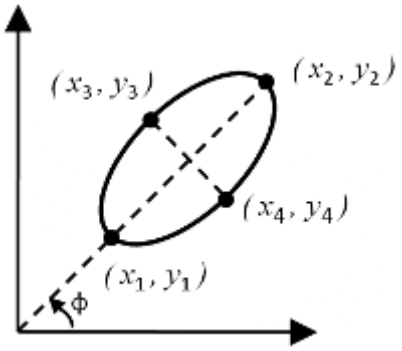

Figure 10. Elliptical fiber cross-section for determining orientation.

Based on the geometric parameters for each fiber within a defined region, the tensor components are found using Equation (2), Equation (3), and Table 12. Equation 2 represents the overall tensor component for the region and represents the tensor component for the *n*th fiber, shown in Table 1. Table 2 is a weighting function used to cope with the biasing that can occur due to fibers lying predominantly perpendicular to the sample section being more likely to appear in the specified region.

$$a_{ij} = \frac{\Sigma(a_{ij})_n F_n}{\Sigma F_n} \quad (2)$$

$$F_n = \frac{M_n}{m_n} \quad (3)$$

Table 2. Tensor components for a single fiber

Tensor component for *n*th fiber	Representation with measured geometrical parameters
$(a_{11})_n$	$X^2\left(\frac{1}{M^2}-\frac{m^2}{M^4}\right)$
$(a_{12})_n=(a_{21})_n$	$XY\left(\frac{1}{M^2}-\frac{m^2}{M^4}\right)$
$(a_{13})_n=(a_{31})_n$	$X\sqrt{\frac{m^2}{M^4}-\frac{m^4}{M^6}}$
$(a_{22})_n$	$Y^2\left(\frac{1}{M^2}-\frac{m^2}{M^4}\right)$
$(a_{23})_n=(a_{32})_n$	$Y\sqrt{\frac{m^2}{M^4}-\frac{m^4}{M^6}}$
$(a_{33})_n$	$\frac{m^2}{M^2}$

By designing the algorithm to use a variable tensor calculation region size, the resolution of the results can be tailored to develop a more local or global understanding of the fiber orientation in the test sample. This can be used to form a more in-depth comparison with predicted results that provide an overall understanding of how the fiber orientation changes in the sample as well as a granular measurement of the accuracy of the Moldflow® predictions.

With the experimental tensor components calculated for the test sample, a method of representing the results was required. Predicted tensor values were plotted across the test geometry in Moldflow® and were sampled at the corresponding tensor regions to determine an explicit value for comparison for each region. The tensor values, measured from 0 to 1, were compared using Equation (4), where 0 represents exact agreement between the experimental and predicted tensor value and 1 represents complete disagreement. These values are represented in a figure of the test geometry with cells varying from white to black to represent the difference values 0 to 1, respectively. An example comparison image, representing the tensor component for an L-channel geometry, is shown in Figure 11.

$$Diff_{ij} = \left|a_{ij,measured} - a_{ij,predicted}\right| \quad (4)$$

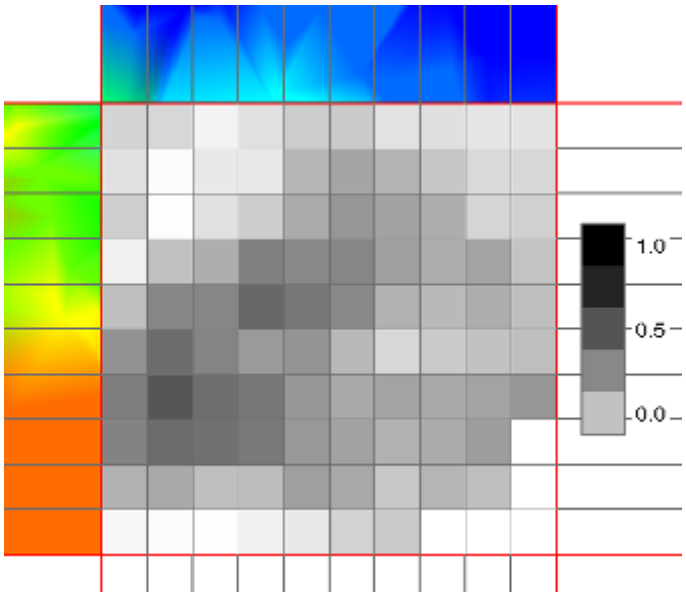

Figure 11. Example comparison between experimental and predicted tensor values.

3.5 Experimentally validated developed model simplification technique

Motivation: A filling-based model simplification technique was developed previously for a single-fin plate geometry. While this method was shown to have good agreement with test geometry, it must be validated for more diverse sample geometries.

Action Plan: A set of randomly-generated finned-plate designs over a range of fin volume concentrations was examined to evaluate the utility of the developed method.

Findings: Randomly generated finned-plate designs were created using the design criteria shown in Table 3, and an example design is displayed in Figure 12. Four sets of five designs were created at varying fin volume concentrations that fell generally into the following categories: 5%, 10%, 20%, > 20%.

Table 3. Design criteria for randomly generated finned-plate designs

Design Criteria	
Parameter	**Value (mm)**
Base Diameter	1000
Base Thickness	2
Fin Width	1-10
Fin Height	10
Fin Length	> 10
Fin Spacing	> 2

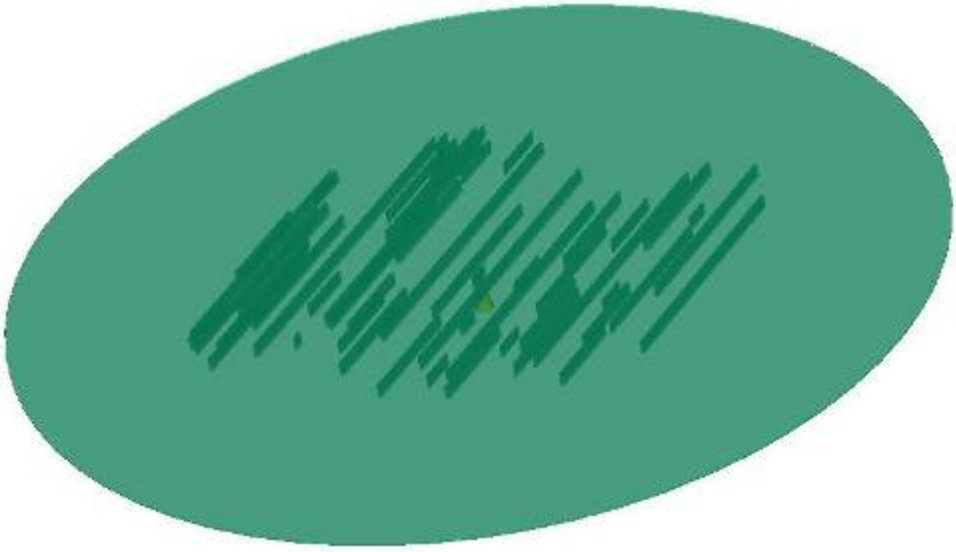

Figure 12. Example design of a randomly-generated finned-plate.

The 20 test designs were simulated in Moldflow® and the results were used in the application of the model simplification technique. Figure 13 shows the relationship between the fin volume concentration and the percent error between the model simplification prediction for mold filling and the Moldflow® results.

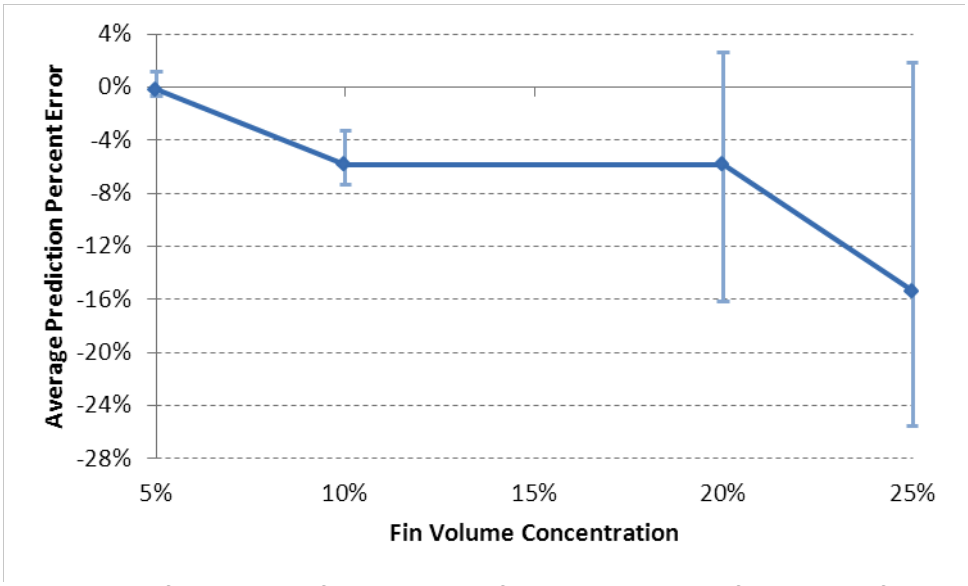

Figure 13. Plot of accuracy of model simplification technique for varying fin volume concentration.

Based on the findings of the 20 test designs, this model simplification technique shows minimal error for geometries with fin volume concentrations less than 10% and is applicable for geometries with up to 20% fins by volume. The large average error and deviation above fin volume concentrations of 20% demonstrate the limits of this simplification method, as the mold filling behavior in the fins begins to dominate the overall filling behavior of the geometry.

3.6 Developed a technique for characterizing mixing of polymer composites in a TSE

Motivation: Mixing of polymer composites is being conducted to enhance mechanical and

thermal properties. We are determining whether specific throughput and screw speed have any effect on the structure and properties of the composites. The overall goal is to determine how to process polymer composites that will meet the mechanical and thermal demands of the polymer heat exchanger.

Action Plan: The factors we have been investigating are connected with the operation of the twin-screw extruder (TSE) that will be used to produce the polymer composite material. These factors include the specific throughput (percentage of the screw channels that are full of melted polymer) and the operating conditions of the extruder (screw speed and throughput). In a previous study done using micro-sized stress beads that break at a specific critical stress, it was found that both specific throughput and operating conditions have an impact on the amount of stress that is induced on the polymer. The more stress that can be produced by the extruder on the polymer melt, the better the mixing of the polymer and any filler that may be added. Composites that have the fillers uniformly distributed as a result of being well mixed will have reduced amounts of voids and be less anisotropic resulting in enhanced thermal and mechanical properties

Findings: We created the experimental grid that would provide the operating conditions for the experiments. This was done by continuously varying the polymer flow rate and extruder screw speed until the maximum torque limit was reached. Polybutylene Terephtalate (PBT) was provided by PolyOne Corporation in Ohio as the base polymer for experimentation. The experimental grid with the operating conditions can be seen in Figure 14.

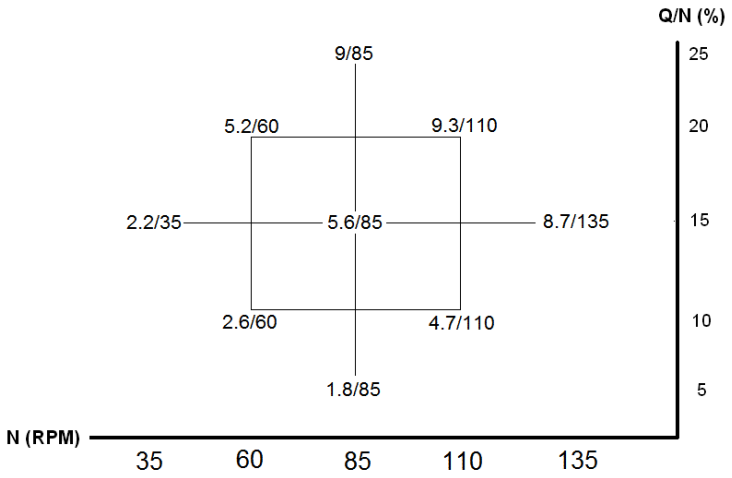

Figure 14. Experimental grid with operating conditions.

The range of the operating conditions in Figure 14 was determined by the capabilities of the extruder. The first number in the represents the throughput in lb/hr, and the second number represents the extruder screw speed in RPM. Due to the expected non-linear relationship between the operating conditions and the mechanical properties of the polymer composites, a central composite design of the experimental grid was selected. This will enable an equation to be developed relating properties and processing conditions.

The initial experiments that were performed were to create sample composite strips using PBT and micro-fillers. This was done by first setting the extruder barrels to 490°F and the die to 480°F and the extruder to the desired screw speed. Three operating conditions were used: 2.2/35, 5.2/60, 4.7/110. These three were chosen because each consisted of a different screw speed and also were on different levels of Q/N (specific throughput). The PBT was then fed into the extruder at the specific rate of the operating condition. The micro-fibers were then fed into the extruder using a second feeder, but at a location closer to the die than that of where the PBT pellets were fed. The micro-fiber used has a diameter of 7 microns and was provided by Toho

Tenax American, Inc. in Tennessee. Three different feed rates of the micro-fiber were used to produce composites consisting of 5, 15, and 25 wt. % of micro-fiber. In total, 9 composite samples were successfully produced from the TSE.

Mechanical and thermal tests will be performed on each of the samples to determine their properties. Some specific tests that will be performed are:

- Strength
- Fatigue
- Toughness
- Elasticity
- Ductility
- Thermal conductivity
- Moisture absorbtion

The samples were sent to Polyone to perform the testing. Some testing will be performed at the University of Maryland as well. Based on the results of these tests, future work that is to be performed has been provided.

4. Difficulties Encountered/Overcome

None.

5. Planned Project Activities for the Next Quarter

- Test prototypes of new candidate PHX design in upgraded experimental test rig.
- Complete research activities for mold filling metamodel, experimental fiber orientation analysis, and model simplification studies.
- Complete thesis on the manufacturability of thermally-enhanced polymer composite heat exchangers.
- Vary geometric parameters (e.g., number of gas side fins, number of waterside fins, fin height, fin thickness, plate thickness) to assess their effect on stress and temperature distributions of orthotropic heat exchanger models.
- Utilize injection mold filling software to approximate full anisotropic structural and thermal material properties and compare the results of this anisotropic model with those of the orthotropic model to ensure similitude.
- The next step for the mixing work is to perform mechanical and thermal testing on the samples that have been produced. The processed samples will be injection molded into dog-bone specimens and mechanical tests can be performed. Additionally, optical and scanning electron microscopy will be used to look at the samples to investigate for any voids or agglomerates in the samples, which will provide insight into the effectiveness of the mixing done by the TSE.
- 5, 15, 25 wt. % composites will be prepared for the mixing work using other operating conditions on the experimental grid and perform mechanical tests will be performed again. Microscopy images of the samples will be looked at to determine how well the fibers are being mixed into the samples.

6. References

[1] Bar-Cohen, A., Luckow, P., Cevallos, J.G., Gupta, S.K., 2010, Thermal Anisotropy in Injection Molded Polymer Composite Fins, International Heat Transfer Conference 14 at Washington DC

[2] Cevallos, J.G., Gupta, S.K., Bar-Cohen, A., Incorporating Moldability Considerations during the Design of Thermally Enhanced Polymer Heat Exchangers (under revisions)

[3] Cevallos, J.G., Bar-Cohen, A., Bergles, A.E., Gupta, S.K., Rodgers, P., Polymer Heat Exchangers – History, Opportunities, and Challenges (in progress)
[4] Luckow, P., A. Bar-Cohen, P. Rodgers, 2009, "Minimum Mass Polymer Seawater Heat Exchanger for LNG Applications," accepted for publication, ASME TSEA, January 2010
[5] Cox, H.L., 1951, "The elasticity and strength of paper and other fibrous materials," Brit. J. Appl. Phys., 3(3), pp. 72-79.
[6] Amado-Becker, A., Ramos-Grez, J., Yanez, M.J., Vargas, Y., and Gaete, L., 2008, "Elastic tensor stiffness coefficients for SLS Nylon 12 under different degrees of desensification as measured by ultrasonic technique," Rapid Proto. J., 14(5), pp. 260-270.
[7] Halpin, J.C., and Kardos, J.L., 1976, "The Halpin-Tsai Equations: A Review," J. Poly. Eng. and Sci., 16(5), pp. 344-352.
[8] Hahn, H.T., and Tsai, S.W., 1980, Introduction to Composite Materials, Technomic Publishing Co., Lancaster, PA.
[9] Pegoretti, A., Fambri, L., Zappini, G., and Bianchetti, M., 2001, "Finite element analysis of a glass fibre reinforced composite endodontic post," Biomaterials, 23, pp. 2667-2682.
[10] Fu, S., and Lauke, B., 1997, "The elastic modulus of misaligned short-fiber-reinforced polymers," Comp. Sci. and Tech., 58, pp. 389-400.
[11] Foye, R.L., 1972, "The Transverse Poisson's Ratio of Composites," J. Comp. Mater., 6(2), pp. 293-295.
[12] "Thermal Graph DKD," Cytec Industries, Accessed 26 May 2010, http://www.cytec.com/engineered-materials/products/cfThermalGraphDKDX.htm.
[13] Robinson, F., Bruck, H., Gupta, S.K., and Bar-Cohen, A., 2010, "Saltwater Hygrothermal Aging Studies of Short Carbon Fiber Reinforced Polyamide 12," ASME International Mechanical Engineering Congress & Exposition, Vancouver, British Columbia, Canada, November 12-18, 2010.

Appendix

Goals

The goal of the proposed 3-year EERC II polymer composite heat exchanger (PCHX) project is to develop the science and technology needed to underpin the systematic design of polymer-fiber composite heat exchanger modules that address the needs of the fossil fuel industry. The project team, lead by A. Bar-Cohen, brings together expertise in thermal science and technology (Bar-Cohen, Rodgers) with polymer composite molding and manufacturing (Gupta, Bigio). Design studies and molding simulations, as well as fabrication and testing of laboratory-scale polymer composite heat exchangers, during the first phase of this project, have provided the foundation for aggressive pursuit of such polymer composite heat exchangers.

Successful development of cost-effective, high-performance PCHX's will require a detailed understanding of the limitations imposed on the thermal performance, mechanical integrity, and cost of such heat exchange devices by the candidate polymer material; carbon fiber geometry, orientation, and concentration; thermal and mechanical anisotropy of the polymer-fiber composite; molding processes; thermal and structural failure mechanisms in the molded heat exchanger; and the energy investment in the fabrication and formation of the heat exchangers. The development and experimental as well as numerical validation of a multi-disciplinary computerized design methodology, along with the fabrication and testing of scaled polymer heat exchanger modules, would provide a unique knowledge-base from which low-life-cycle-cost heat exchange systems for the petroleum and gas industries could be developed.

Project Tasks

A. Thermal Design and Characterization of Polymer Composite Heat Exchanger Module
(Prof. Avram Bar-Cohen - UMD, Prof. Peter Rodgers - PI)

1. ***Design and thermofluid evaluation of PHX concepts for LNG applications***, including sensitivity of thermal performance to key parameters, quantification of primary thermal and exergy figures-of-merit (metrics), comparison to conventional heat exchangers, and identification of least-mass/least-energy designs;

2. ***Detailed design, fabrication, and thermal characterization of least-energy PCHX module***, including mold fabrication for most promising design, assembly and instrumentation of laboratory prototype, analysis of thermal and structural performance under simulated LNG processing conditions;

3. ***Development of predictive models for anisotropic heat exchanger modules***, including use of molding CFD software for prediction of fiber orientation and effective thermal/ structural properties, numerical and analytical models for molded anisotropic fins, derivation of least-material anisotropic fin equations, determination of heat flow sensitivity to fiber geometry/concentration/orientation;

4. ***Evaluation of convective enhancement features in molded channels***, including identification of "best practices" in conventional heat exchangers, manufacturability analysis of candidate features with attention to mold complexity, part ejection, and warpage, polymer composite molding of 3-5 candidate enhanced channels; thermofluid characterization of candidate enhanced channels under simulated LNG processing conditions; and

5. ***Determination of seawater effects on polymer composite finned plates***, including design and molding of test samples, immersion in saltwater tanks at different temperatures and concentrations for pre-determined periods, surface/bulk imaging and mechanical characterization before and after immersion, analysis and correlation of effects.

B. Manufacturability Analysis and Mold Design for Polymer Composite Heat Exchanger Module (Prof. SK Gupta – UMD):

1. *Development of an improved meta-model for mold filling predictions*: We plan to develop an improved meta-model for predicting mold filling for typical heat exchanger geometries. This meta-model will account for multiple gates with adjustable spacing. The data for developing this meta-model will be generated using mold flow simulations. We plan to utilize radial basis function based meta-models to provide the right balance of accuracy and computational speed.

2 *Creation of a computational framework for gate placement to optimize fiber orientation*: We plan to develop a computational framework for placing gates to optimize the fiber orientation, utilizing simulated fiber orientations to select the gates. The sensitivity of the gate locations on fiber orientation will be developed. Gradient-based optimization techniques will be used to optimize the fiber orientation. The optimization problem will incorporate the constraint satisfaction formulation of the weld-line locations to ensure that the fiber orientation formulation produces acceptable weld-lines.

3. *Generation of insert molding process models to incorporate connectors at the weld-lines*: In order to ensure that the weld lines do not compromise the structural integrity, we plan to embed metal connectors at the expected weld-lines locations. In order to accurately place these metal connectors in the structures, we plan to develop process models of the insert molding process and mold design templates for performing insert molding.

C. Polymer-Fiber Interactions in Polymer Composite Heat Exchanger Modules (Prof. David Bigio):

1. ***Develop key relationships for the dependence of fiber orientation on the flow geometry of the finned-plate PCHX module,*** in commercially available polymer composites, including the effect of carbon fiber length and diameter, for high and low fiber concentrations, for both base plate and fin passages in the mold, and the effect of fiber orientation/distribution on thermo-mechanical properties, verify relationships with suitable small scale experiments;

2. ***Determine achievable thermo-mechanical property enhancement*** through control of carbon fiber orientation, in the commercially available polymer composites, with attention to flow regimes, mixing processes in the flow of the melt, and heat exchanger module design, and verify experimentally;

3. ***Explore optimization of PCHX polymer composite properties through the creation of novel polymer composite compositions***, including multi-scale filler geometries, develop the molding methods for the desired geometries, create the novel composites and experimentally verify improved thermo-mechanical polymer composite properties.

Study on Microchannel-Based Absorber/Stripper and Electrostatic Precipitators for CO_2 Separation from Flue Gas

UMD Investigators: S. Dessiatoun, A. Shooshtari, M. Ohadi
GRAs: Arndt-Magnus Herzog
PI Investigators: M. Alshehhi, E. Al-Hajri, A. Goharzadeh
Start Date: Oct 2006

1. Objective/Abstract

This project is focused on research leading to the development of a high-efficiency CO_2 separation mechanism with application to a diverse range of processes in the oil and gas industry, including CO_2 separation separation/injection in petrochemical and refining processes, gas sweetening, and CO_2 capture for enhanced oil recovery applications.

The removal of acidic gases such as carbon dioxide from gas streams is an important process in the natural gas industry. In gas sweetening at least 4% by volume of raw natural gas consists of CO_2 which needs to be lowered to 2% to prevent pipeline corrosion, to avoid excess energy for transport, and to increase heating value. The separation of CO_2 from flue gases and its use for enhanced oil recovery and CO_2 sequestration applications is an increasing area of importance, as evidenced by the large investments in this area by ADNOC and its group companies, as well as affiliated government agencies in Abu Dhabi. A typical CO_2 separation process involves three stages: cooling down the flue gas; separating the solid particles and condensed water droplets; and finally capturing the CO_2 using the absorption process. The microchannel-based CO_2 separator being developed in this project, will significantly increase controllability of the thermal state of the reaction and the efficiency of the separation process while decreasing the reaction time and energy consumption, as well as potential substantial reduction of equipment footprint and the associated capital investment.

Flue gas also usually contains many contaminants in solid and liquid forms, the bulk of which are separated in gravity and inertia-driven feed gas separators. However, fine particles are carried on with the flow and can damage compressors, contaminate the gas absorption process, and reduce the quality of gas products. Electrostatic separation is one of the most effective techniques for separation of such particles and will be used in this project. The present project will address separation of droplets and particles using an EHD gas-liquid separation technique to remove liquid particles suspended in a moving gaseous medium, followed by the proposed micro channel-based separation of the CO_2 from the stream once the fine particles in the flow have been removed.

The project is being conducted jointly by the team at UMD and at PI. The team at PI is focusing on EHD separation process and absorption modeling, while the team at UMD has focused on the experimental work utilizing microchannel-based CO_2 separation and the absorption solution.

2. Executive Summary of Accomplishments in the Current Reporting Period

During this reporting period additional in-depth study of the processes and analysis of our experimental results contributed to our collective enhanced understanding of the physics and reaction kinetics. The team effort advanced on two fronts, mathematical modeling and experimental study. The main focus of the collaborators at the Petroleum Institute has been in mathematical modeling of the absorption process in microchannels, and during this period the team focused on implementing the chemical absorption into computational model, which is still ongoing. The focus of collaborators at UMD has been on the experimental study of the process

and visualization study of the absorption of CO_2 in microchannels. During this period, new sets of data on effect of diameter on the rate of absorption were collected. The results successfully demonstrated that reduction of diameter and miniaturization enhances the absorption rate. Some of the major results collected in this period and the outline of the future work are presented in the current report. In this reporting period, the collaborators from the PI and UMD continued on joint review of the project progress and milestones and sharing idea through weekly video conferences and exchange of emails.

3. Milestones/Deliverables for the Completed Quarter

- Improvement of experimental setup
- Experimental study of absorption of CO_2 in a single microchannel reactor for various diameters
- Design/fabrication of a second-generation laboratory-scale microchannel CO_2 separator

4. Summary of Project Activities for the Completed Quarter

Experimental setups

The entire experimental setup is presented in Figure 1. The syringe pump drives a precise amount of DEA solution to the microchannel reactor. The CO_2 gas is derived by pressurized gas cylinder. The flow rate, temperature and pressure of the flowing gas is measured by the laminar-based gas flow meter. The flow rate of the gas is adjusted manually via a needle valve (not shown in this figure).

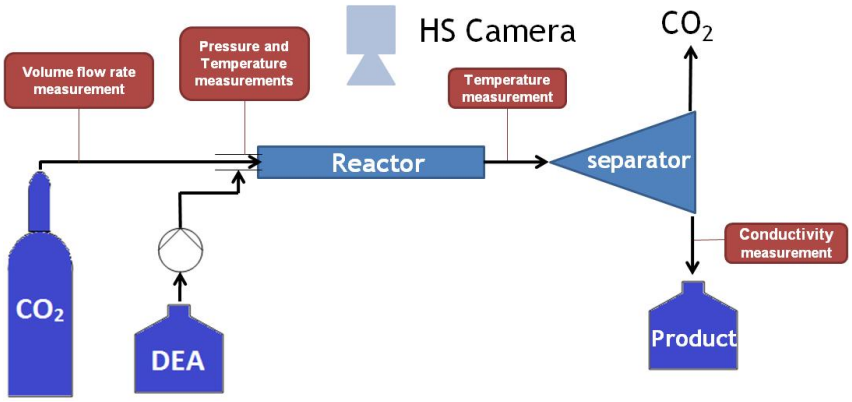

Figure 1. Experimental setup.

Experimental results

Change of inner reactor diameter

The objective of these experiments is to investigate the relation between the inner reactor diameter and the absorption rate. For this experiment, we used the microchannel setup described in Figure 1. Three different inner diameters of 0.6 mm, 0.75, and 0.9 mm were tested. The microchanel length and DEA flow rate were kept constant at 500mm and 10 ml/min, respectively, whereas the CO_2 flow rate varied. The results of this study are presented in Figure 2. As can be seen in Figure 2, there is no clear separation between the results of different diameters, and the results are clustered. This behavior can be explained by considering the way these experiments are conducted. In all these experiments the volume flow rates were identical for different

diameters. This means that the gas and liquid velocities were significantly higher in narrower channels and the residence time was considerably shorter.

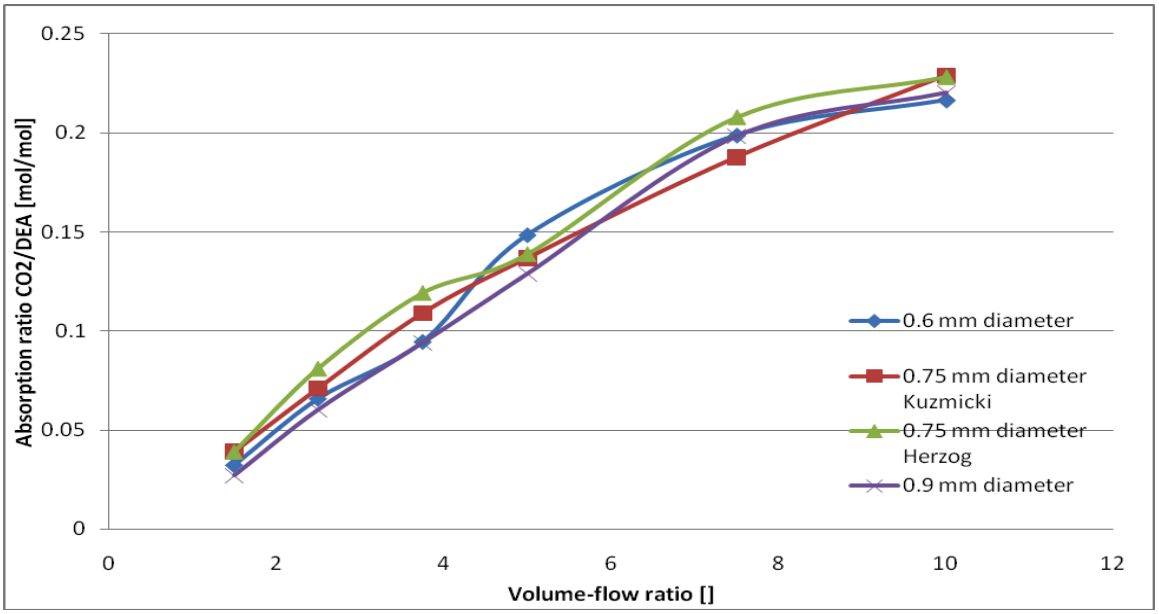

Figure 2. Comparison of different diameters: Absorption ratio versus gas to liquid volume flow rates ratio.

To achieve a fair comparison between different microchannel reactors, the gas and liquid velocities must be kept identical. To calculate the superficial velocities we used the standard equation given as:

$$u = \frac{\dot{V}}{A} \tag{1}$$

$$u : velocity \left[\frac{m}{s}\right]$$

$$\dot{V} : volume\ flow \left[\frac{m^3}{s}\right]$$

$$A : area\ cross\ section\ [m^2]$$

where the volume flow ratio V_r and the velocity ratio u_r remained constant. With the help of Equation (1) we are able to see that the velocity ratio equals the volume flow ratio:

$$V_r = \frac{\dot{V}_{CO_2}}{\dot{V}_{DEA}} \tag{2}$$

$$u_r = \frac{u_{CO_2}}{u_{DEA}} \tag{3}$$

$$u_r = V_r \tag{4}$$

$$u_r : velocity\ ratio$$

$$V_r : volume\ flow\ ratio$$

For all the experiments volume flow rate and velocity ratios of 7.5 were used, and the following diameters and velocities were tested (Table 1):

Table 1. Tested diameters and velocities

Tested Diameters [mm]	Tested DEA Solution velocities u_{DEA} [m/s]	Tested CO2 Velocities u_{CO2} [m/s]
0.45	0.566	4.24
0.58	0.471	3.54
0.9	0.377	2.83
	0.283	2.12
	0.189	1.41

Theoretically, a decrease in diameter will be followed by a decrease in diffusion time scale, which leads to an increase of the absorption ratio. Also an increase in velocity will lead to a decrease of the residence time and a decrease in the absorption ratio. Therefore we expect to get a higher absorption ratio for a smaller diameter and a lower velocity. The result of variation of absorption mole ratio versus velocity of DEA solution is presented in Figure3. In Figure 4, the inlet absolute gas pressure versus velocity of DEA solution is shown.

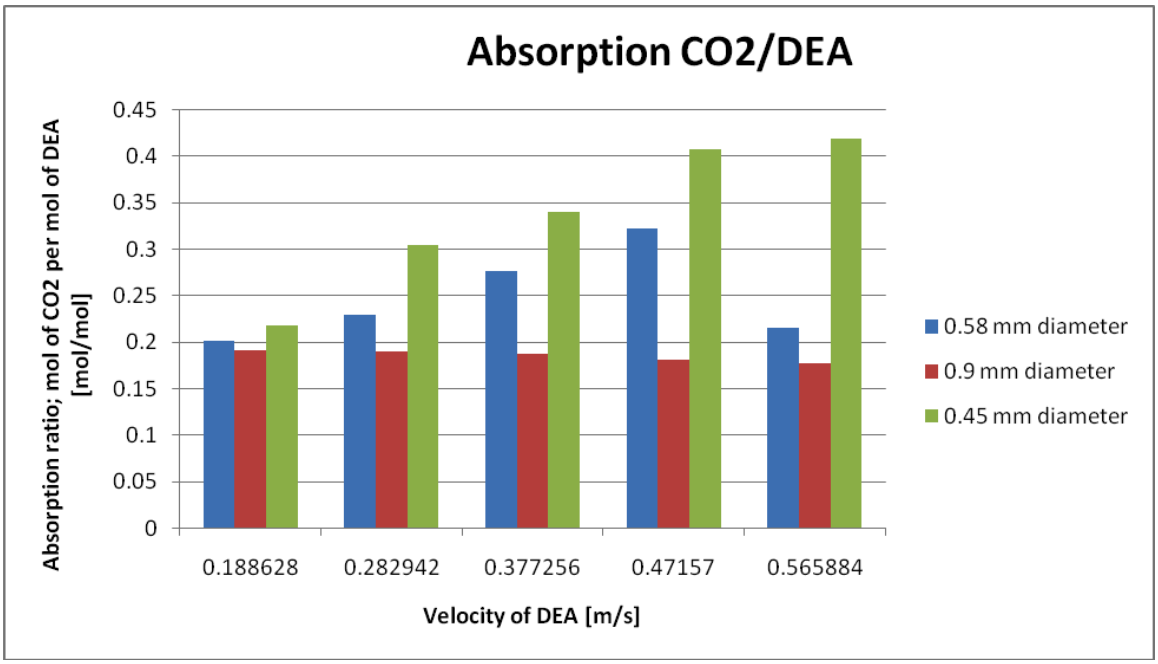

Figure 4. Absorption mole ratio of CO_2/DEA for various velocity of DEA for different diameters.

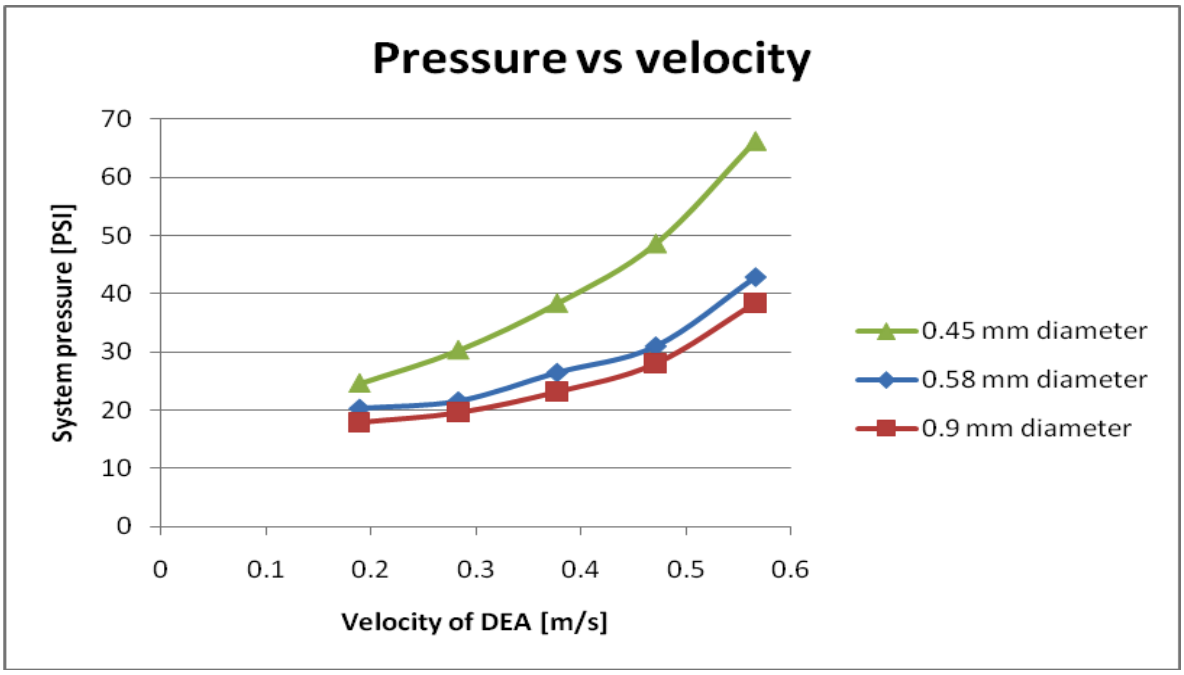

Figure 4. Pressure of CO_2 at the flow meter versus the velocity of DEA solution for different diameters.

The results in Figure 3 fulfill our expectations. As can be seen, each diameter shows a maximum in the absorption ratio, and this maximum occurs at different velocities for different diameters. If we take a closer look at the 0.58 mm reactor it is obvious that at first there is an increase in the absorption mole ratio with the DEA solution superficial velocity. This is because as the superficial velocity increases, the flow regime varies from bubbly flow towards more elongated slugs. Therefore, the contact surface area increases, and the rate of absorption intensifies. However, afterwards a drop in the absorption ratio was observed. This is because a higher velocity has led to a shorter resident time, which reduces the absorption rate. The decrease of internal diameter also resulted in higher absorption rate, which as also expected. As shown in Figure 3, the absorption ratio for a smaller diameter is always higher than the absorption ratio of a bigger diameter.

Figure 4 also matches our expectations. It is logical for the pressure to rise for any given diameter in response to the increase of the velocity of the DEA solution. With a higher velocity, friction between the fluids and the reactor wall increases the resistance that the fluid has to overcome. Also it is logical that the pressure increases as the diameter is getting smaller. As long as the velocity remains constant during the test runs, the pressure has to increase to compensate for the friction. Note that the pressures reported in Figure 4 are the absolute gas pressure measured by flowmeter. However, since the pressure at the separator is atmospheric, the difference between this pressure and atmospheric pressure also represents the pressure drop across the microchannel.

Efficiency of CO_2 absorption for different diameters and velocities

The efficiencies of absorption for the different diameters and velocities are compared to study the effect of geometry on the performance of the reactor. First we need to define the absorption efficiency as given below:

$$\eta = \frac{\dot{n}_{CO_2,inlet} - \dot{n}_{CO_2,outlet}}{\dot{n}_{CO_2,inlet}} \quad (5)$$

$$\eta = \frac{\dot{n}_{CO_2,absorbed}}{\dot{n}_{CO_2,inlet}} \tag{6}$$

$$\eta : absorption\ efficiency$$
$$\dot{n} : molar\ flow$$

Using the conductivity measurement method we are able to determine the absorbed molar flow of CO_2 divided by the molar flow of DEA denoted.

$$R = \frac{\dot{n}_{CO_2,absorbed}}{\dot{n}_{DEA,inlet}} \tag{7}$$

$$\dot{n}_{CO_2,absorbed} = R * \dot{n}_{DEA,inlet} \tag{8}$$

$$R : absorption\ ratio\ of\ mole\ CO_2\ per\ mole\ of\ DEA$$

Therefore, the efficiency can be calculated from the following equation:

$$\eta = \frac{R * \dot{n}_{DEA,inlet}}{\dot{n}_{CO_2,inlet}} \tag{9}$$

R is the absorption ratio, which is defined as the absorbed amount of moles of CO_2 per the amount of moles of DEA at the beginning of the reaction. This value is calculated with a correlation that depends on the average conductivity S measured in our setup.

$$R = 1.847 * 10^{11} * S^3 - 6.26 * 10^7 * S^2 + 1.028 * 10^4 * S - 2.125 * 10^{-2} \tag{10}$$
$$S : average\ conductivity$$

The molar flow rate of the DEA at the inlet can be calculated as

$$\dot{n}_{DEA,inlet} = \dot{V}_{DEA-sol} * C_{DEA} \tag{11}$$

$$\dot{V} : volume\ flow$$
$$C : concentration$$

The molar flow rate of the CO_2 at the inlet of the reactor can be calculated with the ideal gas equation.

$$p * \dot{V} = \dot{n} * R * T \tag{12}$$

This can be written as:

$$\dot{n} = \frac{p * \dot{V}}{R * T} \tag{13}$$

$$p : system\ pressure\ at\ the\ inlet\ of\ the\ reactor$$
$$R : ideal\ gas\ constant$$

$$T : absolute\ temperature\ [K]$$

Now the final equation to calculate the absorption efficiency can be generated:

$$\eta = \frac{R * \dot{V}_{DEA-sol} * C_{DEA} * R * T_{inlet}}{p_{CO_2,inlet} * \dot{V}_{CO_2,inlet}} \quad (14)$$

The results of this study are shown in Figure 5. As can be seen, the trend of the efficiency does not reflect the trend of the absorption ratio shown in Figure 3, but there seems to be a certain velocity for each diameter that has the highest absorption efficiency. This phenomenon is acceptable because the flow pattern and residence time of the particles depend on the velocity of the DEA-solution, the velocity of CO_2 and on the inner diameter of the reactor. However, for the range of measurements, the higher efficiency typically occurs at lower DEA and CO_2 velocities. It must be noted that in all these experiments the superficial velocity of gas over superficial velocity of liquid remains constant at 7.5.

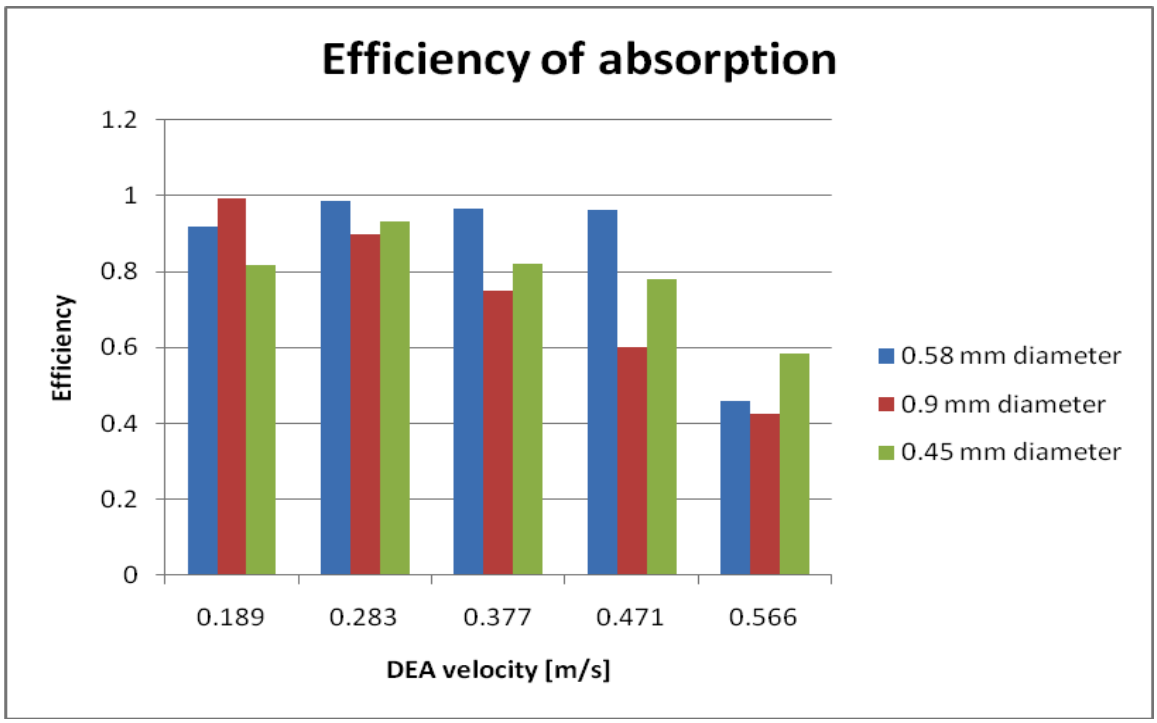

Figure 5. Efficiency of absorption for different diameters and velocities.

A correlation for the calculation of the liquid-side volumetric mass transfer coefficient for Taylor flow

During this period a study on calculation of volumetric liquid-side mass transfer coefficient in the microreactor was conducted. For this purpose several correlations were tested. This is important because mass transfer coefficient enables us to compare the performance of the microchannel reactor with the performance of other conventional reactors. This work is still ongoing, as there are several correlations available that can be tested. One approach to calculate mass transfer coefficient for Taylor flow is based on the following correlation:

$$k_L a = \frac{2}{d_h} * \left(\frac{D * U_B}{L_B + L_S}\right)^{0.5} * \left(\frac{L_B}{L_B + L_S}\right)^{0.3} \quad (15)$$

where the parameter's definition is as follows:

$k_L a$: liquid side volumetric mass transfer coeficcient $[s^{-1}]$
L_B : Length of Taylor bubble L_B : Length of Taylor bubble
D : liquid phase diffusivity
U_B : Taylor − bubble mean velocity
d_h : hydraulic diameter

The liquid phase diffusivity can be calculated from the following equation:

$$D_{AB}^0 = \frac{7.4 * 10^{-8} * (\varphi * M_{wB})^{0.5} * T}{\mu_B * {v_A}^{0.6}} \quad (16)$$

D_{AB}^0 : diffusion coefficient of solute A in solvetn B $[\frac{cm^2}{s}]$
M_{wB} : molecular weight of solvent B $[\frac{g}{mol}]$
T : absolute temperature $[K]$
v_A : molal volume of solute A at its normal boiling point temperature $\left[\frac{cm^3}{mol * g}\right]$
volume and moles of solute A and grams of solvent B
μ_B : viscosity of solvent B $[cP] = [mPa * s]$
φ : association factor of solvent B, e.g = 1 for unassociated solvents, = 2.6 for water

Equation (15) requires visualization analysis of the flow pattern in the microchannel reactor, and it is only applicable to Taylor flow. To solve Equation (16) several values are taken from other sources, such as the viscosity and the density. A literature research was conducted to determine the variation of these parameters with temperature. The results of this research are summarized in Table 2 [1]. Based on those values, correlations for the density and the viscosity of a 20wt% DEA-solution were created and used for further calculations of the liquid side volumetric mass transfer coefficient, as can be seen in Figure 6 and Figure 7.

Table 2. Viscosity and density for a 20wt% DEA-solution for different temperatures [1].

Temperature[C]	Viscosity 20wt% DEA-solution[mPA*s]	Density [g/ml]
20	2.171	1.022
40	1.304	1.0142
60	0.848	1.0052
80	0.606	0.9931
100	0.448	0.9804

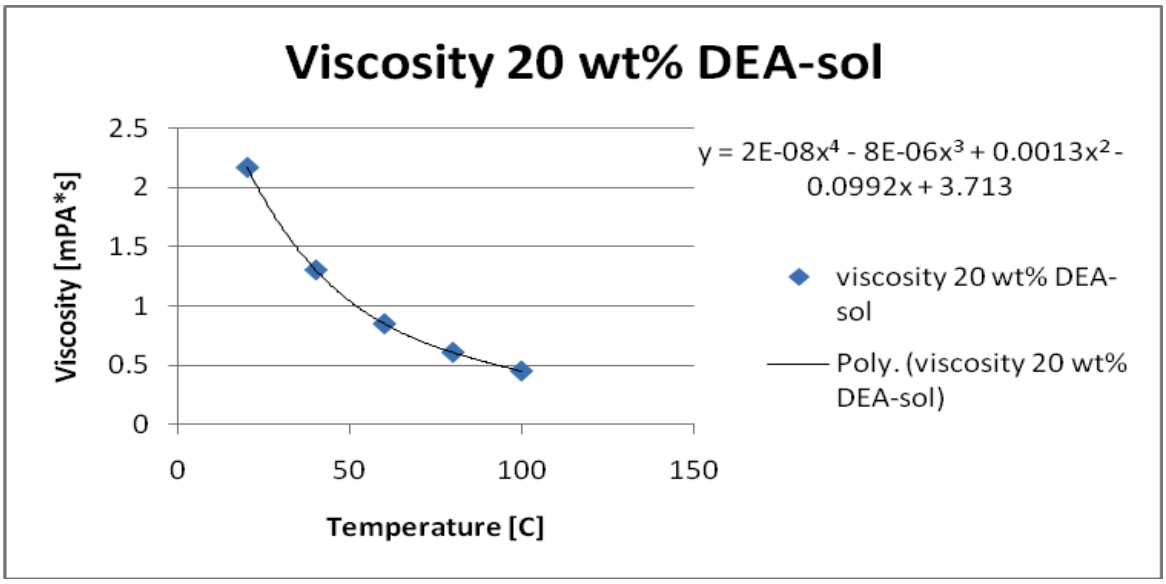

Figure 6. Viscosity of a 20wt% DEA-solution versus the temperature.

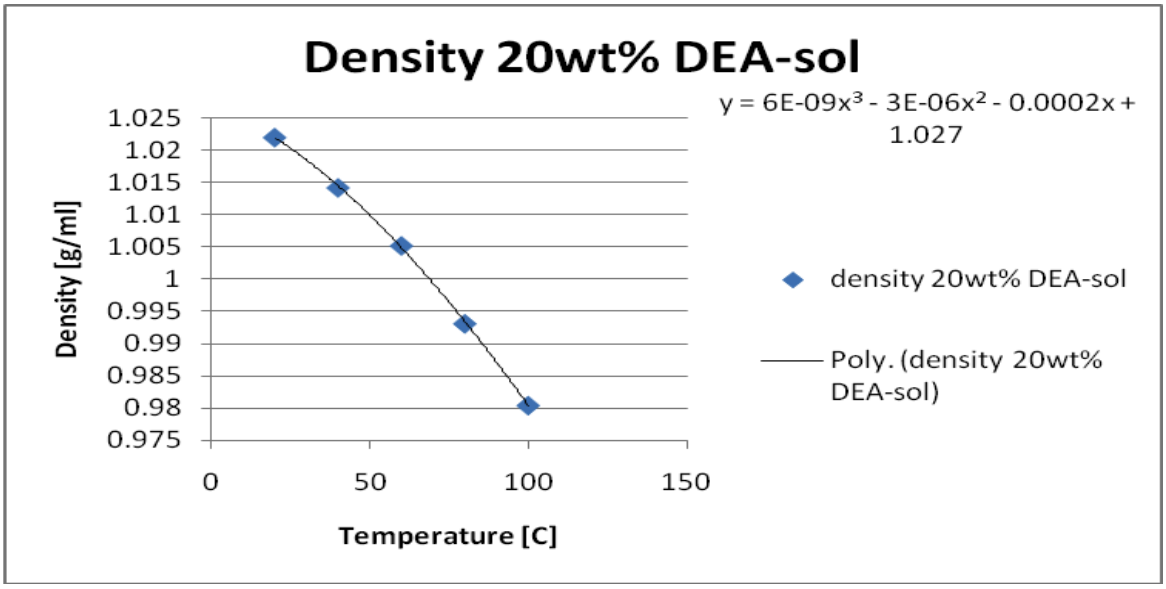

Figure 7. Density of a 20wt% DEA-solution versus the temperature.

Figure 8 shows the calculated values of mass transfer coefficient for different inner reactor diameters (0.45 mm, 0.58 mm and 0.9 mm) with a length of 500 mm each and for constant superficial velocities of 0.094 m/s and 0.705 m/s for the DEA-solution and CO_2 gas stream, respectively. As can be seen, a smaller diameter has a higher mass transfer coefficient than a larger diameter. This trend clearly demonstrates the advantages of channel size reduction for enhancement of mass transfer.

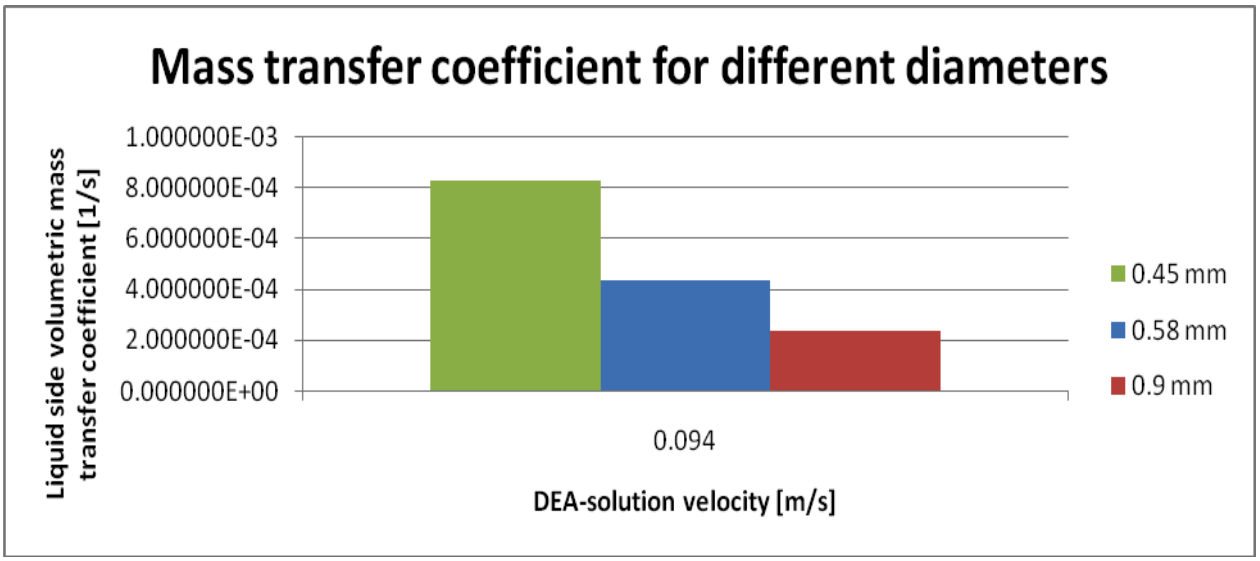

Figure 8. Liquid-side volumetric mass transfer coefficient for different channel diameters.

The second-generation reactor

Based on the experience acquired by working with the first-generation reactor, a second-generation reactor was designed and fabricated. The second-generation reactor features a more compact design, allowing a longer reactor length in lesser space, and also provides a better way to visualize the flow. Also in this construction there is an integrated heating and cooling system, which allows us better control of the thermal conditions in the experimental loop. The innovative spool-like design and the covering glass plate on top enable us to record and analysis images of the flow patterns at different reaction steps in a single frame. The design of the second-generation reactor is shown in Figure 9 and the fabricated prototype is presented in Figure 10.

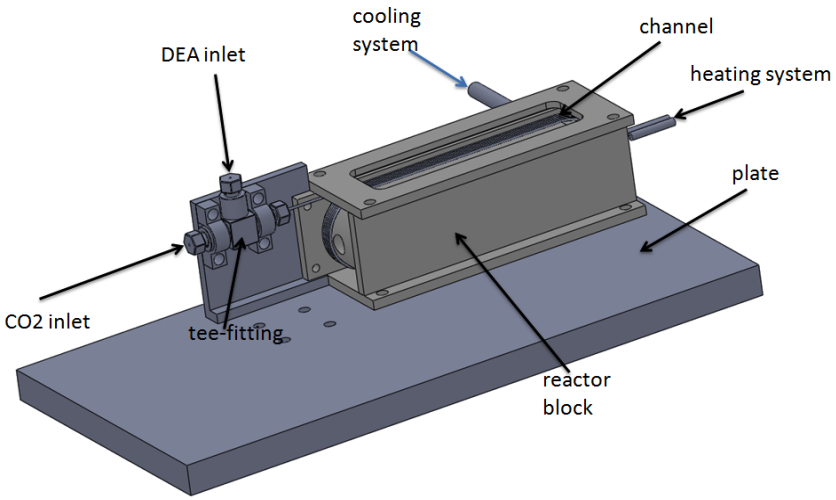

Figure 9. Schematic 3D-model of the second-generation reactor.

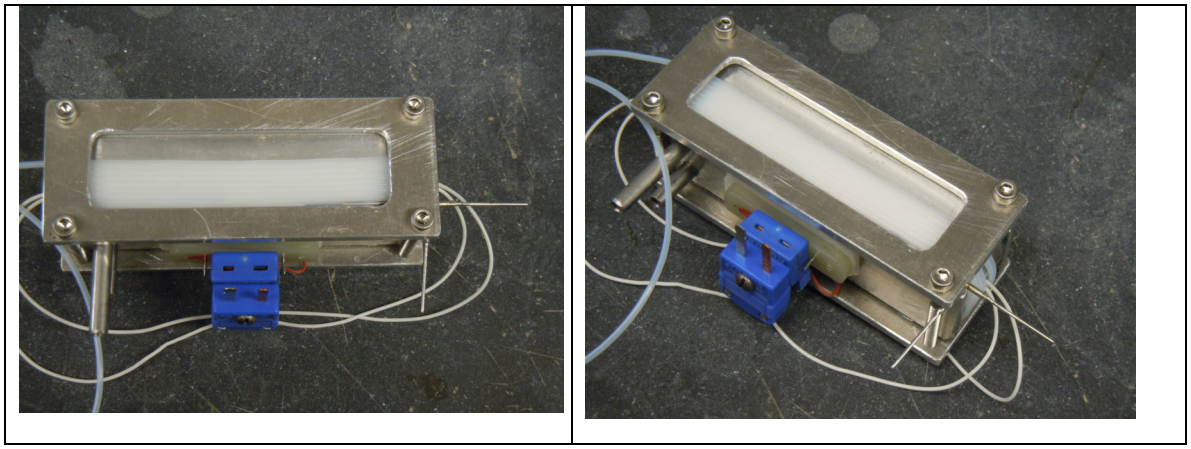

Figure 10. Second-generation reactor prototype.

Summary of results

In this reporting period different experiments were conducted and the results were collected. Most of the time the results fulfilled the expected trends. In addition, various correlations were tested to calculate the liquid-side volumetric mass transfer coefficient for different reactor diameters. One correlation which seemed to be applicable to the measurements we made was used and the mass transfer coefficient was estimated. Also, the results shown in Figure 3 closely match our expectations. The absorption ratio for a smaller diameter is always higher than the absorption ratio of a larger diameter, and it is expected that the pressure will rise for any given diameter in response to increase the velocity of the DEA. The efficiency of the absorption process was calculated for different diameters and velocities. A very high efficiency was obtained at lower velocities. It was also noticed that there is an optimum for the absorption efficiency for each diameter. A design for the second-generation reactor is finished and the prototype is currently under fabrication.

5. Difficulties Encountered/Overcome

None to report.

6. Planned Project Activities for the Next Quarter

- Fabricate second-generation design and prepare the test-section
- Conduct experiment on absorption of CO_2 in gas mixture
- Conduct parametric and visualization studies
- Continue collaboration work with the PI partners to compare experimental results with numerical modeling results for the absorption process

7. References

[1] *J. Yue et al. / Chemical Engineering Science 64 (2009) 3697 -- 3708*

[2] Gonzalo Va'zquez et al. J. Chem. Eng. Data 1996, 41, 806-808

Appendix

Justification and Background

The development of environmentally friendly process in industry is one of the major goals that have to be achieved. One way to approach cleaner environment is capturing or minimizing harmful gas components before emission to the atmosphere. One of the main gases which contribute significantly in global warming is CO_2. Due to a necessity to develop more efficient techniques for CO_2 capturing, scientific research in this area has been expanded rapidly. Since in the past very little R&D was devoted to CO_2 capture and separation technologies, opportunities for revolutionary improvements in CO_2 separation technologies is very high To maintain its competiveness and bring environmental friendly industry to the region, ADNOC has adopted various policies and approached it via many plans including "zero-flare" policy, acquiring more energy efficient process and the agreement signed with MASDAR to develop CO_2 capture technology. CO_2 separated from flue gases will be re-injected in oil wells, increasing oil production.

One of the promising concepts which can lead to major technology advancement is microchannel-based absorption units with enhanced kinetics. The objective of this study is to develop a full process of CO_2 separation from flue gas with incorporating micro-channel absorption technology at laboratory scale. The project addresses various stages of separation process: separation of solid particles and condensed water droplets and CO_2 separation using absorption process. Microchannel absorption CO_2 separator developed in this project will, significantly, increase the efficiency of separation process while decreasing energy consumption involved in such operation. Moreover, development of such technology will lead to reduction of equipment's size and, therefore, minimizing the footprint and cost of equipment. An electrostatic separator will be used prior to CO_2 separation to remove solid and liquid contaminants from flue gas. The ultimate objective is to design all separation stages such that the overall performance will be optimized.

Approach

Detailed analysis and identification of the phenomena and the design challenges involved in effective implementation of the mechanism. Parametric study of existing and improved separators. Design iterations, including numerical flow and field simulations, fabrication, and testing. Creation of database and engineering design correlations.

Three-Year Schedule

The schedule below reflects the revised scope approved by both sides

Year 1:

- Conduct literature review to understand the basic of mass transfer in micrreactor and separation of flue gas;
- Evaluate existing technologies and assess their applicability to CO_2 separation of flue gas;
- Repeat and implement some previous classical examples of microchannel separation to get familiarized with fundamentals and basic challenge;
- Analyze mixing in microchannels and possibility to use it in CO_2 separation;
- Continue improving efficiency of EHD separator for the fine liquid and solid particles;
- Conduct visualization study of liquid and solid particles migration in the electrical field.

Year 2:

- Continue on literature survey;

- Selection of the target alkanolamine;
- Simulate mixing and separation phenomena in microreactor via modeling and analytical means;
- Develop laboratory scale microchannel absorber and desorber for CO_2 separation;
- Conduct Experimental study and design optimization study;
- Continue on visualization study of liquid and solid particles migration in the electrical field.
-

Year 3:

- Conduct visualization study on absorption and desorption in microchannels;
- Design iterations and implementation;
- Parametric study of CO_2 separation process and experiment on different designs;
- Continue on simulation of mixing and separation phenomena in microreactor via modeling and analytical means;
- Present the best design to ADNOC group of companies;
- Develop design correlation;
- Prepare report.

Microreactors for Oil and Gas Processes Using Microchannel Technologies

UMD Investigators: Serguei Dessiatoun, Amir Shooshtari
GRA: Meera Mahadevan
PI Investigators: Afshin Goharzadeh, Ebrahim Al-Hajri
Start Date: Oct 2006

1. Objective/Abstract

Microfabrication techniques are increasingly used in gas and petrochemical engineering to realize structures with capabilities exceeding those of conventional macroscopic systems. In addition to already demonstrated chemical analysis applications, microfabricated chemical systems are expected to have a number of advantages for chemical synthesis, chemical kinetics studies, and process development. Chemical processing advantages from increased heat and mass transfer in small dimensions are demonstrated with model gas, liquid and multiphase reaction systems.

Evaluation of different application of microreactors and their impact on UAE industry economics has been conducted in this quarter. The application of microreactors in the polymerization of ethylene and propylene is feasible and may provide significant economic benefits, and therefore will be considered for further investigation in the current project

2. Milestones/Deliverables Scheduled for the Completed Quarter

Design and fabrication of microreactor
Experiments to initiate polymerization

3. Summary of Project Activities for the Completed Quarter

Co-polymerization kinetics

We have been considering ethylene hompolymerization so far. We now consider copolymerization kinetics of ethylene with any other monomer like butene or hexene to produce high-density polymers.

Consider 2 different monomers A and B undergoing copolymerization in the presence of a single site catalyst. Given below is the reaction mechanism.

Initiation

$$C^* + A \xrightarrow{k_{iA}} P_{1,A}$$

$$C^* + B \xrightarrow{k_{iB}} P_{1,B}$$

Propogation

$$P_{r,A} + A \xrightarrow{k_{pAA}} P_{r+1,A}$$

$$P_{r,A} + B \xrightarrow{k_{pAB}} P_{r+1,B}$$

$$P_{r,B} + A \xrightarrow{k_{pBA}} P_{r+1,A}$$

$$P_{r,B} + B \xrightarrow{k_{pBB}} P_{r+1,B}$$

Chain transfer to

a) Monomer

$$P_{r,A} + A \xrightarrow{k_{tmAA}} C^* + M_r$$

$$P_{r,A} + B \xrightarrow{k_{tmAB}} C^* + M_r$$

$$P_{r,B} + A \xrightarrow{k_{tmBA}} C^* + M_r$$

$$P_{r,B} + A \xrightarrow{k_{tmBB}} C^* + M_r$$

b) Hydrogen

$$P_{r,A} + H_2 \xrightarrow{k_{thA}} C^* + M_r$$

$$P_{r,B} + H_2 \xrightarrow{k_{thB}} C^* + M_r$$

c) Cocatalyst

$$P_{r,A} + Al \xrightarrow{k_{tAlA}} C^* + M_r$$

$$P_{r,B} + Al \xrightarrow{k_{tAlB}} C^* + M_r$$

d) β-Hydrogen

$$P_{r,A} \xrightarrow{k_{\beta A}} M_r + C^*$$

$$P_{r,A} \xrightarrow{k_{\beta B}} M_r + C^*$$

Deactivation

$$P_{r,A} \xrightarrow{k_{dA}} M_r + C_d$$

$$P_{r,B} \xrightarrow{k_{dB}} M_r + C_d$$

$$C^* \xrightarrow{k_d} C_d$$

where

C^* – Activated Catalyst

C_d - Deactivated Catalyst

A&B- Monomers

k_{ij}- Rate constants

M_r-Dead polymer

n- Chain length

P_r - Live Polymer

Copolymerization composition distribution

- Reactivity Ratios: Ratio of homo propagation to cross propagation.

$$r_1 = \frac{k_{pAA}}{k_{pAB}} \qquad r_2 = \frac{k_{pBB}}{k_{pBA}}$$

- F_1- Instantaneous mole fraction of A in the copolymer
  f_1 –instantaneous mole fraction of A in the bulk phase

$$F_1 = \frac{r_1 f_1^2 + f_2 f_1}{r_1 f_1^2 + 2 f_2 f_1 + r_2 f_2^2}$$

Stockmayer's bivariate distribution

- Stockmayer's bivariate distribution describes the instantaneous bivariate distribution of chain length and chemical composition of linear polymers made with single-site-type coordination polymerization catalysts.

$$w(r,y)drdy = r\tau^2 \exp(-r\tau)dr \frac{1}{\sqrt{2\pi\beta / r}} \exp(\frac{-y}{2\beta / r}^2)dy$$

$$\beta = \overline{F}_1(1-\overline{F}_1)[1+4\overline{F}_1(1-\overline{F}_1)(r_1 r_2 - 1)]^{0.5}$$

$$y = F_1 - \overline{F}_1$$

Ethylene-Propylene Copolymerization

- Monomer A-Ethylene; Monomer B-Propylene
- A:B=4:6
- Temperature -50°C
- Reactor Length- 1m
- Residence Time-30mins
- Steady State Reactor
- Axial Dispersion Neglected

Monomer concentration curves

The monomer concentration curves are given in Figure 1.

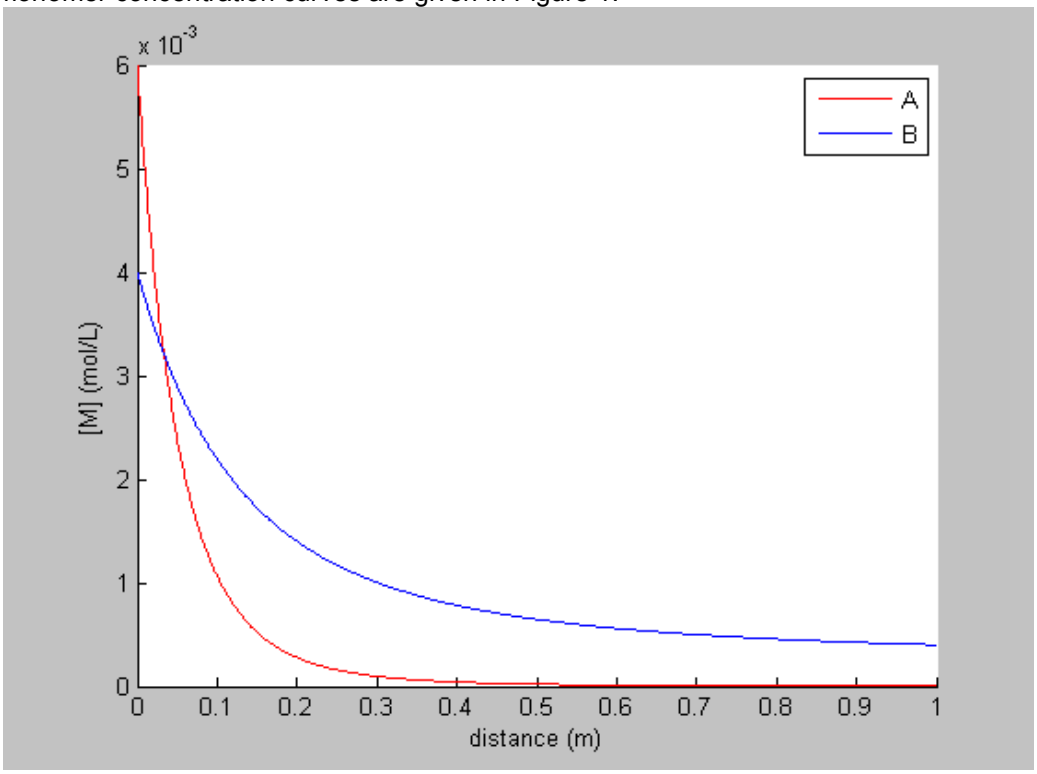

Figure 1. Monomer concentration curves.

Polymer yield

The polymer yield is given in Figure 2.

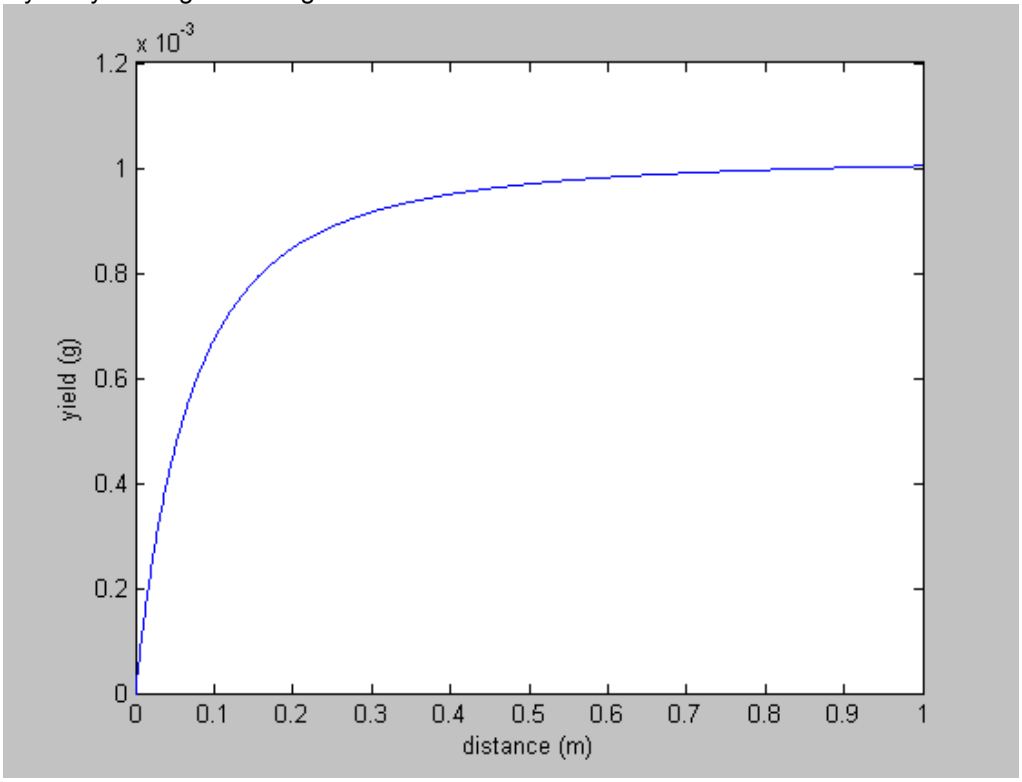

Figure 2. Polymer yield.

Copolymer Composition Curve

The copolymer composition curve is given in Figure 3.

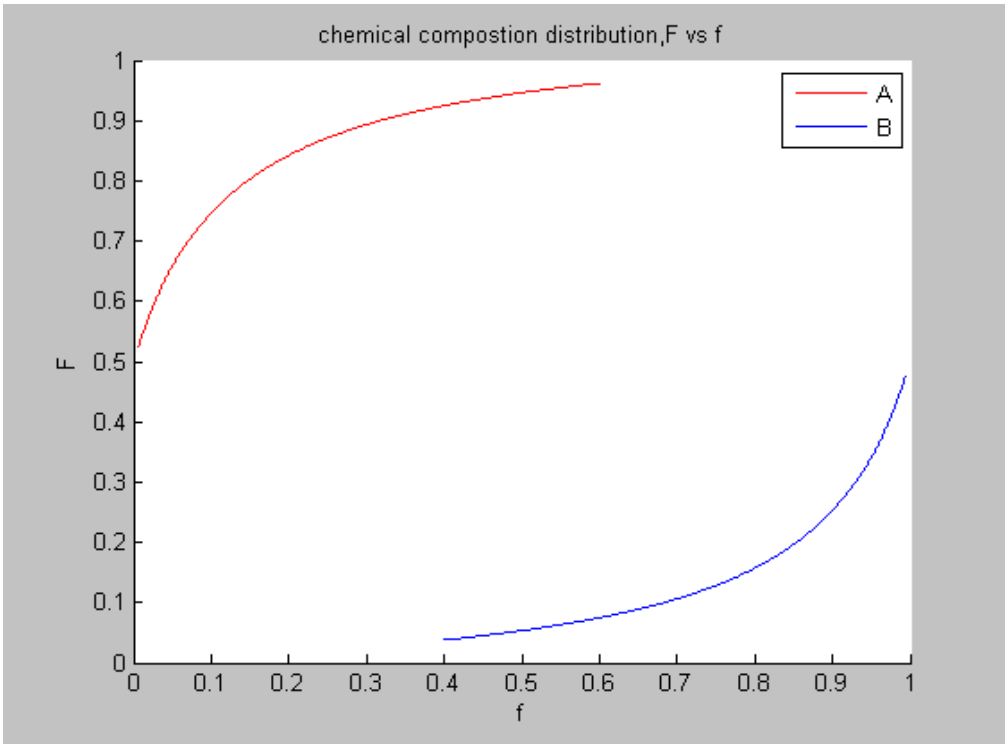

Figure 3. Copolymer composition curve.

Variation of F along the length of the reactor

The variation of F along the length of the reactor is given in Figure 4.

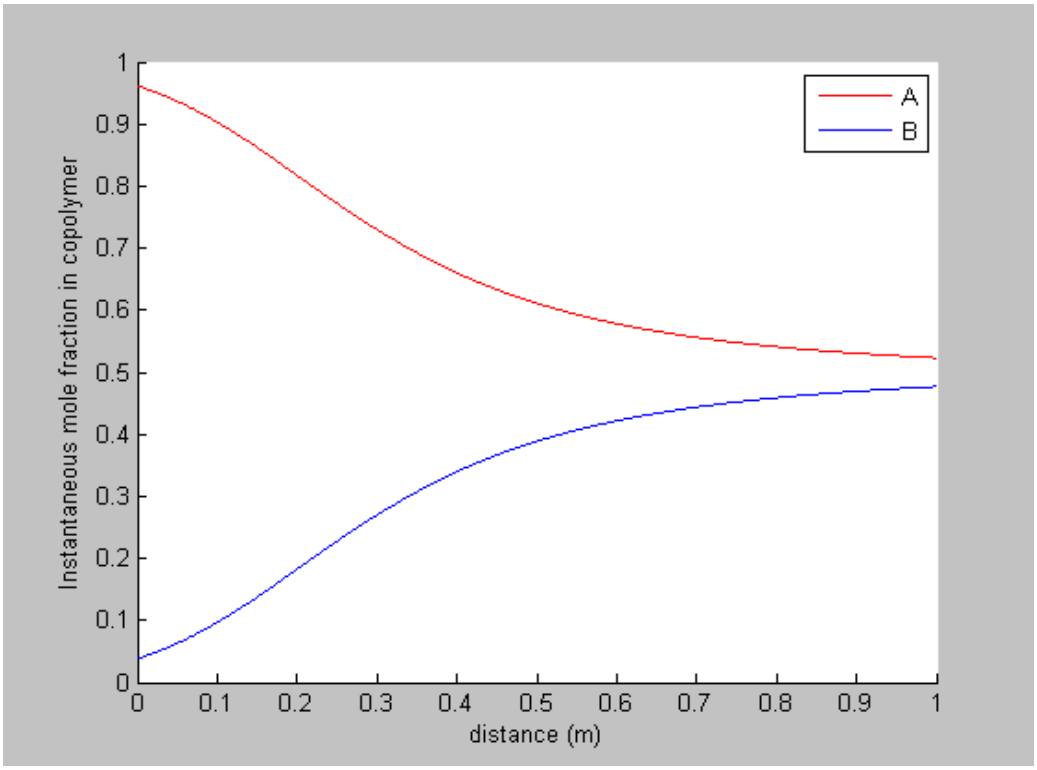

Figure 4. Variation of F along the length of the reactor.

Cumulative composition

$$< F_1 >= \frac{\text{total number of repeating units of } M_1 \text{ in the copolymer}}{\text{total number of repeating units in the copolymer}}$$

The cumulative composition is given in Figure 5.

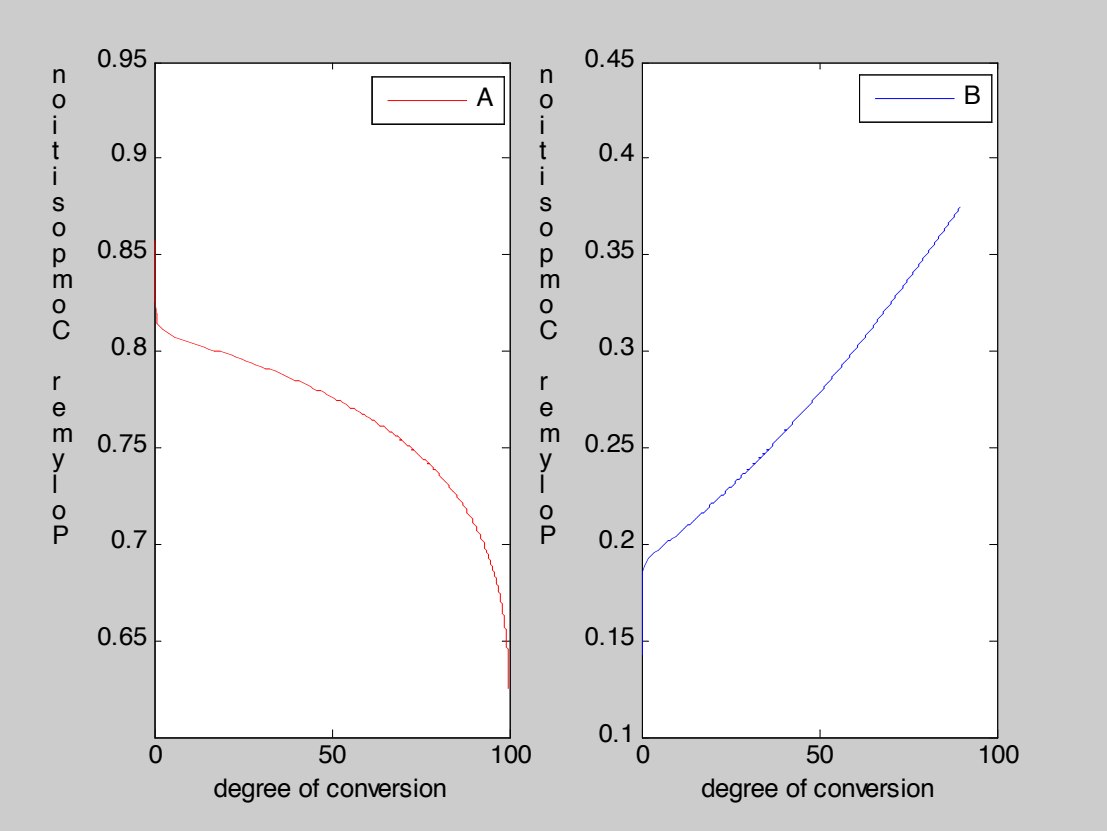

Figure 5. Cumulative composition.

Conclusions

- The copolymerization model helps in studying the effect of different ratios of varied monomers and the composition of copolymer formed.
- The model suggests the need for additional monomer input points in the reactor.
- Inclusion of axial dispersion model
- Studying the effects of a micro-scale reactor on the particle flow and growth and its impact on the rate constants.
- Experiments will allow us to tweak the model by addition of different correlations.

Microreactor Setup

The microreactor setup is shown in Figures 6 and 7.

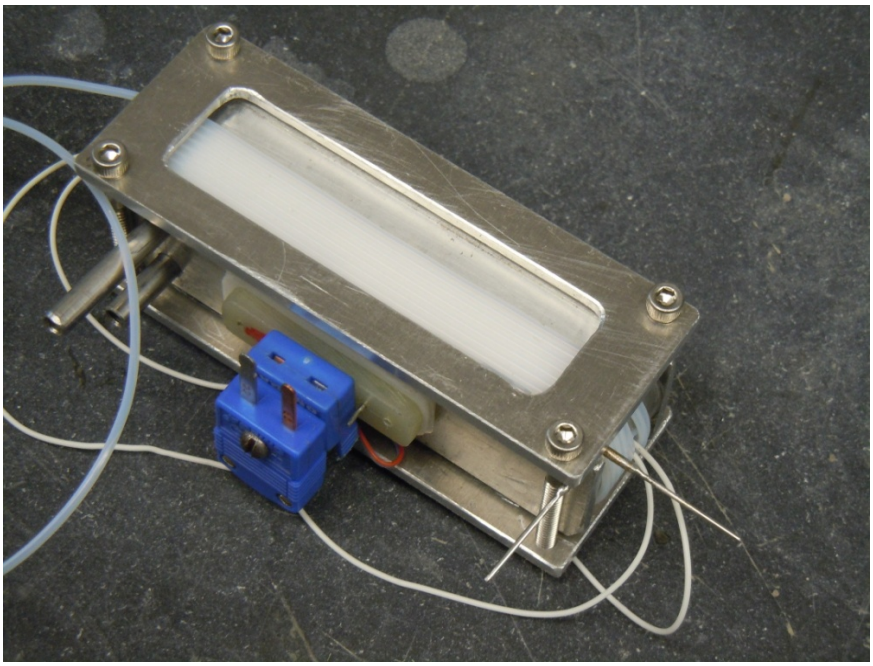

Figure 6. Microreactor setup.

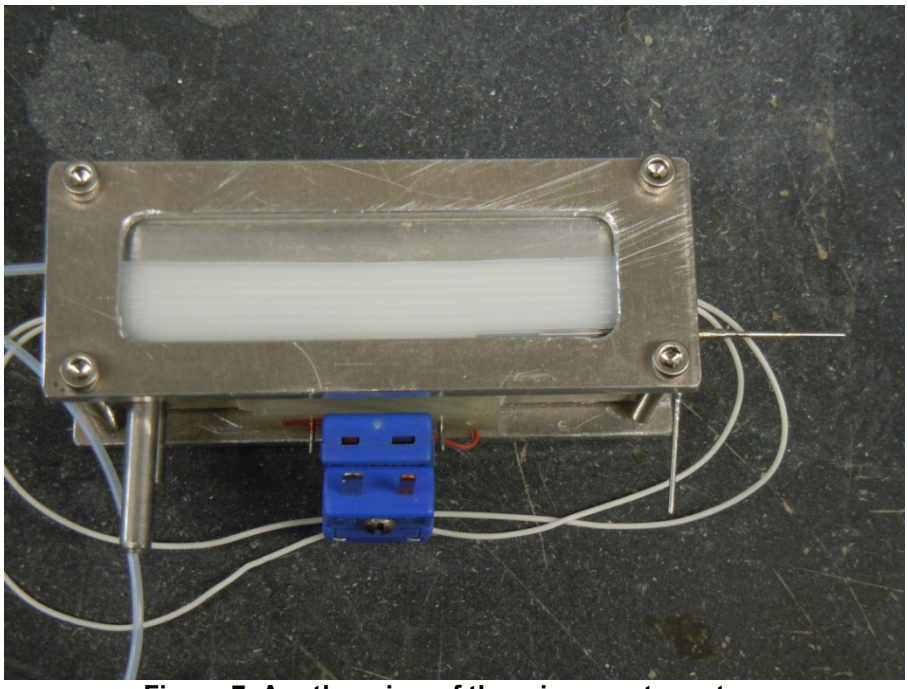

Figure 7. Another view of the microreactor setup.

Silica Support Particle Synthesis (300-400nm)

Prepared using measured quantities TEOS, ethanol, ammonia and water. The particles were viewed under SEM, shown in Figure 8.

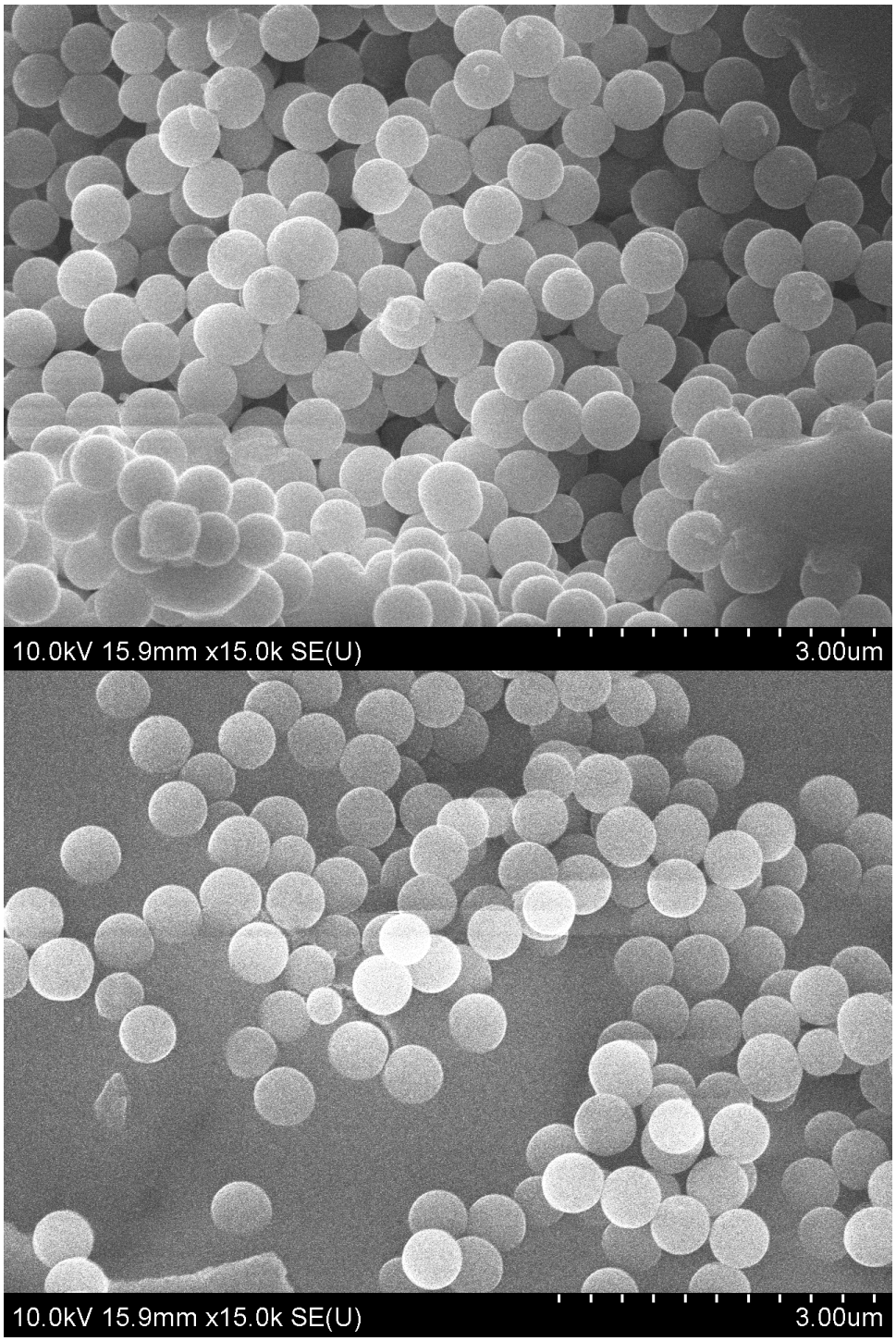
10.0kV 15.9mm x15.0k SE(U)
3.00um
10.0kV 15.9mm x15.0k SE(U)
3.00um

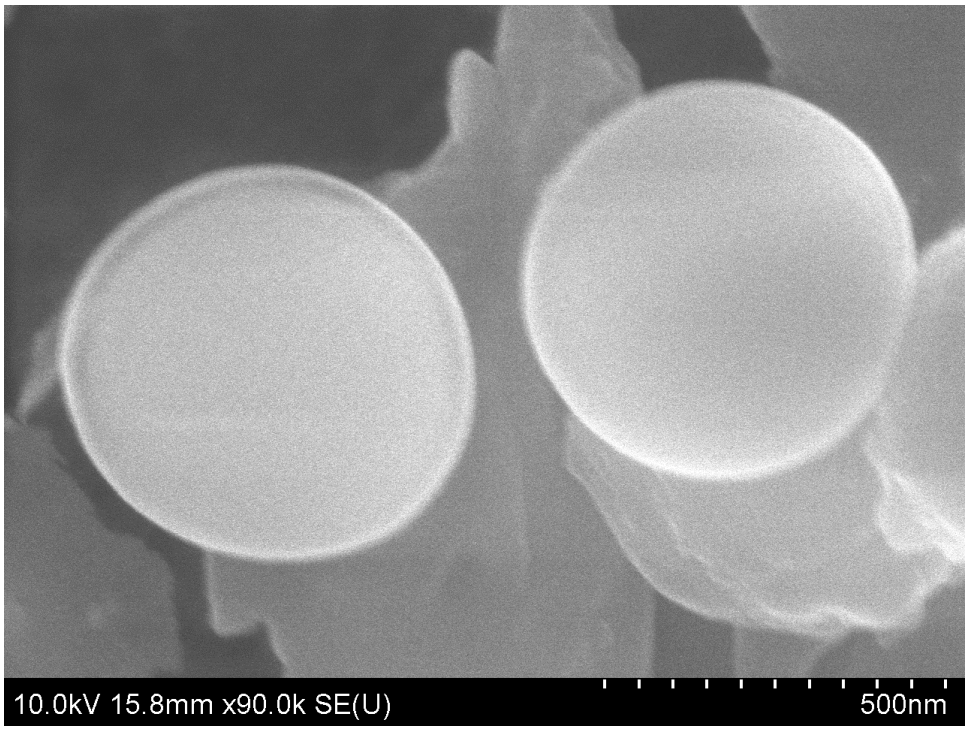

Figure 8. Silica support particles viewed under SEM.

BET Analysis

The pore size distribution is shown in Figure 9, and the isotherm (A) is shown in Figure 10.

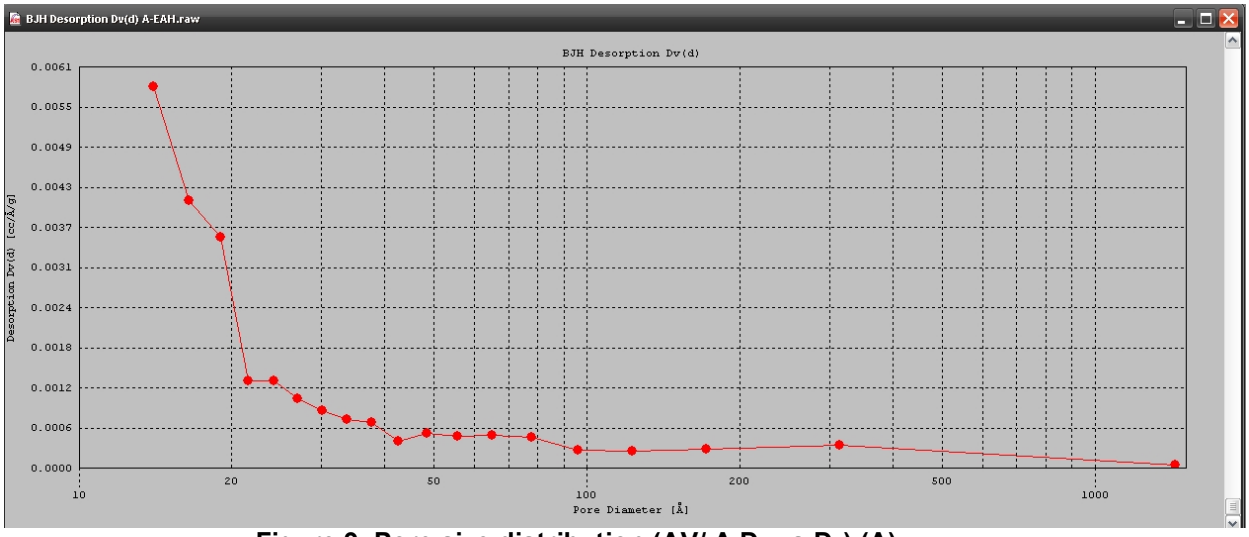

Figure 9. Pore size distribution (ΔV/ Δ D_p vs D_p) (A).

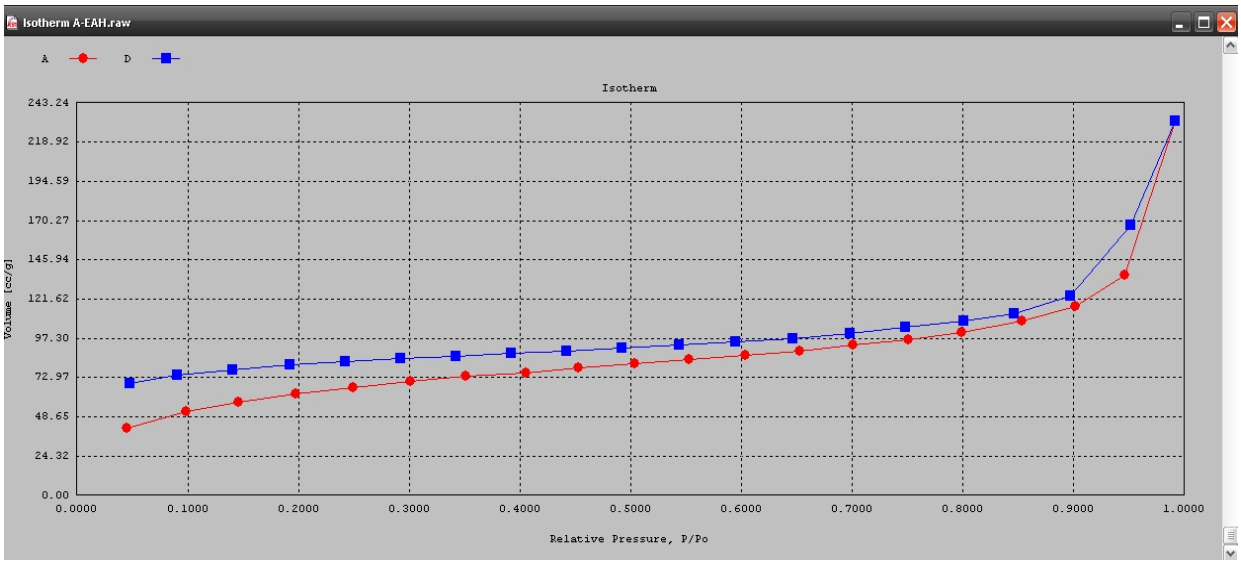

Figure 10. Isotherm (A).

Table 1. Porosity dimensions

Sample	Area (m^2/g)	Pore Volume(cm^3/g)	Mean Pore Diameter (nm) (approx.)
A	**248.1**	**0.359**	**5.78**
B	**288.7**	**0.4228**	**5.85**
C	**405.6**	**0.2099**	**2.07**

From Figures 9 and 10 and Table 1, it can be concluded that

- Porosity=Pore volume/Bulk volume
- They have a very high porosity.
- The isotherms resemble the Type H4 hysteresis plot.
- The silica particles offer a large surface area for catalysis.

Experiments

The procedure for anchoring the catalyst onto surface-treated silica particles is shown in Figure 11.

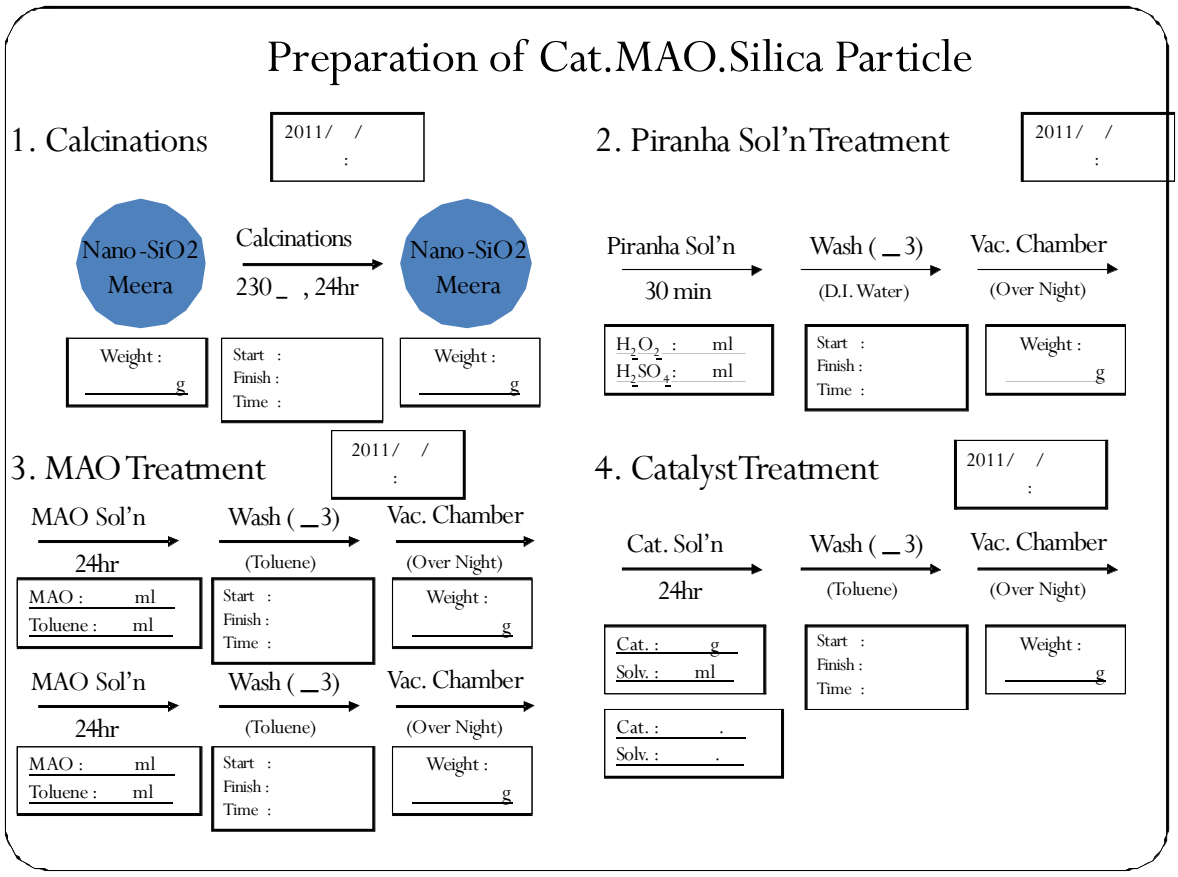

Figure 11. Semi-batch reaction using the above catalyst and ethylene monomer to observe particle morphology.

4. Difficulties Encountered/Overcome

- Visualization of actual polymerization process at high pressure and temperature in microreactor.
- Mass production of homogenous silica particles without loss during purification process.

5. Planned Project Activities for the Next Quarter

JUNE

Experimental:

- Handling catalyst particles: loading them onto silica
- Batch polymerization to understand the type of polymer being formed
- Flow testing in the current microreactor set up

Theoretical:

- Compare the developed models to research papers.
- Verify the model for the batch reaction carried out.
- Expand the copolymerization model
- Quarterly Report

JULY

Experimental Work:

- Ethylene polymerization reaction in micro reactor set up.
- Remodeling the apparatus to include copolymer and other changes
- Polymer characterization (SEM)

Theoretical work:

- Microreactor modeling and design of experiments
- Improve the model by addition of unsteady state behavior, axial dispersion

AUGUST

- Further experiments on microreactor set up with varying parameters
- Qualitative and quantitative study of polymer produced
- Define the desired polymer characteristics.
- Particle level mass transfer modeling

Other Work

- Paper for conference or journals. Get the preliminary data (like fundamental model equations and experimental results compiled and constantly updated)
- Alternative catalysts and their advantages
- Look for novel polymer applications
- Begin work flow and heat transfer modeling.

6. References

[1] Development of a Microchannel In Situ Propellant Production System- September 2005 Prepared for the National Aeronautics and Space Administration Lyndon B. Johnson pace Center by KP Brooks, SD Rassat and WE TeGrotenhuis

[2] Catalytic synthesis of hydrogen peroxide in microreactors, Chemical Engineering Research and Design, volume 86, Issue 4, April 2008, Pages 410-415. S. Maehara, M. Taneda, K. Kusakabe

[3] Kinetics of hydrogen peroxide synthesis by direct combination of H2 and O2 in a microreactor, Catalysis Today, Volume 125, Issues 1-2, 15 July 2007, Pages 40-47 Yury Voloshin, Raghunath Halder, Adeniyi Lawal

[4] Auto-oxidation production of hydrogen peroxide via oxidation in a microreactor United States Patent 7416718, Sethi, Dalbir S. (Cranbury, NJ, US), Dada, Emmanuel A. (Bensalem, PA, US), Hammack, Kevin (League City, TX, US), Zhou, Xinliang (Sugar Land, TX, US)

[5] Experimental studies on hydrogenation of anthraquinone derivative in a microreactor Catalysis Today, Volume 125, Issues 1-2, 15 July 2007, Pages 48-55 Raghunath Halder, Adeniyi Lawal

[6] Chinese Journal of Chemical Engineering, 16(4) 503-516 (2008), “A State-of-the-Art Review of Mixing in Microfluidic Mixers” , Elmabruk A. Mansur, YE Mingxing , WANG Yundong and DAI Youyuan, The State Key Laboratory of Chemical Engineering, Department of Chemical Engineering, Tsinghua University,Beijing 100084, China.

[7] Morini, G.L., “Viscous heating in liquid flows in micro-channels”, Int. J. Heat Mass Transfer, 48, 3637-3647 (2005).

[8] Judy, J., Maynes, D., Webb, B.W., “Characterization of frictional pressure drop for liquid flows through microchannels”, Int. J. Heat Mass Transfer, 45, 3477-3489 (2002).

[9] Glasgow, I., Batton, J., Aubry, N., “Electroosmotic mixing in microchannels”,Lab Chip, 4, 558-562 (2004).

[10] Engler, M., Kockmann, N., Kiefer, T., Woias, P., “Numerical and experimental investigations on liquid mixing in static micromixers”,Chem. Eng. J., 101, 315-322 (2004).

[11] Yu, H.Y., Xiao, S.S., Chen, H., Fan, S.F., “Influence of flow velocity profile on mixing in micromixer”, Nanotechnology and Precision Engineering (China), 3 (4), 290-294 (2005). (in Chinese).

[12] Bothe, D., Stemichb, C., Warnecke, H., “Fluid mixing in a T-shaped micro-mixer”, Chem. Eng. Sci., 61, 2950-2958 (2006).

[13] Zhao, Y.C, Ying, Y., Chen, G.W., Yuan, Q., “Characterization of micro-mixing in T-shaped micro-mixer”, J. Chem. Ind. Eng. (China),57, 1884-1890 (2006). (in Chinese).
[14] Goullet, A., Glasgow, I., Aubry, N., “Effects of microchannel geometry on pulsed flow mixing”, Mech. Res. Commun., 33, 39-746 (2006).
[15] Johnson, T., Ross, D., Locascio, L., “Rapid microfluidic mixing”,Anal. Chem., 74, 45-51 (2002).
[16] Seok Woo Lee, Dong Sung Kim2, Seung S. Lee, and Tai Hun Kwon, “SPLIT AND RECOMBINATION MICROMIXER BASED ON PDMS THREE-DIMENSIONAL MICRO STRUCTURE”, Korea Advanced Institute of Science and Technology, Pohang University of Science and Technology.
[17] The Engineering ToolBox, “Thermal Conductivity of some common Materials”, Online Resources, Tools and Basic Information for Engineering and Design of Technical Applications, Available at: http://www.engineeringtoolbox.com/thermal-conductivity-d_429.html Lass accessed on July 17, 2009
[18] DuPont Teflon fluoropolymer manufacturer, Fluoropolymer Typical Properties, available online at: http://www2.dupont.com/Teflon_Industrial/en_US/tech_info/techinfo_compare.html last accessed on July 17, 2009
[19] Rodgers P, 2009, “MEEG376 Core measurements Uncertainty analysis”, The Petroleum Institute, spring 2009
[20] A.Y. Tonkovich, S. Perry, D. Qiu, T. LaPlante, W.A. Rogers, Microchannel process technology for compact methane steam reforming. Velocys, Inc., Technology Development, 7950 Corporate Drive, Plain City, OH 43064, USA. Y.Wang (Battelle, Pacific Northwest National Laboratory, Richland, WA 99352, USA)
[21] “The discovery and progress of MgCl2-supported TiCl4 catalysts”. N. Kashiwa, J. Polym. Sci. A: Polym. Chem. 42 (1–8) (2004) 1.
[22] J.J.A. Dusseault, C.C. Hsu, J. Macromol. Sci. Rev. Macromol. Chem. Phys. C 33 (2) (1993) 103.
[23] S. Kojoh, T. Fujita, N. Kashiwa, Recent Res. Dev. Polym. Sci. 5 (2001) 43.
[24] J.T.M. Pater, G. Weickert, J. Loos, W.P.M. van Swaaij, Chem. Eng. Sci. 56 (2001) 4107.
[25] J.T.M. Pater, G.Weickert,W.P.M. van Swaaij, J. Appl. Polym. Sci. 87 (2003) 1421.
[26] G.Weickert, G.B. Meier, J.T.M. Pater, K.R.Westerterp, Chem. Eng. Sci. 54 (1999) 3291.
[27] L. Noristi, E. Marchetti, G. Baruzzi, P. Sgarzi, J. Polym. Sci. A: Polym. Chem. 32 (1994) 3047.
[28] X. Zheng, J. Loos, Morphology evolution in the early stages of olefin polymerization, Macromol. Symp., 236, 249-258, (2006).
[29] X. Zheng, M.S. Pimplapure, G. Weickert, J. Loos, Influence of porosity on the fragmentation of Ziegler-Natta catalysts in the early stages of propylene polymerization, e-Polym., 028, 1-10, (2006).
[30] M. Bartke, in: J.R. Severn, J.C. Chadwick (Eds.), Tailor-Made Polymers. Via Immobilization of Alpha-Olefin Polymerization Catalyst, Wiley–VCH Verlag GmbH & Co. KGaA,Weinheim, 2008.
[31] G. Cecchin, E. Marchetti, G. Baruzzi, Macromol. Chem. Phys. 202 (2001) 1987.
[32] Adiwinata G., Prashant M., Panagiotis D. C., Fault-tolerant control of a polyethylene reactor, Journal of Process Control 17 (2007) 439–451

Appendix

Justification and Background

Microreactors form a basis for the potential future downscaling of existing chemical processes, allowing tremendous reductions in capital and operating cost. They provide finer control of conditions, allow for faster process times, and improve safety in operation. Also, they should not encounter a significant problem in scaling from laboratory-sized systems to commercial-sized systems, since their operating principle will simply allow them to be stacked together modularly.

Of critical importance to the microreactors' capability to make the jump into industrial applications is the mixing efficiency, which controls the reaction rates and the yield expected from a reactor. Due to the scale of the systems, laminar flow is almost always encountered, which means that the vortices typically associated with turbulent flow are often missing. Instilling vortices into the flows to encourage mixing is accordingly a matter of construction of mixer channels.

Correct design parameters of microreactor influence the process yield. Designing microreactor for appropriate reaction conditions is very important for the reactions to be fast. Microreactors can be energy efficient too by appropriately designing and visualizing heat transfer. The channel dimensions have direct impact on diffusive mixing of reactants.

Approach

- Literature survey of the microreactor technologies as well as microchannel fabrication technologies.
- Selection of the target process for realization in microreactors with maximum benefit.
- Selection of microchannel fabrication technology suitable for microchannel mass production.
- Design and fabrication of a microreactor using microchannel fabricating technology suitable for mass production.
- Microreactor demonstration.
- Prepare experimental set-up and conduct the experiments.

Two-Year Schedule

Year 1:

- Conduct literature review to study current technologies for micoreactors, micromixers, and incorporation of catalysts into microreaction technology.
- Evaluate existing microchannel formation techniques and their applications to microreactor construction.
- Selection of the target process for realization in microreactors with maximum benefit to ADNOC.
- Selection of microchannel manufacturing process most suitable for mass production.
- Preparation of a microreactor testing facility.
- Visualization study of mixing in microchannels.

Year 2:

- Literature survey of the olefin polymerization technologies focus on microchannels
- Selection of the target polymerization process for realization in microreactors with maximum benefit.
- Design and fabrication of a microreactor capable of realization of selected polymerization process
- Select type and size of catalyst particles to be used in the process

- Investigate propagation of selected catalyst particles in microchannels
- Investigate polymerization and polymer particle behavior in microchannels
- Parametric study of polymerization process at different temperatures, catalyst and reactant concentration.
- Microreactor demonstration.
- PI-side participation:

1. Selection in cooperation with Borouge of the catalyst for the target polymerization process for realization in microreactors.
2. Prepare a microreactor testing facility.
3. Visualization study of mixing in microchannels
4. Combine PI/UMD testing of the microreactor
5. Microreactor demonstration to ADNOC representatives
6. Prepare final project report and recommendations.

Thrust 3
Energy System Management

Integration of Engineering and Business Decisions for Robust Optimization of Petrochemical Systems

UMD Investigators: Shapour Azarm, P.K. Kannan
PI Investigators: Ali Almansoori, Saleh Al Hashimi
UMD GRA: Weiwei Hu
PI GRA: Adeel Butt
Acknowledgement: Zhichao Wang, Khaled Saleh
Start Date: Oct 2006

1. Objective/Abstract

The overall objective of this project is to develop a framework for integrating engineering and business decisions. In view of this objective, a robust decision support system is being developed that can be used for multi-objective and multi-disciplinary optimization and sensitivity analysis under uncertainty in oil, gas and petrochemical systems. In this quarter, the Decision Support System (DSS) framework with dashboard was further improved for oil refinery performance management. Under the proposed framework, the decision-maker and dashboard served as two independent decision-making agents; however, each agent's decision was contingent on the decisions made by the other agent. By way of a case study, it was shown that as the two agents interacted with each other; using the proposed approach, the performance of the refinery model gradually reached an equilibrium state and the final converged decisions for engineering and business operations were obtained. To alleviate the computational cost in the optimization-based DSS, a previously developed Approximation Assisted Multi-Objective Robust Optimization (AA-MORO) approach was implemented. AA-MORO allowed the dashboard and the proposed DSS framework to be applied in an efficient and practical manner. Two case study scenarios were used to demonstrate the applicability of the dashboard in oil refinery management. For the case study considered, it was shown that the decision-maker was able to make informed decisions using the dashboard while increasing profit at the oil refinery plant.

2. Deliverables for the Completed Quarter

- Continued the development of the dashboard for oil refinery performance management, with user-interface and improved functions:
  - Extended the previous dashboard framework by considering interactions between the decision-maker and the optimization-based decision support system.
  - Refined the decision support role of dashboard and introduced additional functions for user-interface.

- Implemented and integrated a non-regret learning algorithm for simulating the decision-making process by the decision-maker:
  - Developed a decision strategy function that was used to represent the likelihood that the decision-maker selects a particular value for a decision variable.
  - The decision strategy function was updated according to a profit model for a process example in oil refinery.

- Developed and tested two case study scenarios for a demonstration of dashboard:

  - The case study showed the applicability of the proposed dashboard for oil refinery performance management.
  - The case study results indicated that the decision-maker was able to make more informed decisions and improve profit.

- Submitted an abstract titled “An Agent-Based Approach to an Integrated Corporate Dashboard for Oil Refinery” to the Canadian Society of Chemical Engineering Conference 2011.

- Finished and submitted an abstract of a book chapter titled “Robust Multi-Objective Genetic Algorithm with Interval Uncertainty.”

- Progress on recent joint publications:

  Journal Papers:

  [1] Hu, W., M. Li, Azarm, S. and Almansoori, A., 2011, "Multi-Objective Robust Optimization Under Interval Uncertainty Using Online Approximation and Constraint Cuts," Journal of Mechanical Design, 133(6), pp. 061002-1 to 061002-9.

  [2] Hu, W., A. Almansoori, Kannan, P.K., Azarm, S. and Wang, Z. 2010, "Corporate Dashboards for Integrated Business and Engineering Decisions in Oil Refineries: an Agent-Based Approach" Decision Support Systems, submitted, under revision.

  Working Conference Presentation:

  [3] Butt, A., Almansoori, A., Elkamel, A., Hu, W., Wang, Z., Kannan, P.K. and Azarm, S., "An Agent-Based Approach to an Integrated Corporate Dashboard for Oil Refinery," Canadian Society of Chemical Engineering Conference, October 23–26, 2011, London, Ont.

  Working Journal Papers:

  [4] Hu, W., Azarm, S. and Almansoori, A., 2011, "Uncertain Interval Reduction Approach with Multi-Objective Robust Optimization with Online Approximation," under preparation.

  [5] Hu, W., Azarm, S. and Almansoori, "Approximation Assisted Multi-objective collaborative Robust Optimization (AA-McRO) under Interval Uncertainty," to be submitted to Structural of Multidisciplinary Optimization.

  Working Book Chapter:

  [6] Hu, W., Butt, A., Azarm, S., Almansoori, A. and A. Elkamel, 2011, *Robust Multi-Objective Genetic Algorithm under Interval Uncertainty*, in *Multi-Objective Optimization: Techniques and Applications in Chemical Engineering*, Abstract submitted.

3. Summary of Project Activities for the Completed Quarter

Project meetings held during the ninth quarter were as follows:

- Three teleconference meetings were held between PI and UMD research collaborators on April 25, May 23 and June 1, with Adobe Connection. Highlights of these meetings include:

  (1) Professor Elkamel from PI joined our PI-UMD research collaboration.
  (2) Mr. Adeel Butt from PI planned to visit and work with the UMD team during the summer semester on the research project.

(3) The decision support role of the oil refinery dashboard was refined by taking into consideration manager's decision based on a learning algorithm. The revised model was demonstrated with an oil refinery case study.
(4) Progress on joint publications was reported. The paper on the decision support system has been revised (a rebuttal was being prepared). The paper on multi-objective collaborative robust optimization was revised and under review by Profs. Almansoori and Azarm.
(5) PI proposed to draft a book chapter with a topic in "Multi-Objective Optimization: Techniques and Applications in Chemical Engineering." The proposed book chapter was based on a robust multi-objective genetic algorithm with a comprehensive literature review. Some chemical engineering examples were planned to be developed and included in this chapter.

Research efforts in this quarter included the following:

- Continued developing the dashboard for oil refinery performance management, with user-friendly interface and improved functions.

The conceptual layout of the improved dashboard for oil refinery performance management is shown in Figure 1. One important role of the dashboard is to visualize Key Performance Indicators (KPIs). For example, profit from sales of end product is an indicator of how efficient the company is in turning investment into net income and which products are driving profits. Similarly, stock-out cost and production figures inform the decision-maker how well the production capacity is able to meet market demands. With the current and historical KPIs presented on the dashboard, the decision-maker is able to see the oil refinery's overall performance firsthand. In addition, the dashboard allows decision-makers across various departments to coordinate and implement decisions. When there is a significant deviation on KPIs from their normal value, decision-makers can take actions by changing the selected decision variables through the sliders on dashboard. Since there many decision variables need to be considered in an oil refinery, it is impractical for decision-makers to control all decisions manually on the dashboard. Instead, the proposed decision support framework integrated a multi-objective optimization to obtain optimum decisions for the variables that are not controlled by the decision-makers. The optimum solutions are presented to the decision-makers through dashboard.

Figure 1. Conceptual layout of dashboard for oil refinery performance management.

Figure 2 shows the decision support role of the dashboard in an integrated decision support framework, where x_1 and x_2 represent decision variables controlled by the decision-maker and dashboard, respectively. Particularly, the values of x_1 are determined according to the decision-maker's expertise and previous experience while the value of x_2 is selected based on the optimum solutions from the Approximation Assisted Multi-Objective Robust Optimization (or AA-MORO), which is integrated in the dashboard. When making decisions, the decision-maker needs to consult with the information presented on the dashboard in order to achieve certain goals, e.g. to maintain all the KPIs in the oil refinery at their normal level and to ensure the refinery is profitable. It should be noted, however, that any decision from the decision-maker must comply with market laws, regulations, and other constraints. Furthermore, the objective functions in AA-MORO must be consistent with the goal of the decision-maker. For example, maximizing profit from sales and maximizing the purity of an end-product are the two primary goals in the case study presented later in this report. These goals, such as the profit and the purity, are functions of the decision variables.

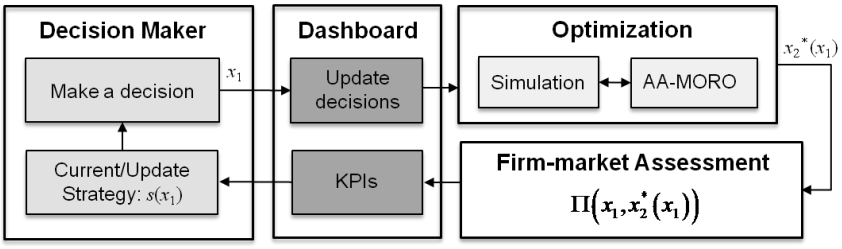

Figure 2. The decision support role of dashboard.

With the help of the dashboard, the decision-making process started with an initial set of decisions (x_1) determined by the decision-maker. The values of decisions (x_1) are updated on the dashboard and then passed on to simulation in the "Optimization" block, as shown in Figure 2. Next, AA-MORO searches for the robust optimum decisions based on the simulation for the given

decisions (x_1) made by the decision-maker earlier. Note the output from the "Optimization" block is the optimum value of decisions which are not controlled by the decision-maker. Therefore, the optimum decisions (or x_2*) is essentially a function of x_1, as represented by x_2*(x_1) in Figure 2. Next, x_2* is forwarded to the oil refinery, where $\prod(x_1, x_2^*(x_1))$ represents profit functions for the given optimum decisions x_2*(x_1) and current value of x_1. Based on the interaction between the oil refinery and market, the profit value is recorded and sent to the dashboard as one of the KPIs. Upon observing profit and the other KPIs on dashboard, the decision-maker needs to update the decision strategy function $s(x_1)$. According to the updated strategy function, the decision-maker determines a new decision on x_1 and updates decisions on the dashboard. Afterwards, the previous steps are repeated until plant performance reaches an equilibrium state or the desired values of KPIs has been achieved.

- Integrated a non-regret learning algorithm for simulating the decision-making process by the decision-maker.

A no-regret learning algorithm is adapted for the decision-making model. It is assumed that any decisions made by the decision-maker follow a decision strategy function. The decision-maker exhibits learning behavior, i.e., updates his/her decision strategy by iteratively making decisions and observing payoffs. We define "action" as the decision, i.e. x_1^k, made in the k'th iteration. We also define "strategy", i.e., $s(x_1)$, as a probability density function representing the likelihood that the decision-maker chooses an action x_1. By letting the decision-maker exhibit learning behavior, we account for the fact that the decision-maker may deviate from making optimal decisions by anticipating the future. In addition, we consider the decision-maker and the dashboard as two decision-makers who collectively affect the firm's profit. The decision-maker's decision is made by learning from the past whereas the dashboard's decision is driven by AA-MORO. It should be noted that a variety of other learning algorithms are also applicable to modeling the decision-making process. In the following, we present the equations used in a non-regret learning algorithm.

Let $\prod(x_1, x_2)$ denote the profit function for the refinery. The decision-maker's payoff function is set to be identical to profit. In every iteration, the decision-maker first computes a regret function defined as:

$$R^k(x_1) = \frac{1}{k}\sum_{t=1}^{k}\left(\Pi(x_1, x_2^t) - \Pi(x_1^t, x_2^t)\right) \quad (1)$$

The regret function reflects the average increase in profit if an action has been always played in previous iterations. The strategy function, i.e. the probability of playing x_1 in the following iteration, is proportional to the regret:

$$s^k(x_1) = \frac{\left[R^k(x_1)\right]^+}{\sum_{x_1 \in X_1}\left[R^k(x_1)\right]^+} \quad (2)$$

in which:

$$\left[R^k(x_1)\right]^+ = \begin{cases} 0, & \text{if } R^k(x_1) \le 0 \\ R^k(x_1), & \text{if } R^k(x_1) > 0 \end{cases} \quad (3)$$

Equations (1) and (2) assume that the decision variable x_1 is discrete. In case the x_1 is continuous, the summation (denominator) on the right-hand side of Equation (2) will be replaced with an integration procedure. When the decision-maker makes a decision, i.e. playing an action, it essentially draws a sample from the updated strategy function defined in Equation (2).

Case Study

This case study is intended to demonstrate the procedure that decision-maker uses to control the dashboard. It is shown that the dashboard allows decision-makers to make better decisions. The simulation used in the dashboard includes both business and engineering models and have been developed beforehand in NetLogo and HSYSY respectively. The simulation models were used to simulate how a refinery plan will react to oil market for a given set of decision variables. For example, the input to the engineering simulation includes three decision variables: mass flow rate of feed air, pressure of cooled mixture and phthalic column reflux ratio, one uncertain parameter: temperature of feed stream to phthalic distillation column, and the feed flow rate of o-xylene (obtained as a output from the business simulation). The output to the engineering simulation includes the purity and flow rate of phthalic anhydride. The input to the business simulation includes three decision variables: daily crude oil purchase, percentage of crude oil sold to external market, percentage of inventory storage sold to external market, one uncertain parameter: price of phthalic anhydride in external market, and the flow rate of phthalic anhydride (obtained as a output from the engineering simulation). The output of the business simulation includes profit and the feed flow rate of o-xylene. In the case study, the engineering and business simulations are connected through an interface program developed in Matlab, which is used to run both simulations programmatically and exchange information between Netlogo and Aspen HYSYS.

- Formulation of Multi-Objective Optimization

Based on the engineering and business simulations, a multi-objective optimization problem is formulated to maximize profit (business objective) and maximize the purity of phthalic anhydride (engineering objective), as defined in Equation (4):

$$
\begin{aligned}
&\underset{x_{2,i}}{\text{Maximize:}} \ \text{Profit (objective 1)} \\
&\underset{x_{2,i}}{\text{Maximize:}} \ \text{Purity of phthalic anhydride (objective 2)} \\
&\text{Subject to:} \ \text{Business (e.g. inventory) constraints} \\
&\qquad\qquad \text{Engineering (e.g. pressure) constraints} \\
&\qquad\qquad \text{Uncertainty in parameters (e.g. price, temperature)} \\
&\qquad\qquad \text{Lower and upper bounds on } x_{2,i} \text{ , } i=1,...,5
\end{aligned}
\tag{4}
$$

Using the AA-MORO approach, $x_{2,i}$, i=1,…,5 (including both business and engineering decision variables) is optimized in a multi-objective optimization framework. Since we consider uncertainties in the business and engineering parameters, the optimizer must also eliminate decisions that are not robust (or too sensitive) to the uncertainty. In the following, we consider two case study scenarios; i.e., in the first scenario, we assume that the decision-maker determines the value of x_1 manually, while in the second scenario, a non-regret learning algorithm replaces a human decision-maker in the decision-making process.

- Scenario 1: x_2 is determined by the decision-maker

In scenario 1, the value of daily crude oil input (x_1) was determined by the decision-maker. A total of four iterations were simulated with the value of daily crude oil input equal to four discrete values: 9.2×10^4, 9.4×10^4, 9.6×10^4 and 9.8×10^4 bbl/day. In each of the iterations, the decision-maker first adjusted the decision control bar to update the decision. The dashboard then forwarded the daily crude oil input as fixed value to the simulation model. Next, the decision-maker engaged the “optimization” level on the dashboard to initiate AA-MORO and obtain the multi-objective robust optimal solutions. After that, the decision-maker was required to select one desirable solution from a set of optimum solutions based on the objective values. After the optimum decision is selected, the optimum values for the decision variables were implemented in

the oil refinery by the dashboard.

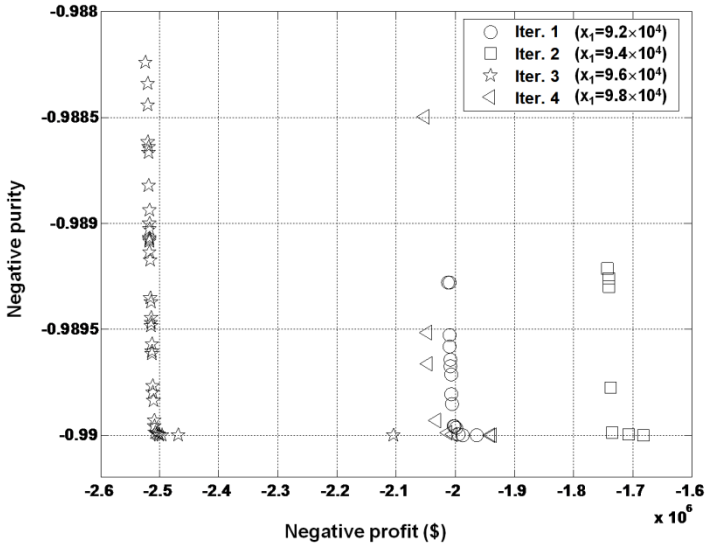

Figure 3. Optimum design solution for case study scenario 1.

Figure 3 shows the optimum solutions in the objective function space with four different iterations characterized by different values of daily crude oil input. It can be seen that the two objective functions, profit and purity, are in conflict with each other. Therefore, as profit increases (its negative value decreases), the purity of phthalic anhydride decreases (its negative value increases). Comparing the optimum solutions with different values of daily crude oil input, their range in purity of phthalic anhydride (the second objective function) is similar. However the largest profit (the first objective function) is achieved when the amount of daily crude oil input is 9.6×104 bbl/day in iteration 3.

- Scenario 2: x_2 is determined by non-regret learning

In scenario 2, instead of the decision-maker manually determining the value of daily crude oil input (decision on x_1), a non-regret learning algorithm was used to simulate and replace the decision-making process. Based on the non-regret learning, a total of 300 iterations were simulated. In each iteration, a sample was first drawn from the strategy function $s(x_1)$ which was characterized as a distribution profile (PDFs). Drawing a sample from the strategy function was comparable to the procedure in which the decision-maker makes a decision. As soon as the dashboard was informed of the new decision, it forwarded it to the simulation model. Similar to scenario 1, AA-MORO obtains robust optimum solutions, and it was assumed that the decision-maker always selected a solution with maximum profit. When the selected solution was implemented, the outcome profit was used to update the strategy function from which another sample (decision) was drawn, and the iteration continued.

The simulated distribution profiles (PDFs) for $s(x_1)$ in iterations 10, 50, 150 and 300 are shown in Figure 4. It can be seen that initially (i.e., in iteration 10), the distribution profile is diffusive because the decision-maker has no information about the past. By iteratively making decisions through interacting with the dashboard and observing the outcome (profit), the decision-maker gradually shifts his/her decision to a more profitable position, as represented by the shift of distribution of the PDFs. Furthermore, the shrinkage of the distribution profile reflects that the decision-maker strengthens her/her belief on the more profitable decisions.

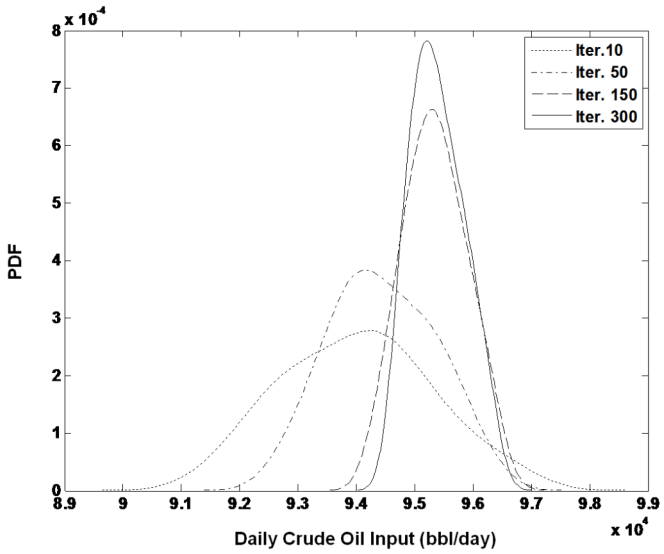

Figure 4. Simulated distribution profile (PDFs) of daily crude oil input.

Note that in reality, a decision-maker's learning process may not follow the no-regret learning algorithm exactly. The simulation in Scenario 2 is primarily aimed at demonstrating how a human decision-maker and an automated decision agent (i.e., AA-MORO) can interact and collectively improve a firm's performances (e.g., profit), even though the DSS framework based on AA-MORO and dashboard, as proposed in this research, is still applicable.

4. Difficulties Encountered/Overcome

The dashboard for oil refinery performance management considers both a human decision-maker and an optimization-based automated decision support system (DSS). The computational cost in the optimization-based DSS was alleviated using an approximation-assisted optimization approach, i.e. AA-MORO. AA-MORO makes it very practical to implement the dashboard in the real-world. However, computational difficulty arose when we designed two case study scenarios to demonstrate the applicability of dashboard. Particularly in the second case study scenario, a non-regret learning algorithm required many simulation calls to calculate the regret function for profit and update the decision strategies. These simulation calls made the second case study scenario intractable. To overcome this difficulty, a surrogate model was used to approximate the actual simulation. While constructing the surrogate model for the case study, we used a fixed number of sample points and validated the surrogate to ensure its accuracy to within an acceptable range. Because the surrogate model was rather inexpensive compared to the actual simulation, the computation cost for running the non-regret algorithm became computationally affordable.

5. Planned Project Activities for the Next Quarter

- Develop a heat-integrated simulation process using HYSYS and increase complexity to the current process by considering its applicability to processes used by ADNOC companies.
- Formulate an approximation-assisted multi-objective robust optimization problem with uncertainty based on the update on the HYSYS simulation model and obtain optimum solutions.
- Continue improving dashboard based on the update in the engineering models.

- Revise and submit the paper in multi-objective collaborative optimization and continue working on the remaining papers.
- Develop a schedule for writing the proposed book chapter, including developing and testing of a few chemical engineering applications.
- Create a draft for the sections in the book chapter, covering literature review, techniques and methodologies.

6. References

[1] Anderson, S. P., Palma, A.d., and Thisse, J., 1992, “Discrete Choice Theory of Product Differentiation”, Cambridge, MA, MIT Press, 1992.

[2] Aspen HYSYS, 2009, http://www.aspentech.com, Aspen Technology.

[3] Deb, K., 2001, Multi-Objective Optimization using Evoluionary Algorithms, John Wiley & Sons, Ltd, New York.

[4] Douglas, J.M., 1988, “Conceptual Design of Chemical Processes”, McGraw-Hill, New York, USA.

[5] Forbes, R.J., 1948, “Short History of the Art of Distillation”, Brill, Leiden, Holland.

[6] Gargeya, V., 2005, “Plant Level Performance Measurement: An Exploratory Case Study of a Pharmaceutical Encapsulation Company”, Technovation, 25(12), pp.1457-1467.

[7] Gattu, G., Palavajjhala, S., and Robertson, D., 2003, “Are Oil Refineries Ready for Non-Linear Control and Optimization?” International Symposium on Process Systems Engineering and Control, Mumbai, India.

[8] Grossmann, I. E., 2005, “Enterprise-Wide Optimization: A New Frontier in Process Systems Engineering,” AIChE Journal, 51(7), pp. 1846-1857.

[9] Halemane K. P., Grossmann I. E., 1983, “Optimal Process Design under Uncertainty,” AIChE Journal, 29(3), pp. 425-433.

[10] Hu, W., M. Li, Azarm, S. and Almansoori, A., 2011, "Multi-Objective Robust Optimization Under Interval Uncertainty Using Online Approximation and Constraint Cuts," Journal of Mechanical Design, 133(6), p. 061002.

[11] Jackson, J., Hofmann, J., Wassick, J. and Grossmann, I., 2003, “A nonlinear multi-period process optimization model for production planning in multi-plant facilities”, Proceedings FOCAPO2003, pp. 281-284..

[12] Janak, L., Lin, X. and Floudas, C. A., 2007, “A New Robust Optimization Approach for Scheduling Under Uncertainty: II. Uncertainty with Known Probability Distribution,” Computers and Chemical Engineering, 31(3), pp. 171-195.

[13] Kaplan, R. and Norton, D., 1996, “Using the Balanced Scorecard As a Strategic Management System”, Harvard Business Review, 74(1), pp. 75-85.

[14] Kleijnen, J. and Smits, M., 2003, “Performance metrics in supply chain management”. Journal of the Operational Research Society, 54(5), pp. 507–514.

[15] Koehler, J.R., Owen, A.B., 1996, "Computer Experiments," Handbook of Statistics, Elsevier Science, New York. pp. 261-308.

[16] Lin, X., Janak, S. L. and Floudas, C. A., 2004, “A New Robust Optimization Approach for Scheduling Under Uncertainty: I. Bounded Uncertainty,” Computers and Chemical Engineering, 28(6-7), pp. 1069-1085.

[17] Li, M., and Azarm, S., 2008, "Multiobjective Collaborative Robust Optimization with Interval Uncertainty and Interdisciplinary Uncertainty Propagation," Journal of Mechanical Design, 130(8), p. 081402.

[18] Li, M., N. Williams and Azarm, S., 2009, "Interval Uncertainty Reduction and Single-Disciplinary Sensitivity Analysis With Multi-Objective Optimization," Journal of Mechanical Design, 131(3), p. 031007.

[19] Micheletto, S. R., Carvalho, M. C. A. and Pinto, J. M., 2008, “Operational Optimization of the Utility System of an Oil Refinery,” Computers and Chemical Engineering, 32(1-2), pp. 170-185.

[20] Netlogo, http://ccl.northwestern.edu/netlogo/

[21] Pinto, J., Joly, M. and Moro, L., 2000, “Planning and scheduling models for refinery operations”, Computers and Chemical Engineering, 24(9), pp. 2259–2276.
[22] Sahdev, M., Jain, K., Srivastava, P., “Petroleum Refinery Planning and optimization Using Linear Programming”, The Chemical Engineers' Resource Page, http://www.cheresources.com/refinery_planning_optimization.shtml
[23] Simpson, T. W., and Mistree, F., 2001, “Kriging Models for Global Approximation in Simulation-Based Multidisciplinary Design Optimization," AIAA Journal, 39(12), pp. 2233-2241.
[24] Suresh, S. Pitty, Li, W., Adhitya, A., Srinivasan, R., Karimi, A., 2008, “Decision support for integrated refinery supply chains”, Computer and Chemical Engineering, 32, pp. 2767–2786.
[25] Z. Wang, S. Azarm, and P. K. Kannan, 2011, “Strategic Design Decisions for Uncertain Market Systems Using an Agent Based Approach,” Journal of Mechanical Design,” 133(4), p. 041003

Appendix

Justification and Background

Many oil, gas and petrochemical systems involve numerous coupled subsystems. These systems and their subsystems usually have uncertain inputs and thus it can be difficult to make the "best" engineering and business decisions in terms of independent operations of these complex systems. It becomes even more difficult to make those decisions when the system consists of many units or plants producing different products. This difficulty presents an opportunity taken on in this project. A review of mainstream literature has revealed that previous models in management of petrochemical systems have been based on either engineering or business decisions but not both. There is a significant gap in the literature as to how these two types of decisions should be devised and integrated. To address this important gap, the focus of this investigation is to develop an integrated robust decision support framework considering both engineering and business models under uncertain conditions. Our overall objective has several underlying research questions, including: (i) how to develop business models that include management decisions in a multi-unit organization and at the same time account for engineering aspects; (ii) how to determine the relative importance and effects of uncertain system and/or subsystem input parameters on subsystem and/or system outputs (e.g., system performance); (iii) how to define a set of metrics, by way of a dashboard, that will serve as a visualization tool to keep track of a company's financial status in view of competition and market systems and provide for easy communication between various levels in the company, and (iii) how to extend our current single-level robust optimization method to multi-subsystem problems and maintain reasonable computational complexity for the method. These underlying questions and corresponding investigations will be organized into tasks throughout the time frame allocated to the project. The details of these tasks are explained in the next section.

Approach

There are two main tasks in this investigation as detailed in the following.

Task 1 (PI):
Develop and implement engineering analysis models, in a Matlab (or Matlab compatible) environment, for a crude distillation unit case study model.

- Task 1.1: Develop a multi-input multi-output analysis model for a representative petrochemical system with corresponding subsystem analysis models.
- Task 1.2: Extend the analysis model in Task 1.1 to include: (i) additional complexity, (ii) subsystem details and uncertainty to include reasonable representation of engineering side of a plant. The ultimate goal is to develop an integrated multi-subsystem petrochemical analysis model for a plant or a group of units in a plant.

Task 2 (UMD):
Develop and implement a Robust Decision Support System (RDSS).

Engineering Tasks

- Task 2.1: Develop a single level (all-at-once) approximation-assisted robust optimization technique that is able to significantly reduce the computational efforts of making robust decisions.
- Task 2.2: Demonstrate an application of the approach from Task 2.1 with a case study in petrochemical systems which will be developed by PI as a part of Task 1.
- Task 2.3: Develop an approximation assisted multi-objective multi-disciplinary robust optimization approach, which is an extension to Task 2.1.
- Task 2.4: Demonstrate an application of the approach from Task 2.3 with a case study in petrochemical systems which will be developed by PI as part of Task 1.

Business Tasks

- Task 2.5: Develop business models in Netlogo and/or Matlab and solve a simplified refinery supply chain optimization problem with Matlab.
- Task 2.6: Develop a Dashboard and test the robustness and sensitivity of the Dashboard's elements for the model in Task 2.5.

Integration Tasks

- Task 2.7: Inspect engineering and business problems to determine coupling variables between two problems.
- Task 2.8: Integrate Tasks 2.1 to 2.4 with Tasks 2.5 to 2.6 to formulate a refinery optimization problem that considers both engineering and business objectives and constraints.
- Task 2.9: make the supply chain management problem more realistic by considering more decision levels, more finished products and a wider market, and by increasing the size of the refinery's internal network and then repeat Task 2.8.
- Task 2.10: Verify and validate the integrated model.

Dynamics and Control of Drill Strings

UMD Investigator: Balakumar Balachandran
PI Investigators: Hamad Karki and Youssef Abdelmagid
GRA: Chien-Min Liao (started in Spring 2007)
Other Participants: Nicholas Vlajic
Start Date: Oct 2006

1. Objective/Abstract

Drill-string dynamics need to be better understood to understand drill-string failures, control drill-string motions, and steer them to their appropriate locations in oil wells. Although a considerable amount of work has been carried out on understanding drill-string vibrations (for example, Leine and van Campen, 2002; Melakhessou *et al*., 2003; Spanos *et al*., 2003; Liao *et al*., 2009), the nonlinear dynamics of this system are only partially understood given that the drill string can undergo axial, torsional, and lateral vibrations, and operational difficulties include sticking, buckling, and fatiguing of strings. In addition, the prior models focus on either bending or torsional or axial motions. Hence, it is important to consider coupled axial-bending-torsional vibrations and contact instability in oil and gas well drilling. A better understanding of these vibrations can help keep the drill string close to the center of the borehole and help realize near-circular bores during drilling operations.

The overall goal of the proposed research is to understand the nonlinear dynamics of the drill string and develop a control-theoretic framework for its stabilization enabling energy efficient drilling with longer life span for the equipment. Specific research objectives of this project are the following: i) building on Phase I efforts, develop and study control-oriented models for the drill strings through analytical and numerical means, ii) investigate the control of an under-actuated nonlinear system (drill string) with complex interactions with the environment, and iii) use the drill-string test-beds constructed at the Petroleum Institute (PI) & the University of Maryland (UMD) to validate the analytical findings and suggest possible strategies to mitigate drill-string failures in fixed and floating platform environments.

2. Summary of Results

In the previous report, the investigators presented a distributed parameter model, which can be adapted to study horizontal drilling dynamics. Additionally, a novel drill string-wellbore force model was introduced, and the phenomenon predicted by the model was also observed in the experimental apparatus during similar operating conditions. The current report expands on the model previously presented by specifically explaining what motions the model is able to capture. Most notably, the model is able to predict backward whirling while in contact with the outer shell. This specific motion, which is thought to be detrimental to the drill string, is explained in detail later in this document.

To date, most of the research has focused on the nonlinear interactions between the drill string and wellbore while drilling in a vertical configuration. However, other nonlinearities may exist due to the geometry of the structure itself. These geometric nonlinearities become even more pronounced for horizontal drill strings. Therefore, preliminary experimental results are shown for a vertical drill string in the absence of an outer shell. This allows the authors to explore the dynamic effect that is due to geometry, and this effect is expected to play a dominant role in horizontal drilling.

The rest of this section is organized as follows. In Section 2.1, further details of the drill string-wellbore force interaction model are given. In Section 2.2, modifications made to enhance the experimental apparatus are explained, and experimental results that provide evidence for the presence of geometric nonlinearities are given. In Section 2.3, an outline of future work is provided.

2.1 Force-Interaction Model

A novel force-interaction model was presented in the previous report, and the numerical predictions provided were found to be in good agreement with experimental data. In the current section, some of the phenomena that are captured by this model id discussed. This discussion is used to explain the physics underlying the dynamical behavior, which assists in interpreting the experimental results and can also serve as a basis for determining operating procedures for drilling operations.

2.1.1 Force-Interaction Model

A schematic depicting the forces acting on a section of the drill string while in contact with the other shell is shown in Figure 1. Also, in order to reacquaint the reader, some of the relevant equations are revisited. The normal and tangential force components acting on the rotor are determined, after first introducing the following definitions:

$$\delta = \frac{1}{2}(D_S - D_D) \tag{1}$$

$$\rho = \sqrt{W^2 + V^2} \tag{2}$$

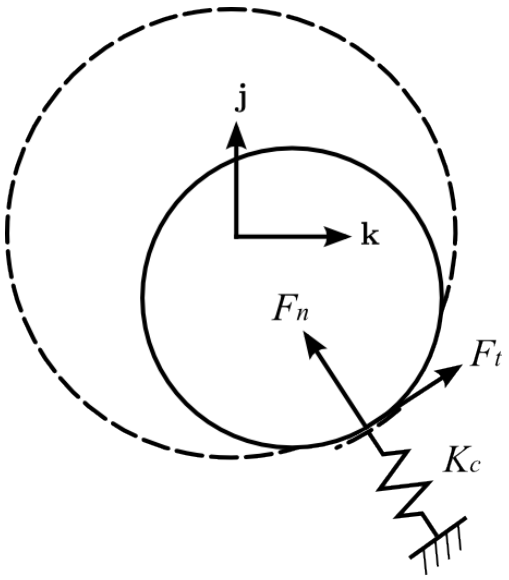

(a)

Figure 1. Schematic of force components acting on the rotor when in contact with the outer shell.

$$\lambda = \begin{cases} 0 & \text{for } \rho \le \delta \\ 1 & \text{for } \rho > \delta \end{cases} \tag{3}$$

Here, D_D is the diameter of the rotor and D_S is the diameter of the shell. Furthermore, λ is the contact parameter, which is equal to zero when there is no contact, and equal to unity in the presence of contact. The forces that act upon the rotor are then governed by the following set of equations:

$$F_{normal} = \begin{cases} 0 & \text{for } \rho \le \delta \\ K_c(\rho - \delta) & \text{for } \rho > \delta \end{cases} \tag{4}$$

$$\mu = \begin{cases} \left|\dfrac{V_{rel}}{V_{min}}\right| \mu_o & \text{for } |V_{rel}| < V_{min} \\ \mu_o & \text{for } |V_{rel}| \ge V_{min} \end{cases} \tag{5}$$

$$F_{tan} = -\mu \cdot \text{sign}(V_{rel}) F_{normal} \tag{6}$$

In the context of rotor-stator interactions, there are various classifications of phenomena and dynamic behavior. *Rubbing* occurs when the rotor is in contact with the outer shell, and there exists a finite, nonzero relative speed between the rotor and stator at the point of contact. An extreme case of rubbing is forward whirling with contact. This phenomenon occurs when the tangential force cannot overcome the inertia force of the rotor, and this is likely to occur in cases with low friction. The term *rolling* is used when the relative speed between the rotor and outer shell is exactly zero. As discussed in the previous report, during rolling the response frequency of the lateral response is much greater than that of the driving frequency of the drill string, and this is likely to cause higher levels of stress on the string itself, which may be a contributing factor in drill-string failures. Typically, the rotor can undergo combinations of rolling and rubbing, referred to as *roll-rub* phenomena. Additionally, the rotor may exhibit *impacting* motions, where the rotor does not settle into a state of continuous contact with the stator. From numerical investigations, it is found that impacting motions are more prevalent with low friction forces. Impacting models, which are commonly found in the literature, are not able to capture rolling or rubbing. The current model allows for rolling, rubbing, and also impacting behavior.

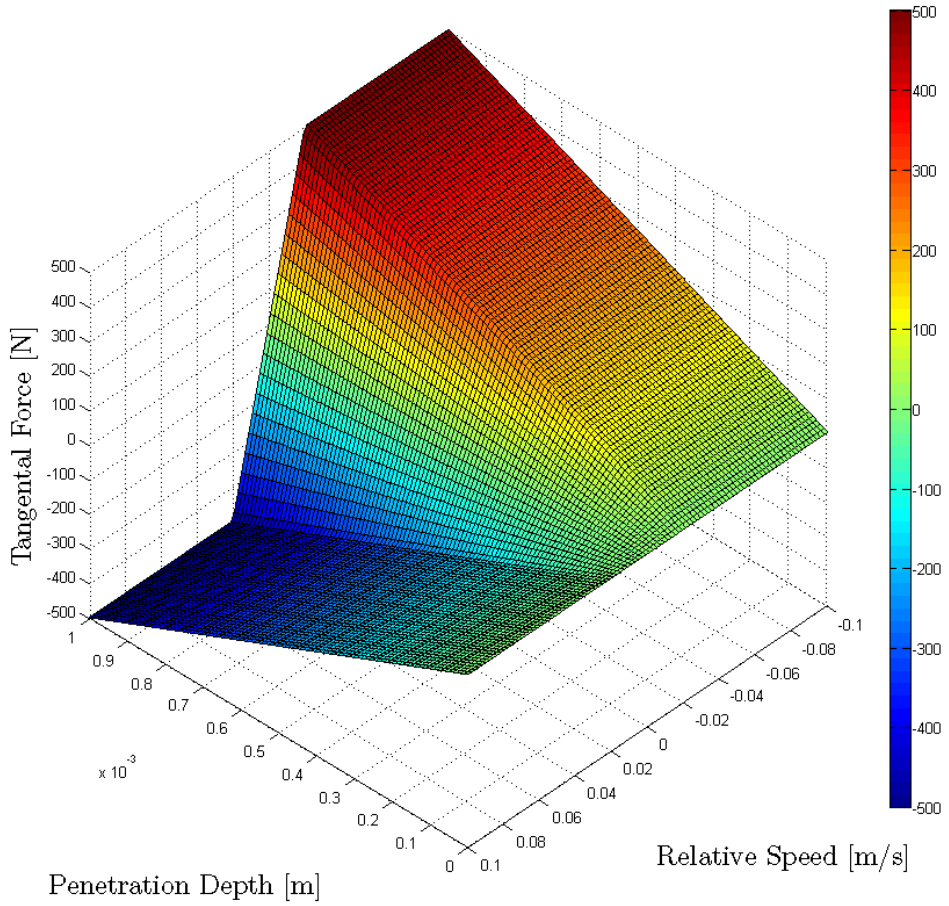

Figure 2. Magnitude of the tangential force component acting on the rotor for $K_c = 1kN/m$, $V_{\min} = 0.02m/s$, and $\mu_o = 0.5$ for a range of penetration depths.

As shown in Figure 1, the direction of the normal force always starts at the point of contact and points towards the geometric center of the shell. The magnitude of the normal force is linearly proportional to the penetration depth $p = \rho - \delta$. The direction of the tangential force, by definition, acts to produce a negative moment about the x-axis. In other words, it opposes the direction of rotation. The magnitude of the tangential force is a continuous function of the normal force and a discontinuous function of the relative speed. Therefore, the magnitude of the tangential force acting on the rotor changes in a non-smooth manner at certain relative speeds. A graphical representation of the magnitude of the tangential force is shown in Figure 2. The non-smooth jump in the tangential force, as well as change in the sign direction, occurs when the relative velocity approaches zero. This jump is thought to excite torsional vibrations in an actual drilling operation.

2.2 Experimental studies

Previous experimental studies had focused on the rotor dynamics of the drill string, and also, on the contact dynamics between the rotor and outer shell. Numerical and experimental studies have

shown the impact dynamics and response of the rotor due to the interaction forces. However, other nonlinearities, which originate from the structure itself, may also exist in the system. Two possible types of nonlinearities are material nonlinearities, which can arise in the constitutive material relations of the structure, and geometric nonlinearities which can occur due to large displacements or complex structural geometry. Geometric nonlinearities are expected to play a dominant role in the dynamics of horizontal drilling, which requires the use of an initially prestressed, curved structure. Therefore, for the current study, the outer shell is removed and the response of the drill string is recorded for different driving speeds in order to determine the possible presence of geometric nonlinearities.

2.2.1 Experimental arrangement

In Figure 3, the experimental arrangement is presented along with details used for studying the string dynamics under different rotational speeds. The experimental arrangement has been enhanced through the addition of a slip ring and self-centering, three-jaw chuck (referred to as chuck in the later sections) into the setup. The chuck is the connector between motor and string, which is shown in Figures 3(a) and (c), and this chuck is able to secure different string diameters to the motor, which will be useful for horizontal experiments. The slip ring allows researchers to place sensors, such as strain gauges or accelerometers, in the rotating reference frame. The mechanism prevents the wires from the sensors wrapping around the shaft while in operation.

In Figure 3(b), a snap shot of the string with the bottom disc in a camera view is shown. This system is driven by a motor with a constant rotating speed that ranges from 20 rpm (revolutions per minute) to 160 rpm. These rotating speeds correspond to motor driving voltages of 100 milivolts (mV) and 400 mV, respectively. The attached unbalanced mass for these experiments is fixed at 28.1 grams. The unbalanced mass is recognized as being representative of the curvature of the drill string. For instance, the case of zero unbalanced mass corresponds to a straight drill string, while a non-zero unbalanced mass is representative of a drill string in a curved orientation.

The video camera, which was used to capture the video frames of the disk during operation, is shown in Figure 3(c). These images were used for monitoring the system response during the experiments. Rotor trajectories were traced and constructed by analyzing the location of the rotor center in each video frame through a gradient-based image processing procedure. The image capture rate from the camera is 87 FPS (frames per second), which is sufficient for capturing the response excited over the range of rotation speeds, which extend up to a maximum rotation speed of 160 rpm.

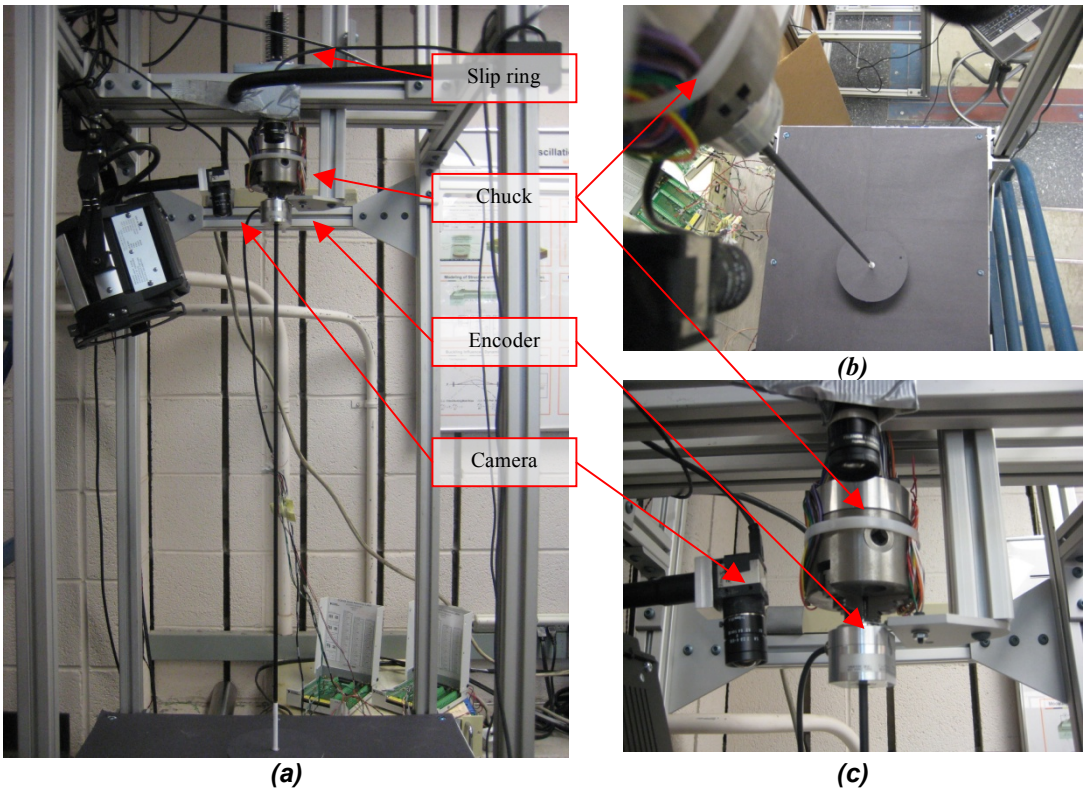

Figure 3. Experimental setup with details: (a) system overview, (b) top view, and (c) self-centering, three-jaw chuck (chuck), camera, and encoder.

2.2.2 Experimental Results

In the previous studies, the rotor motions changed significantly with increase in driving speed. The interaction between the rotor and outer shell has a significant influence on the system dynamics. While contained within the shell, with increasing driving speed, the rotor moves from forward whirling to pure sticking subsequently followed by backward whirling. In the current experiments, with the absence of the outer shell, the rotor exhibits forward whirling motions, but does not exhibit any backward whirling as shown in Figure 4.

In Figure 4(a), the rotor motions are close to the origin when the driving speed is low. For a driving speed of 55.3 rpm, the amplitude of radial displacement is approximately 1 cm. With increase of the drive speed to 64.8 rpm, as shown in Figure 4(b), the amplitude of radial displacement increases to 9 cm. For a slight increase in the driving speed to 69.4 rpm, the amplitude of the radial displacement increases to 19 cm, as shown in Figure 4(c). In Figure 4(d), the observed speed at a drive speed of 71.5 rpm is shown. For this drive speed, for which the corresponding frequency coincides with the first natural frequency of the system, the maximum amplitude of radial displacement occurs. As the driving speed is increased further, the rotor moves closer to the origin, with a small amplitude of radial displacement.

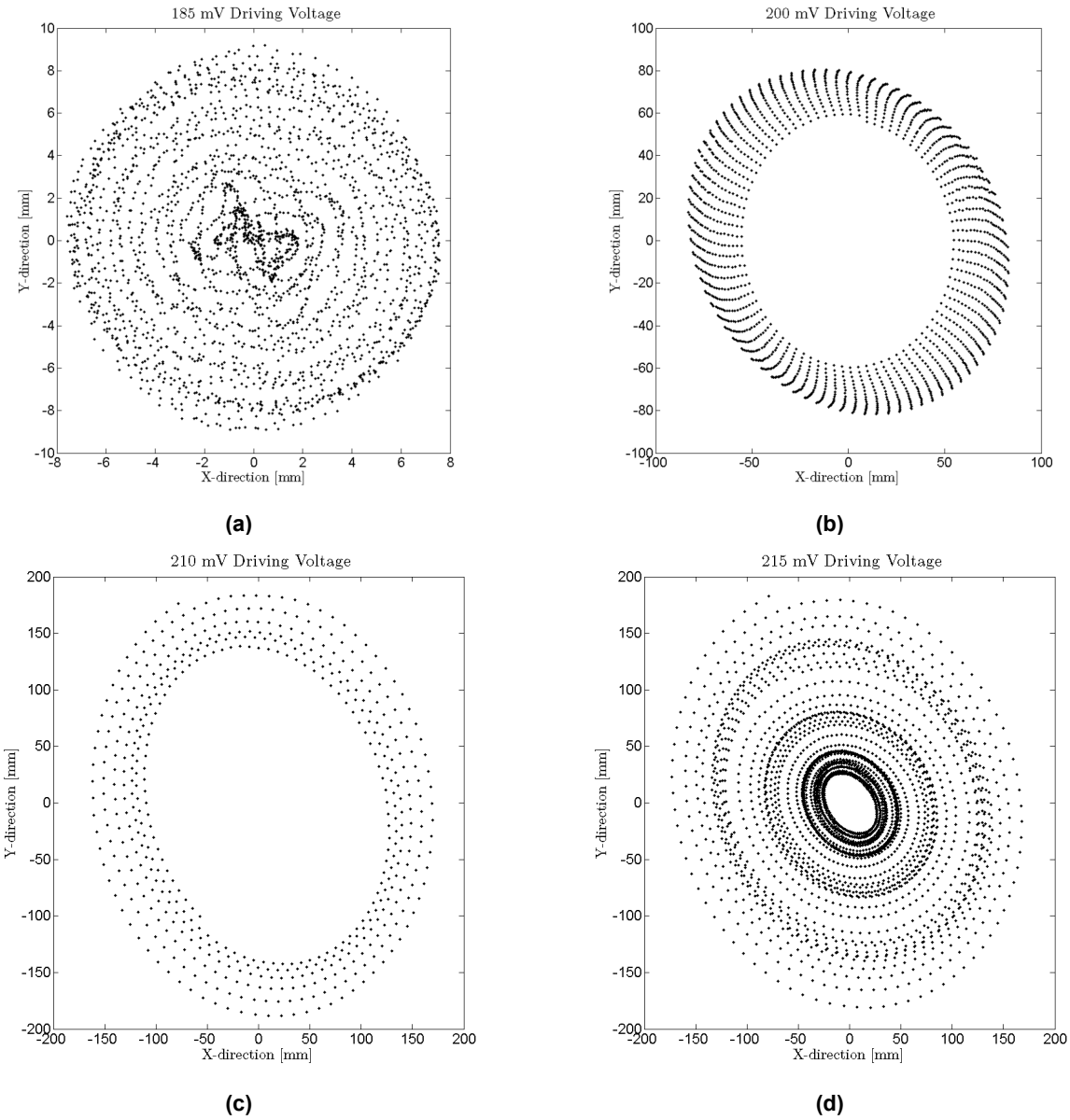

Figure 4. Rotor response trajectories by different level of driving speed: (a) driving speed of 55.3 rpm (drive voltage of 185 mvolts), (b) driving speed of 64.8 rpm (drive voltage 200 mvolts), (c) driving speed of 69.4 rpm (drive voltage 210 mvolts), and (d) driving speed of 71.5 rpm (drive voltage 215 mvolts).

Experimental data were collected over a driving voltage of 100 mV to 400 mV. The maximum amplitude of radial displacement in each case with respect to different driving speeds is shown as Figure 5. In order to examine the possible nonlinear behavior of the string system, a forward and backward sweep was performed in the experiments, following similar experimental nonlinear dynamics studies (e.g., Nayfeh and Balachandran, 1995, 2006). During forward sweep of the drive frequency, the driving frequency is varied from a low frequency to a high frequency and the displacements are recorded for each frequency value. On the other hand, during backward sweep of the drive frequency, the system is driven at first at a high driving frequency and this control parameter is quasi-statically varied from a high frequency to a low frequency.

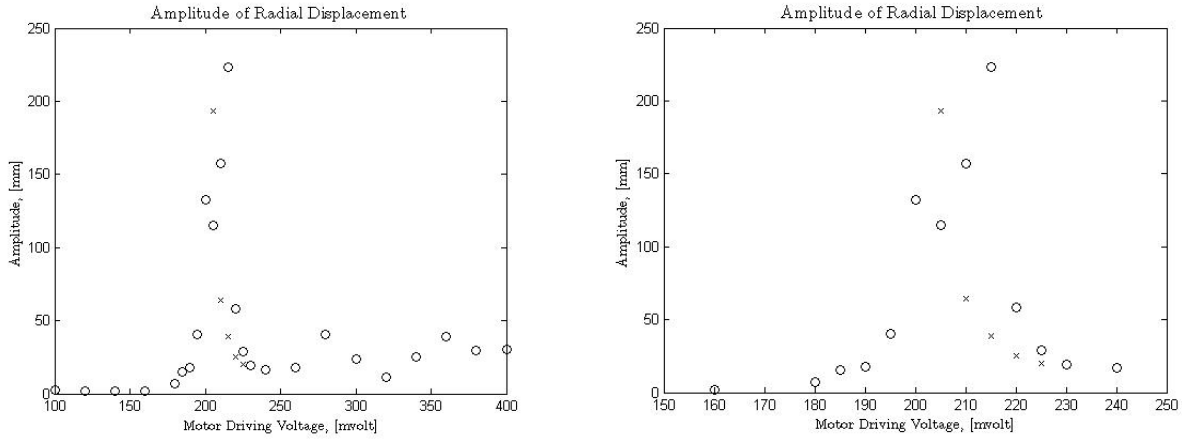

Figure 5. Response of rotor radial displacement during quasi-static sweep of drive speed: (a) response over drive speed range of 100 to 400 mV and (b) response over the region of 150 to 250 mV. (legend: o- forward sweep, x- backward sweep).

The response curves suggest a behavior similar to that observed with a Düffing oscillator with a positive cubic stiffness term or a hardening spring. This type of nonlinearity can arise due to geometric nonlinearities, which are expected to play an important role in horizontal string dynamics.

3. Discussion and Future Work

The complex forces acting on the rotor have been explored through a simple switching model, which is able to predict rotor motions, such as rubbing, rolling, combinations of both, as well as impacting motions. This model could prove to be useful while studying drill strings in a horizontal configuration. Furthermore, experimental results have shown that other nonlinearities exist in the vertical system, and geometric nonlinearities need consideration while modeling horizontal drill-string dynamics.

The current focus of the research is moving from vertical drill strings to horizontal drill strings with an accompanying experimental apparatus that has an aspect ratio close to those of "real" drill strings. Future reports are to contain findings and results pertaining to horizontal drilling studies.

References

[1] Akgun, F. 2004, "A Finite Element Model for Analyzing Horizontal Well BHA Behavior," J. of Petrol. Sci & Eng., Vol. 42, pp. 121-132.

[2] Bednarz, S., 2004, "Design and Exploitation Problems of Drill Strings in Directional Drilling," Acta Montanistica Slovaca, Vol. 9, pp. 152-155.

[3] Downtown, G., 2009, "*New Directions in Rotary Steerable Drilling*", Oilfield Review, pp. 18-29.

[4] Feng, Z., and Zhang, X., (2002). "Rubbing phenomena in rotor-stator contact". Chaos, Solitons, & Fractals, 14(2), August, pp. 257–267.

[5] Leine, R. I., van Campen, D. H., and Keultjes, W. J. G. (2002). "Stick-Slip Whirl Interaction in Drill String Dynamics," *ASME Journal of Vibration and Acoustics*, Vol. 124 (2), pp. 209-220.

[6] Liao, C.-M., Balachandran, B., and Karkoub, M., (2009). “Drill-String Dynamics: Reduced Order Models,” To appear in Proceedings of ASME IMECE 2009, Nov. 13-19 Lake Buena Vista, FL, USA, 2009; Paper No. IMECE2009-10339.
[7] Melakhessou, H., Berlioz, A., and Ferraris, G. (2003). “A Nonlinear Well-Drillstring Interaction Model,” *ASME Journal of Vibration and Acoustics*, Vol. 125, pp. 46-52.
[8] Mihajlović, N., van Veggel, A. A., van de Wouw, N., and Nijmeijer, H. (2004) “Analysis of Friction-Induced Limit Cycling in an Experimental Drill-String System,” *ASME Journal of Dynamic Systems, Measurement, and Control*, Vol. 126(4), pp. 709-720.
[9] Mihajlović, N., van de Wouw, N., Rosielle, P.C.J.N., and Nijmeijer, H. (2007) “Interaction between torsionalal and lateral vibrations in flexible rotor systems with discontinuous friction,” *Nonlinear Dynamics*, Vol. 50, pp. 679-699.
[10] Nayfeh, A. H. and Balachandran, B. (1995, 2006). *Applied Nonlinear Dynamics: Analytical, Computational, and Experimental Methods*, Wiley, New York.
[11] Spanos, P. D., Chevallier, A. M., Politis, N. P., and Payne, M. L. (2003). “Oil and Gas Well Drilling: A Vibrations Perspective,” *Shock and Vibration Digest* Vol. 35(2), pp. 85-103.
[12] Short, J. A. “Introduction to Directional and Horizontal Drilling ” Pennwell Pub, 1993.
[13] Singh, S. P. and Balachandran B. (2009). “Rolling Rub Translations of a Flexibility Connected Disk,” pre-print.
[14] Vlajic, N., Liao, C.-M., Karki, H., & Balachandran, B. (2011) “Stick-Slip and Whirl Motions of Drill Strings: Numerical and Experimental Studies,” 2011 ASME IDETC MSNDC Conference, Washington, D.C., accepted for publication.

Appendix

Approach

A combined analytical, numerical, and experimental approach is being pursued at the University of Maryland and the Petroleum Institute. Specifically, the drill string is being modeled as a reduced-order nonlinear dynamical system. Appropriate attention is also to be paid to the interactions with the environment. The experiments at UMD and PI are tailored to address specific aspects of the drill-string dynamics as well as complement each other. Actuator and sensor choices are also to be explored to determine how best to control the system dynamics, in particular, through the rotational speed. The studies will be initiated with drill strings located on fixed platforms, and later extended to systems located on floating platforms.

Three-Year Schedule

Phase II:

January 1, 2009 to December 31, 2009: Carry out quantitative comparisons between experimental results and predictions of reduced-order models for open-loop studies; understand stick-slip interactions and explore continuum mechanics based drill-string models for fixed platform environments; examine different configurations including horizontal drilling

January 1, 2010 to December 31, 2010: Construct control schemes; carry out experimental, analytical, and numerical studies; and identify appropriate schemes; study horizontal drilling configurations through experiments and analysis

January 1, 2011 to December 31, 2011: Continue horizontal drilling studies; carry out experiments, analysis, and numerical efforts and also examine drill-string operations in off-shore environments

January 1, 2012 to May 1, 2012: Compile results obtained for drill-string operations in vertical and horizontal configurations and provide guidelines for enhancing operations.

Studies on Mobile Sensor Platforms

UMD Investigators: Balakumar Balachandran, Nikil Chopra
GRAs: Rubyca Jaai
PI Investigator: Hamad Karki, Sai Cheong Fok
GRAs: Hesham Ishmail (ADNOC Fellow)
Start Date: April 2009

1. Objective/Abstract

Mobile sensor platforms can be employed in a variety of operations including environmental and structural health monitoring operations in harsh and remote environments. In the proposed work, cooperating sensor platforms are to be studied for potential use in oil storage tanks, which are periodically tested for corrosion, cracks, and leaks. These platforms are envisioned for estimating geometrical profile parameters, such as, the tank bottom thickness. To this end, simultaneous localization and mapping (SLAM) algorithms (also known in the literature as concurrent mapping and localization (CML) algorithms) for co-operating sensor platforms operating in harsh environments are being investigated. While many solutions have been suggested for the single agent SLAM problem, multi-agent SLAM is still a difficult problem from an analytical and practical perspective. The use of multiple agents can allow for greater and faster coverage in the exploration and searching tasks and provide a certain degree of redundancy in the completion of tasks. Additionally, map merging using overlapping information from different agents can possibly compensate for sensor uncertainty (Dudek *et al*., 1996).

The overall objective of this project will be to carry out a combined analytical, numerical, and experimental effort to develop mobile sensor platforms and appropriate simultaneous localization and mapping (SLAM) algorithms for cooperative sensor platforms to operate in a harsh environment. Research objectives are the following: i) develop SLAM algorithms based platforms taking into account system constraints such as constrained communication, the type of sensors considered, allowable dynamics, and factors such as sensor failures and reliability of the considered sensors and ii) carry out experimental and supporting simulation studies by using mobile platform test platforms at the University of Maryland and the Petroleum Institute.

In this report, results of experiments and simulations carried out to demonstrate SLAM are presented. In Section 2, the different sections involved in solving the SLAM problem are discussed, followed by the scheduled work in Section 3. Experimental and simulation results are presented in Section 4, and an outline of the future work is provided in Section 5.

2. Summary of Results

In this report results obtained from experiments carried out to demonstrate SLAM are presented. Additionally, simulation work completed on the feature extraction and data association algorithms is shown.

2.1 Experimental setup

In order to carry out experiments to demonstrate simultaneous localization and mapping algorithms, a test setup was created, as shown in Figure 4.1. This setup includes mobile platforms and a scaled version of a corridor-like environment using plexiglass structures. Suitable ground-based mobile agents, necessary to carry out the experimental measurements for simultaneous localization and mapping, were acquired at UMD. The ground-based platforms are

capable of being controlled using the Matlab Simulink environment via wireless communication. Information from sensors such as encoders, infrared sensors, and ultrasonic sensors collected by the mobile platform can also be communicated in real time to the controlling computer as the experiments are performed. Additionally, cameras are used to collect ground truth data on the path followed by the mobile platform during the experiments. The path information is used to compare the results from the algorithms to the actual path taken by the mobile platform. The path information is extracted from the videos through image processing, which is also carried out in Matlab.

Image processing results obtained from an experiment with two mobile platforms are presented in Figure 4.2. The data from the cameras were used to extract the path information and the position of the plexiglass walls. The black lines indicate the positions of the plexiglass walls, and the red and blue lines indicate the paths followed by the two mobile platforms.

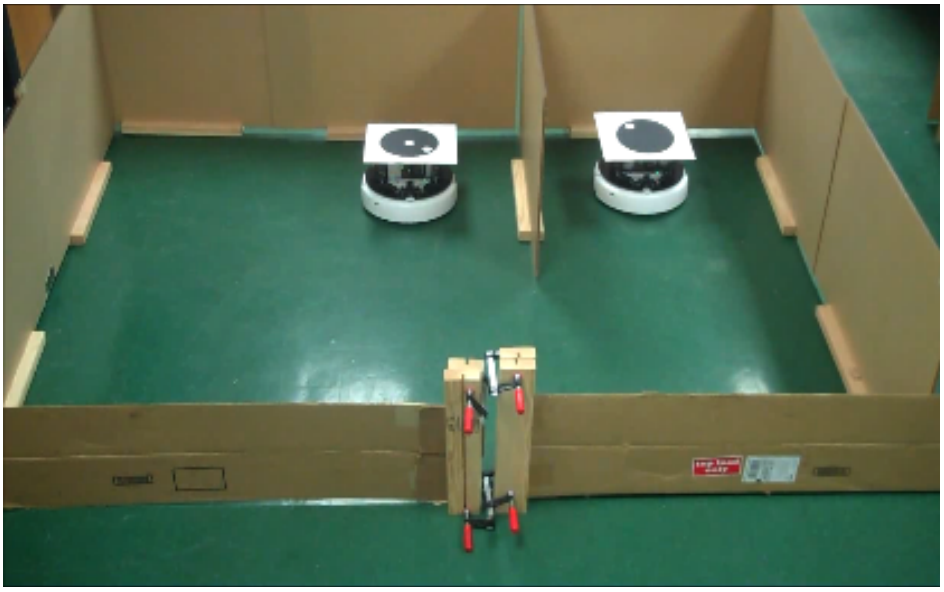

Figure 1. Experimental setup.

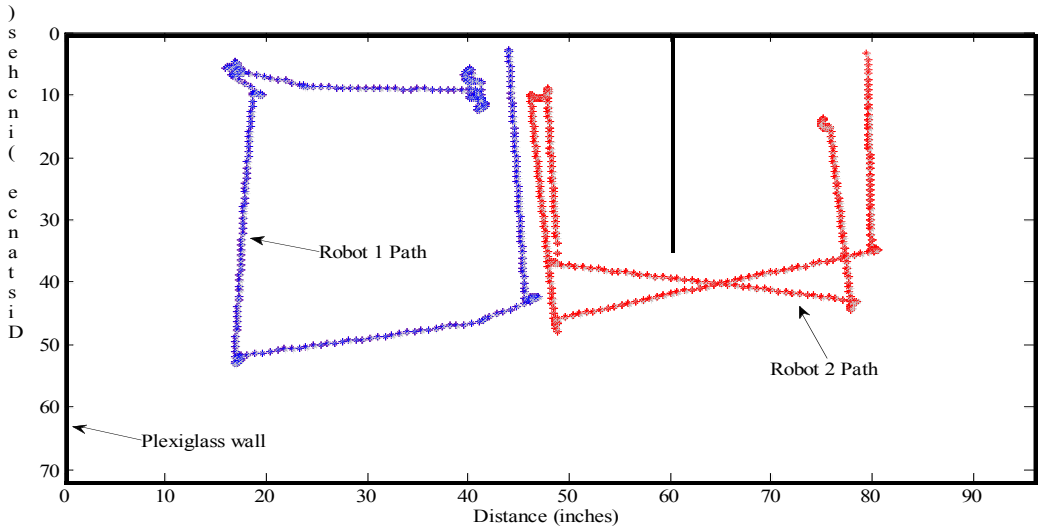

Figure 2. Path information obtained from the video of the experiment.

2.3 Simulation results

Simulation results obtained using the data association for point landmarks are shown in Figure 3. The results are based on nearest neighbor matching of the point landmarks using a gating technique. Data association using the gating technique is based on the distance between landmarks observed (Dissanayake *et al*., 2001). With every new measurement, the landmark's position is estimated and its distance from the other landmarks already present in the map is computed. If the nearest neighbor is at a distance that is less than a predefined threshold, the measurement is associated with the nearest neighbor. A certain minimum number of associations is required for any landmark to become a valid landmark in the map.

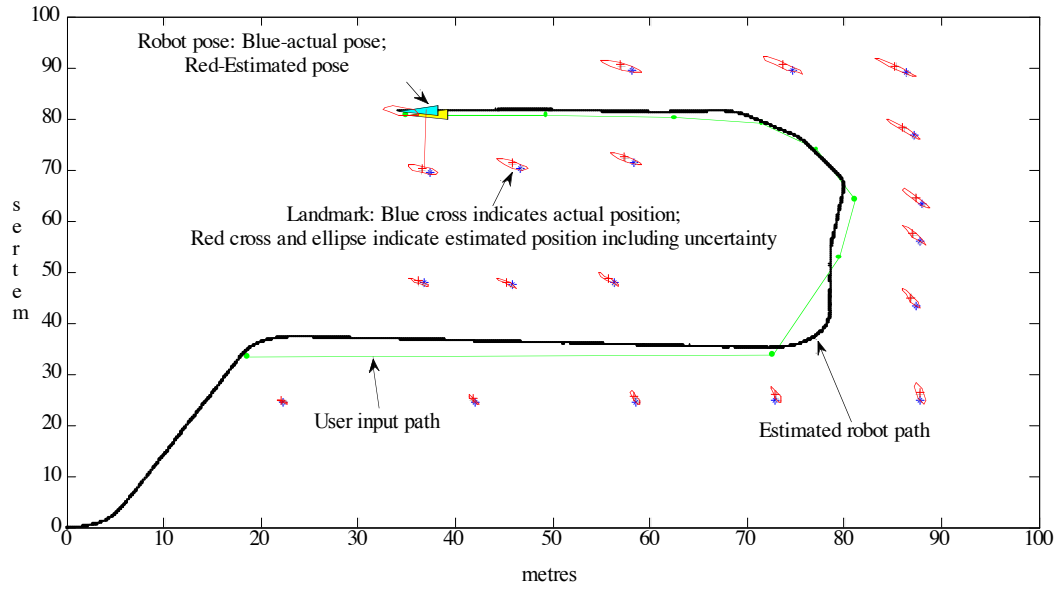

Figure 3. Simulation results with data association for point landmarks.

Two lists of landmarks are maintained, one for the valid landmarks that have had the required number of data associations and the other for potential landmarks that have not had the required number of data associations validated. The distance calculations are based on the Mahalanobis distance. Measurements that are not associated with any previous landmarks are placed in the list of potential landmarks until they reach the required minimum number of associated measurements. Additionally, if any member of the potential landmarks does not reach the threshold for validation within a certain number of measurements, it is removed from the list. The algorithm used to carry out the SLAM prediction and update steps is based on the extended Kalman filter.

When the environment can be described by line segments, for example, corridors with walls and doors, the line extraction algorithms can be used for extracting line segments from laser and/or sonar sensors. Coding of the following line extraction algorithm has been completed, and testing will be carried out on experimental data.

For extracting line segments from the group of sonar scans, the randomized Hough transform (RHT) technique is used (Yap and Shelton, 2009). Before line segments are extracted, each sonar measurement is plotted as a point (in the global reference frame) representing the object in the environment with respect to the robot pose. The Hough transform is used to find groups of almost collinear points and extract the parameters of the lines that fit those groups of points from the set of measurements. The Hough transform is a technique used in digital image processing for extracting features such as lines and curves. It is a voting scheme in which each point (pixel) in the image votes for a set of features (lines, curves) that pass through it. To use the RHT for line segment extraction, the lines are represented in polar coordinate parametrization (ρ, θ), where ρ is the length of the normal from the origin to the line and θ is the angle that the normal makes with the positive x-axis.

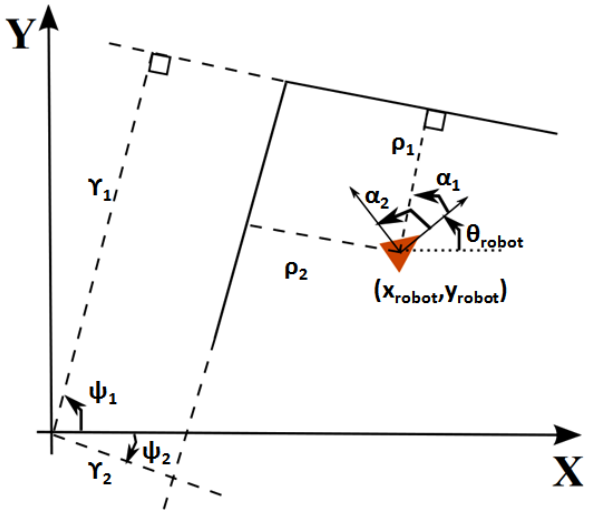

Figure 4. (following Yap and Shelton, 2009**). Extraction of line segments (α,ρ) with respect to the robot and (ψ,θ) with respect to the origin. The extracted values are then used as part of the SLAM algorithm.**

An alternative algorithm uses a sliding window technique where a window of constant size sweeps over the ordered set of range readings (Arras, 2003). The sensor readings are in polar coordinates. At every step of the sliding window, the model (in this case the line) is fitted to the points within the window and a measure of the fit of the model is calculated. The algorithm is used to fit a line in the weighted least squares sense to the points within the window in polar coordinates minimizing perpendicular errors from the points to the line. Uncertainties in the fit parameters are propagated through the fit expressions yielding the parameter covariance matrix. A condition on the fit is used to detect new objects in the environment (this is done to reduce the effect of outliers in the measurements). The result of this step is a segmented range image, which in many cases may be over-segmented since each outlier can give rise to several small segments. At this point, a condition of co-linearity based on a significance level is used to fuse adjacent segments as a final step. The line segments represented in distance and angle measurements (see Figure 4.4) are used as parameters in the SLAM algorithms.

2.4. Interactions

The use of Simulink and Matlab for real time control with the mobile platforms was demonstrated to the interns from the Petroleum Institute visiting the University of Maryland this summer.

3. Planned Project Activities for the Next Quarter

Future work includes incorporating the Kinect sensor with the mobile platforms. The Kinect sensor provides images with depth information to carry out SLAM experiments in three dimensions. Additionally, the required feature extraction algorithms for the image data will also be added and the experiments will be conducted. The three dimensional mapping can be used for mapping of structures such as oil pipelines for inspection. The use of ultrasonic imaging sensors and extending the algorithms from the Kinect sensor to the ultrasonic sensors will also be investigated.

4. References

[1] Arras, K.O., 2003, "Feature-Based Robot Navigation in Known and Unknown Environments", Ph.D. dissertation, Nr. 2765, Swiss Federal Institute of Technology Lausanne, Autonomous Systems Lab, June.

[2] Bay, H., Ess, A., Tuytelaars, T., and Gool, L. V., 2008, "SURF: Speeded Up Robust Features," Computer Vision and Image Understanding, vol. 110, no. 3, pp. 346-359.

[3] Dissanayake, M.W., Newman, P., Clark, S., Durrant-Whyte, H.F., and M. Csorba, 2001, “A Solution to the Simultaneous Localization and Map Building (SLAM) Problem,” Robotics and Automation, IEEE Transactions on, Vol.17, No.3, pp. 229–241, June.

[4] Dudek, G., Jenkin, M., Milios, E. and Wilkes, D., 1996, “A Taxonomy for Multi-Agent Robotics,” Autonomous Robots, vol. 3, no. 4.

[5] Durrant-Whyte, H. and Bailey, T., 2006, “Simultaneous Localization and Mapping: Part I," IEEE Robotics & Automation Magazine, Vol.13, no.2, pp. 99-110, June.

[6] Durrant-Whyte, H. and Bailey, T., 2006b, “Simultaneous Localization and Mapping: Part II State of the Art," IEEE Robotics & Automation Magazine, Vol.13, no.3, pp. 108-117, 2006.

[7] Garulli, A., Giannitrapani, A., Rossi, A., and Vicino, A., 2005, “Mobile robot SLAM for line-based environment representation,” 44th IEEE Conference on Decision and Control, 2005 and 2005 European Control Conference. CDC-ECC '05., pp. 2041 – 2046, December.

[8] Lemaire, T. and Lacroix, S., 2007, "SLAM with Panoramic Vision," Journal of Field Robotics, vol. 24, no. 1-2, pp. 91-111, February.

[9] Montemerlo, M., Thrun, S., Koller, D., and Wegbreit, B., 2002, “FastSLAM: A Factored Solution to the Simultaneous Localization and Mapping Problem," in Proceedings of the AAAI National Conference on Artificial Intelligence, AAAI, (Edmonton, Canada).

[10] Smith, R., Self, M., and Cheeseman, P., 1990, “Estimating Uncertain Spatial Relationships in Robotics”, pp. 167-193, Springer-Verlag New York, Inc., New York, NY, USA.

[11] Tardós , J. D., Neira, J., Newman, P. M., and Leonard, J. J., 2002, “Robust mapping and localization in indoor environments using sonar data,” International Journal of Robotics Research, vol. 21, pp. 311—330.

[12] Thrun, S., 2003, “Robotic Mapping: A Survey,” in Exploring Artificial Intelligence in the New Millennium, G. Lakemeyer and B. Nebel, eds., pp. 1-35, Morgan Kaufmann Publishers Inc., San Francisco, CA, USA.

[13] Thrun, S., Burgard, W., and Fox, D., 2006, “Probabilistic Robotics,” MIT Press.

[14] Yap, T.N., and Shelton C.R., 2009, "SLAM in Large Indoor Environments with Low-Cost, Noisy, and Sparse Sonars," Proceedings of the IEEE International Conference on Robotics and Automation, pp. 1395-140.

Appendix

SLAM and its Components

The basic aim of the simultaneous localization and mapping (SLAM) algorithm is to make a mobile platform autonomous by providing the capability to navigate through an unknown environment from an initially unknown location. This is achieved by iteratively building a consistent map and by simultaneously determining the platform's location within the map (Durrant-Whyte and Bailey, 2006). Therefore, SLAM is the process by which a mobile platform can build a map of the environment and at the same time use this map to compute the platform's location within the map (Thrun, 2003). This ability is useful particularly in applications such as search and rescue, inspection and surveillance, and exploration, which require accurate localization within unknown environments. For example, in the inspection problem, by using SLAM techniques, the mobile sensor platform can determine locations of faults, thereby providing an autonomous solution and reducing the need for external sensors to perform the same task.

In the SLAM problem, an agent or a mobile sensor platform uses relative sensing information between the agent and the surrounding environment in order to determine a map that constitutes the locations of landmarks or features in the surrounding environment as well the platform's position within the map.

Well known solutions to the single-robot SLAM problem include the use of extended Kalman filter (EKF) algorithm to estimate the positions of landmarks and the pose (i.e., position and heading) of the robot as Gaussian distributions or particle filters that allow for non-Gaussian representations or their combinations (known as FastSLAM) (Smith *et al*., 1990, Montemerlo *et al*., 2002).

One of the important components of the SLAM solution is data association. Before fusing new sensor data into the SLAM map, new measurements are associated with existing map landmarks. The problem is that incorrect data association can cause the map estimates to diverge. Additionally, the incorrect data association can lead to failure in the localization of the mobile platform within the map. Practical SLAM solutions are therefore fragile to incorrect association of observations to landmarks. Additionally, it is necessary to solve the loop-closure problem that occurs when a robot returns to observe landmarks that were previously observed after a long route, and the algorithm needs to recognize this has occurred by correctly associating new measurements to landmarks that were observed in the beginning of the robot path. The association problem is compounded in environments that are not simple points (Durrant-Whyte and Bailey, 2006b).

Feature extraction is another critical component of the SLAM problem. In environments that are not simple, correct data association also involves representing the environment by features extracted from the sensors provided on the mobile platform. Some examples include extracting line features in indoor environments typically from sonar and laser sensors (Tardos *et al*., 2002; Garulli *et al*., 2005), and extracting corners and scale invariant features from stereo camera data using techniques from computer vision (Bay *et al*., 2008; Lemaire *et al*., 2007).

Three-Year Schedule

Phase II:

April 1, 2009 to December 31, 2009: Carry out analytical and numerical investigations into SLAM algorithm based mobile platforms for representative geometrical profile measurements, and construction of experimental test platforms.

January 1, 2010 to December 31, 2010: Continuation of analytical, experimental, and numerical efforts, with one of the focus areas to be development of appropriate

communication and motion planning protocols for co-operative multi-agent platforms. Construction of experimental setup for ground based mobile agents with attention to the environment.

January 1, 2011 to December 31, 2011: Continuation of experimental and numerical studies and formulation of recommendations for appropriate sensor and mobile platform configurations for use in oil tanks and pipes.

January 1, 2012 to March 31, 2012: Continuation of experimental and numerical studies for proof of concept for appropriate sensor and mobile platform configurations for use in oil tanks and pipes.

Development of a Probabilistic Model for Degradation Effects of Corrosion-Fatigue Cracking in Oil and Gas Pipelines

UMD Investigator: Mohammad Modarres
PI Investigators: Abdennour Seibi
GRA: Mohammad Nuhi
Start Date: Oct 2006

1. Objectives/Abstract

This research continues Phase I mechanistic modeling of the corrosion-fatigue phenomenon for applications to pipeline health, risk and reliability management. The objective of this study is to perform additional mechanistic-based probabilistic models derived from physics of failure studies and validate them using the state-of-the-art experimental laboratory being developed at the PI as part of Phase I of this study. Where possible, observed field data from ADNOC operating facilities will be used to supplement observations from the laboratory experiments based on the well-established Bayesian approach to mechanistic model updating and validation developed in Phase I. Uncertainties about the structure of the mechanistic models as well as their parameters will also be characterized and accounted for when such models are applied. The proposed models will allow the end users (e.g., maintenance analysts and inspection crew) to integrate observed performance data from a wide range of pipelines and selected refinery equipment, such as pumps, compressors and motor-operated valves. Admitting the fact that modeling all degradation mechanisms would be a challenging undertaking, the proposed research will additionally address the following degradation phenomena related to the petroleum industry: creep, pitting corrosion, and stress cracking corrosion (SCC).

2. Summary of Results

The following tasks have been completed in the last three months:

4.1. Theoretical effort in support of model development
4.1.1. Creep (deformation) mechanism map
4.2. Experimental efforts in support of corrosion and creep model development
4.2.1. Experiments on Al-7075-T6 materials
4.2.2. Experiments on X-70 carbon steels

2.1. Creep (Deformation) Mechanism Map

Creep is one of the most serious high-temperature damage mechanisms. It involves time-dependent deformation and high-temperature creep rupture that generally occur in an inter-crystalline manner in materials that fail over an extended time. Boiler superheaters and other components operating at high temperature, petrochemical furnaces and reactor vessel components and gas turbine blades are some examples. At higher temperatures that can occur by local overheating, deformation is more localized, with large plastic strains and local wall thinning. At lower temperatures and under higher stress levels, fracture can be transgranular in nature.

To characterize the type of deformation and the relevant fracture mechanisms or to correlate observed deformation and fracture characteristics, deformation and fracture mechanism maps as developed by Ashby, Mohamed and Langdon [2, 3] can be useful. Deformation maps of pure aluminum and iron are given in Figure 1.

.

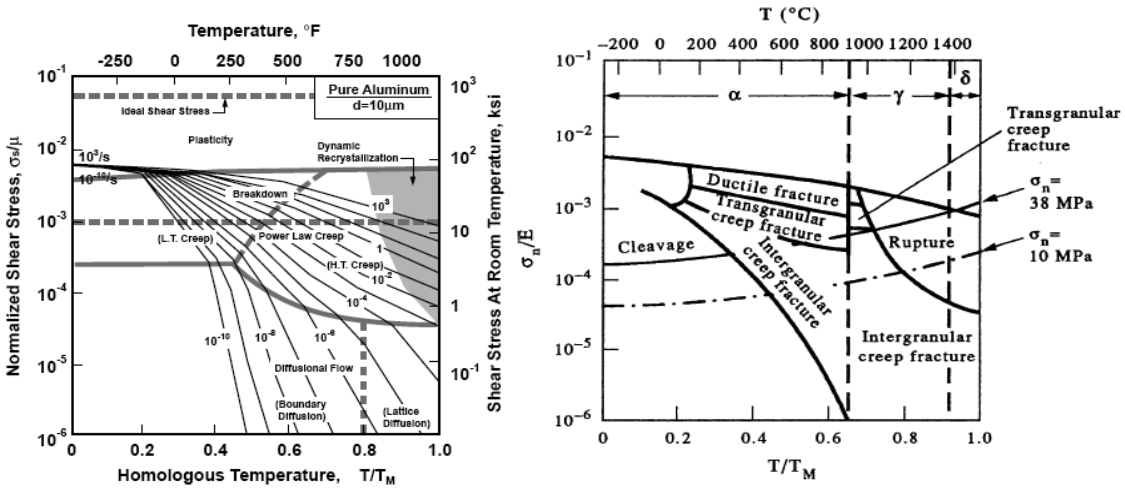

Figure 1. Creep deformation map of pure aluminum (left) and iron (right) with given different fracture modes of trans- and inter-granular rupture mechanisms [2, 3].

Creep experiments can be conducted according to the given temperatures and applied stresses described above for aluminum and steel alloys, and so it is possible to prove the intergranular or transgranular mode of fracture of the samples, accordingly.

2.2. Experimental effort in support of model development

Creep experiments take a lot of time. We tried to make our experiments on a MTS machine and took its grips displacements as the creep strain. Experiments were conducted at high temperature under high stresses (accelerated conditions). Better results can be achieved by appropriate equipment especially designed for creep experiments and high temperature extensometers.

In these experiments two different materials were considered: Al 7075-T6 and X-70 carbon steel (both are used in oil refinery industry).

2.2.1. Experiments on Al-7075-T6 materials

First, creep experiments were done with Al-7075-T6 samples because of its lower creep temperature requirement.

Al-7075-T6 samples were tested at different applied stresses at a given temperature.

To characterize the type of deformation and the relevant fracture mechanisms, microscopic investigations were conducted. The experimental investigations are comparable with the theoretical prediction of grain growth (re-crystallization) of grains and transgranular rupture mode for aluminum samples. Broken aluminum dog-bone samples with the ductile transgranular mode and heat affected re-crystallization (grain growth) form are shown in Figure 2.

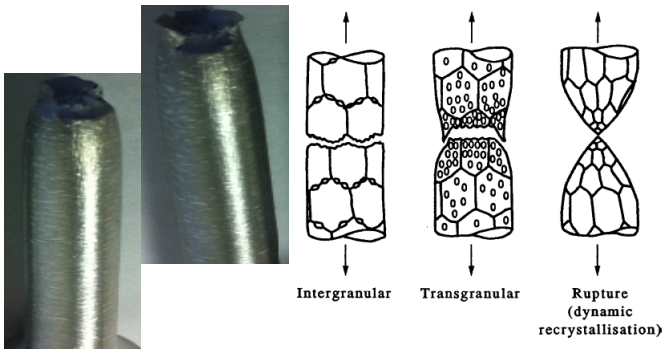

Figure 2. Ductile transgranular mode of rupture form of Al-creep sample at 400°C, with re-crystallized grain growth form and compared picture given in the literature [4].

2.2.2. Experiments on X-70 carbon steels

To conduct creep experiments on X-70 carbon steel, the top and bottom threaded CT samples are made. To apply constant force, two long-pin threaded grips were made and connected to the samples. All the creep experiments were performed in a house-made, high-temperature furnace, described in the previous reports on the MTS machine. Figure 3 shows the installed sample in MTS equipment.

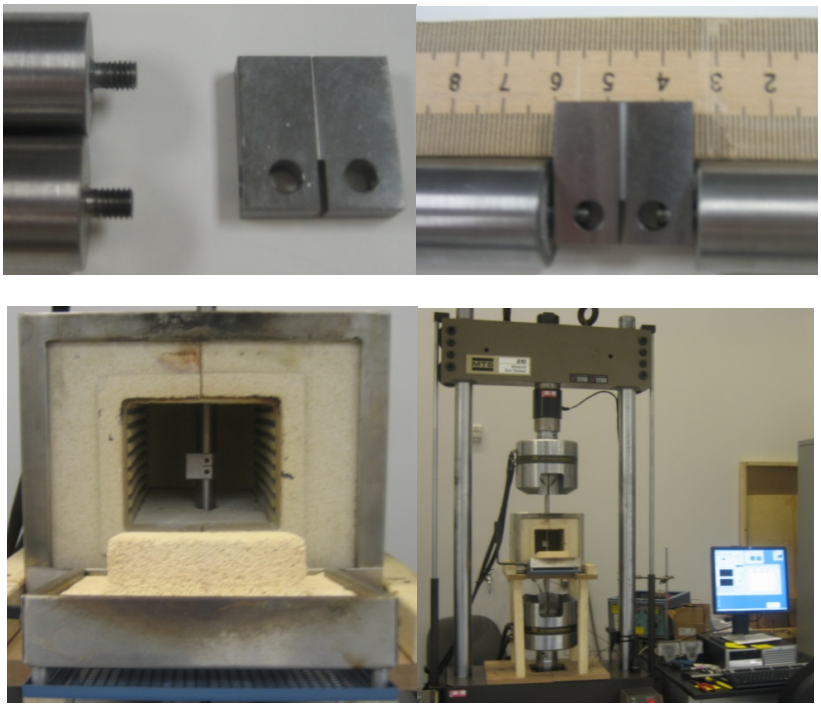

Figure 3. X-70 samples with two long grips (top left), sample connected to the grips, real dimensions (top right), sample connected to grips in furnace (bottom left), and in MTS machine (bottom right).

Since CT samples are very hard (with Vickers hardness of 295 HV at 10 kg [5]), while the grips are made from soft steel material, the following problems arose:

a) Grips could not apply appropriate stresses to the CT samples and therefore were deformed at the threaded top part and slid out from the threaded CT sample part;

b) Filling the threaded part of CT samples with hardened materials, using horizontal pins, and changing the grips didn't work either due to hardness of CT samples;

c) Although extension of the groove part of CT samples with some additional crack (similar to pre-crack) seemed to work at first, it failed finally because of the soft grips connected to the hard samples.

Figure 4 shows the deformed CT samples after the experiment together with the pin before and after the experiments.

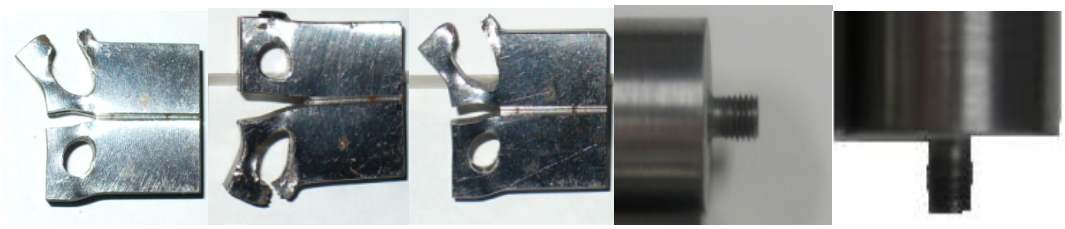

Figure 4. Deformed CT samples and the threaded grip part before and after deformation.

After the unsatisfactory experiments on CT samples, we decided to change the morphology of the samples and made new threaded dog-bones with appropriate grips. To estimate the applied stresses during the creep experiments, we made our own stress-strain curve for the X-70 carbon steel. The dog-bone X-70 carbon steel samples prepared and threaded grips are shown in Figure 5.

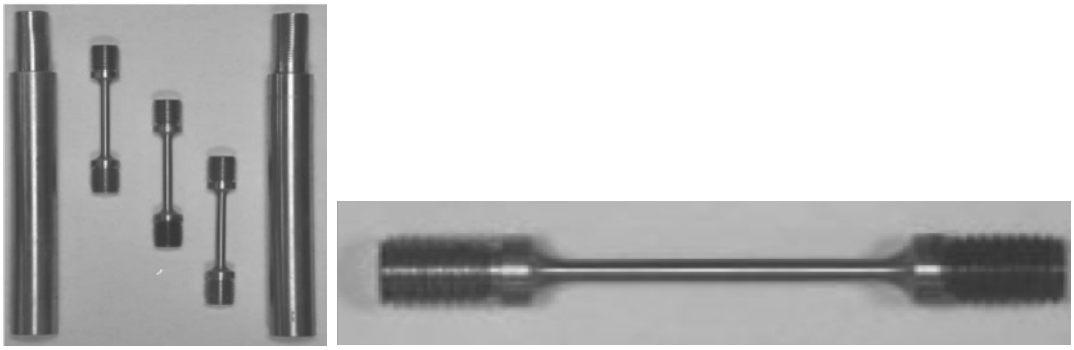

Figure 5. X-70 threaded dog-bone samples, 4mm cross section diameter, and gauge length of 45mm with grips for installation in the creep furnace.

The stress-strain curve of X-70 carbon steel sample was estimated with an extension rate of 1mm/hr. The X-70 carbon steel sample shows a ductile cup and cone form after breakage with elongated grains toward the rupture cross-section. Figure 6 shows the stress-strain curve of X-70 carbon steel. Figure 7a-b shows the cap and cone mode of fracture and the necking and broken sample after stress-strain experiment, respectively. Figure 7c shows grain growth of the sample around the necking part during the stress-strain experiment. Figure 7d shows the schematic of grain cavitations and grain growth before and after rupture (for comparison).

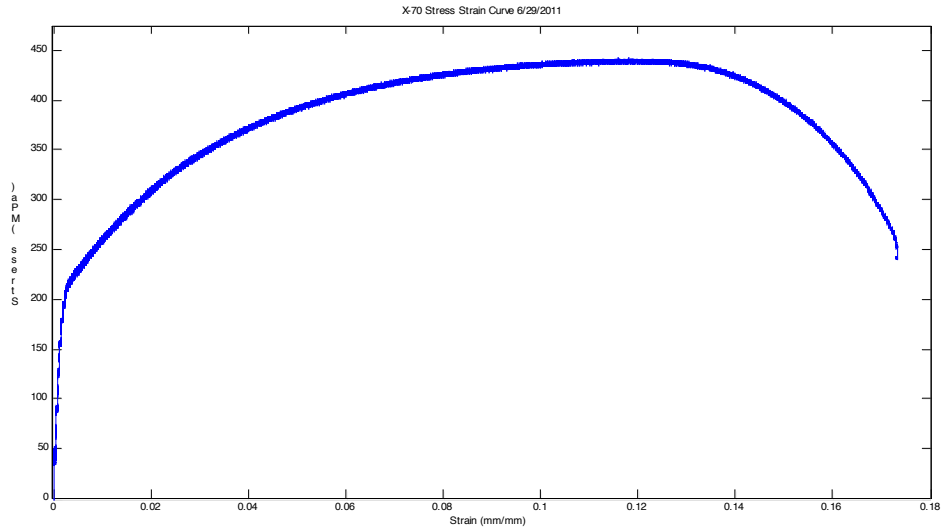

Figure 6. Stress-strain curve of X-70 carbon.

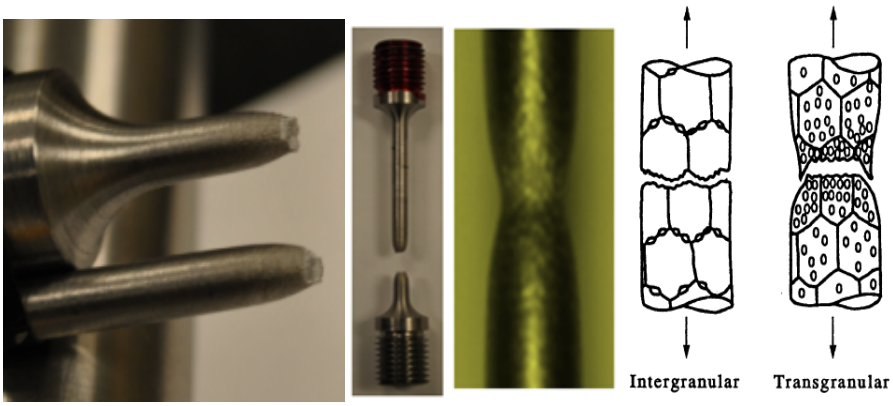

a) b) c) d)

Figure 7. a) ductile cup and cone form of rupture cross section of X-70 carbon steel, b) broken sample parts, c) grain elongation toward the necking region and d) schematic of grain cavitations and growth [4].

We are going to do our creep experiments with X-70 carbon steel with new dog bone samples, and detailed results will be given in the next report. In addition, as mentioned previously, we made a high-temperature furnace for the creep experiment. Due to the high cost of grip materials we will install a copper-winding cooler around the old grips. A special copper winding cooler has been designed, and its workability has been tested. However, the best way to avoid the problem is making the grips and specimens from the same material (X-70 carbon steel), which is expensive.

It should be mentioned here that exact estimation of temperature and stress dependencies of parameters need more time and samples. Creep experiments need their own creep equipment and specific high temperature extensometers (instead of a MTS machine that is more specified for estimation of stress-strain behaviors of metallic materials). We are looking into the possibility of acquiring this capability.

3. Planned Project Activities for the Next Quarter

The model verification and justification by performing creep experiments of Al 7075 and X70 dog-boned shaped specimens are about 60% done and will be continued during the next quarter. The statistical evaluation of the experimental data and nonlinear regression analysis by the MATLAB program is 40% done (i.e., the MATLAB program is formulated), and will be reported in our next report. Finally, we will compare our model with other empirical models and BIC (Bayesian Information Criterion) [6, 7] with experimental data gathered for Al-7075-T6 and X70 carbon steel samples.

Near Future Plans:

1. Simulation and refinement of the stress and temperature dependency of creep parameters of mechanistic models (PoF models) for creep for Al-7075-T6 and X70 carbon steel samples will be performed.
2. The corresponding simulation and statistical tool to help both model development and field applications will be done.

4. References

[1] ASME-B31G, Manual for Determining the Remaining Strength of Corroded Pipelines. A Supplement of ASME B31G Code for Pressure Piping, ASME, New York, 1995.

[2] Ashby, M.F. “A First Report on Deformation-Mechanism Maps”, Acta Met., v. 20, p. 887-897, 1972.

[3] Mohamed, F.A.; Langdon, T.G. Deformation Mechanism Maps: Their Use in Predicting Creep Behavior, J. Eng. Matls. and Technol., v. 98, p. 125-130, 1976.

[4] G. M. OMWEG et.al., Welding research, JUNE 2003, p 136-144, www.matsceng.ohio-state.edu/~FRANKEL/FCC/pubs/.../OmwegweldJ.pdf

[5] D.R.H. Jones “Creep failures of overheated boiler, superheater and reformer tubes”, Engineering Failure Analysis 11 (2004) 873–893

[6] K.P.Burnham and D.R. Anderson,” Model selection and multi-model inference, A practical Information-theoretic Approach, Spriger,2002

[7] Bayesian information criterion, en.wikipedia.org/wiki/Bayesian_information_criterion

Appendix

Background

A number of deterministic models have been proposed to assess reliability and life-remaining assessment of pipelines. Among these models is the ASME B31G [1] code, which is most widely used for the assessment of corroded pipelines. However, these models are highly conservative and lack the ability to estimate the true life of the pipelines and other equipment used in the oil industry. To address this shortcoming one needs to develop a best-estimate assessment of the life (to assess reliability and risk imposed) by these structures and equipment and assess the uncertainties surrounding such estimates. The proposed probabilistic mechanistic models, when fully developed, would integrate the physics of failure of some of the leading failure degradation mechanisms in the oil industry into the formal risk and reliability assessments. Such physical models will be validated using a state of the art reliability assessment laboratory (being developed at PI). Uncertainties about the model structures and parameters will also be quantified. Such models will incorporate inspection data (characterizing limited and uncertain evidences). The rate of degradation is influenced by many factors such as pipeline materials, process conditions, geometry and location. Based on these factors, a best estimate of the structure (pipeline) or equipment (primarily valves, pumps and compressors) service life (reliability and remaining life) is to be calculated and uncertainties associated with the service life quantified. This estimate would serve as a basis that guides decisions regarding maintenance and replacement practices.

Phase I of this research focused on developing a corrosion-fatigue model. It successfully proposed such a model and developed an advanced laboratory for testing this phenomenon at PI. The current research continues in the same line of research by investigating and developing additional degradation phenomena (SCC, pitting corrosion, and creep-fatigue) and integrates these phenomena with reliability and risk assessment through four different tasks. The long-term objective of this research is to develop a comprehensive library of probabilistic mechanistic models for all degradation phenomena pertinent to structures (piping, and pressure vessels) used in the oil industry.

Test Facilities

The test rig for this research exists at the University of Maryland. The rig is used to conduct experimental studies reflecting field conditions for model validation developed in EERC Phase I & II. The equipment include MTS fatigue machine, heating furnace, corrosion test cells, autoclaves, multiphase flow loops, and testing machines for slow strain rate and crack growth testing. This activity also requires a complete line of monitoring equipment for evaluation of corrosion, scaling, and chemical treatment for field and laboratory. This test rig will be a useful tool for performing fatigue, corrosion, corrosion-fatigue, creep, and creep-fatigue, as well as teaching and possibly training field engineers from operating companies.

Two-Year Schedule

This project involves three distinct tasks. The first task is the development of the mechanistic models, development of a corresponding simulation tool to help both model development and field applications. The second task focuses on experimental activities to generate relevant data to validate the proposed models of Task 1. Finally, the third task involves the actual validation of the models proposed in Task 1 with the experimental results obtained in Task 2, including Bayesian estimation of the model parameters.

Task 1: Develop the best estimate mechanistic (physics of failure) empirical models for pitting corrosion, SCC, and fatigue-creep. The model development involves the following activities.

Task1.1: Gather, review and select most promising physics of failure based methods and algorithms proposed in the literature.

- Literature surveys for creep and stress corrosion cracking (SCC) degradation mechanisms are almost completed and will be classified for finding the relevant models (100% done).

Task1.2: Select, develop or adopt a detailed mechanistic model (one deterministic model for each phenomenon) that properly describes the degradation process.

- Development of the mechanistic models and of a corresponding simulation tool to help both model development and field applications after classifying the models and choosing the appropriate one should be done in the next future (90% complete).

Task 1.3: Develop a Monte-Carlo based mathematical simulation routine on MATLAB depicting the detailed mechanistic model of each degradation phenomenon (far faster than real-time).

- This part was completed for the empirical model developed based on the works of the PI interns for pitting corrosion. After proposing the similar models for SCC and creep-fatigue, it will be repeated (85% completed).

Task 1.4: Based on the results of the simulation a simplified empirical model that best describes the results of simulation will be proposed. Such a model relates the degradation (e.g., depth of the pit or the crack growth rate) to applied loads such as pipeline internal pressure and chemical composition of the product inside the pipeline, as a function of time or cycle of load application.

- This part is completed for the Stress Corrosion Cracking, pitting corrosion and corrosion-fatigue (100% complete).

Task 2: A PoF reliability analysis laboratory has been designed and being developed at PI. The advanced corrosion-fatigue purchased by the PI that was installed at the University of Maryland (the Cortest Rig) has been sent to Cortest to ship to PI.(100% done).

Task 2.1: Completing the remaining corrosion-fatigue tests being conducted by Mr. Nuhi and Chookah. (100% Completed)

Task 2.2: Pitting Corrosion Experiments (develop test plan, prepare samples and the facility, perform the test, and evaluate the test results) (100% Completed).

Task 2.3 SCC Experiments (develop test plan, prepare samples and the facility, perform the test, and evaluate the test results). (100% Completed)

- This task will be done in the near future, but SCC specimen holders have already designed and made according to the recent patents and ASTM-Standard.

Task 2.4 Creep-Fatigue Experiments: The equipments and samples are completely ready (100% completed); the tests will be performed in future and the results will be evaluated.

- A small-scaled corrosion-fatigue (or creep) chamber has been designed (not as part of this project), made and tested for dog-bone and CT specimens and checked its workability on the UMD MTS machines using Aluminum alloy samples. Moreover, another chamber has been made for long dog boned specimens.
- A heating chamber has been designed and tested for creep experiments.
- New dial gauges with stand are prepared and tested for four and three points bending of SCC and pitting corrosion experiments.

Task 3: This task involves modification, advancement and use of the WinBUGs' Bayesian formalism for model validation using experimental data and integration of the field data and information including sensor-based data (acoustics and/or optical) to update the empirical models and estimate the remaining life of oil pipelines and structures. (85% Complete)

- The WinBUGs' Bayesian formalism for model estimation and validation was developed as part of M. Chookah's work. This formalism is being updated and new applications of the formalism have been performed using past experimental data and new data. Further work with this software for integration the experimental data has already be done.

Schedule/Milestones/Deliverables

Tasks 1.1-1.3 (5/1/09-12/15/09); Task 1.4 (12/15/09-3/1/10); Task 2.1 (completed 7/1/09); Task2.2 (7/1/09-12/15/09); Task 2.3 (12/15/09 – 6/1/10); Task 2.4 (6/1/10-2/1/11); Task 3 (12/15/09-3/15/11).

The Cortest rig was boxed and shipped to the Cortest Corporation to test and send to **PI.**

The project is on schedules and there is no issue or delay at this point.

Dr. Seibi was appointed as a Co-Advisor of Mr. Nuhi.

Visits

- Dr. A.Seibi visited UMD in July 2009
- Dr. A.Seibi visited UMD in July 2010
- Two PI students Abdullah Al Tamimi, and Mohammad Abu Daghah took parts at summer internship (2009).
- A PI student Taher Abu Seer took parts at summer internship (2010).
- Prof. Modarres attended the 1st Annual PI Partner Schools Research Workshop. The Petroleum Institute, Abu Dhabi, U.A.E. January 6-7, 2010.
- Abdullah Al Tamimi, presented a joint paper on pitting corrosion at the ICM 11 conference in Como, Italy, June 5-9, 2011.

8. Papers Published and prepared for publishing by the Team

1- Development of a Probabilistic Mechanistic Model for Reliability Assessment of Gas Cylinders in Compressed Natural Gas Vehicles, S. Chamberlain, M. Chookah, M. Modarres, Journal of Risk & Reliability, Vol. 233, pp 289-231(2009).

2- A Probabilistic Physics-Of-Failure Model For Prognostic Health Monitoring of Piping Subject to Pitting and Corrosion-Fatigue, M. Chookah, M. Nuhi, and M. Modarres, , Reliability Engineering and System Safety (Accepted for publication, April 2011).

3- Probabilistic Model for Mechanistic Evaluation of Reliability of Oil Pipelines subject to Corrosion-Fatigue Cracking, M. Chookah, M. Nuhi, M. Modarres, A. Seibi, Proceedings of the ASME 2008 International Design Engineering Technical Conferences & Computers and Information in Engineering Conference, IDETC/CIE 2008, New Cork City, NY, August 3-6, 2008.

4- Development of a Probabilistic Model for Assessment of Degradation of Pipelines Due to Corrosion-Fatigue Cracking, M. Chookah, M. Nuhi Faridani, M. Modarres, A. Seibi, Probabilistic Safety Assessment (PSA'08) Conference, Knoxville, TN, Sept. 2008.

5- Assessment Of The Integrity of Oil Pipelines Subject To Corrosion Fatigue And Pitting Corrosion, M. Chookah, M. Nuhi, And M. Modarres, 3rd International Conference on Integrity, Reliability and Failure, Porto, 20-24 July 2009.

6- Reliability Analysis for Degradation Effects of Pitting Corrosion in Carbon Steel Pipes, M. Nuhi, T. Abu Seer, A. M. Al Tamimi, M. Modarres, A. Seibi, 11th International Conference on the Mechanical Behavior of Materials, Lake Como, Italy, June 5-9, 2011.